
ROSETTA Mission Commissioning Results Review Spacecraft Performance Report

Rosetta Project



prepared by	SCI-PRS (H.Fiebrich,D.Martinez Ripoll,J.Noyes,J.Rouquet,D.Stramaccioni)
approved by	J.Ellwood
reference	RO-EST-RP-3226
issue	1
revision	1
date of issue	June 2004

a

ESTEC

Keplerlaan 1 - NL 2201 AZ Noordwijk ZH - The Netherlands
Tel (31) 71 565 3424 - Fax (31) 71 565 5922 - <http://sci.esa.int/rosetta>

D I S T R I B U T I O N

Name	Organization	Name	Organization
J.Louet	SCI-P	H.Fiebrich	SCI-PRS
W.Frank	OPS-O	D.Martinez Ripoll	SCI-PRS
A.Gimenez-Canate	SCI-S	J.Noyes	SCI-PRS
J.F.Kaufeler	OPS-G	J.Rouquet	SCI-PRS
J.Ellwood	SCI-PR	D.Stramaccioni	SCI-PRS
J.van.Casteren	SCI-PRS		
G.Schwehm	SCI-SB	P.Ferri	OPS-OPR
M.Kessler	SCI-SD		
A.F.Smith	OPS-OF	R.Best	Astrium-GmbH
C.Alexander	NASA		
A.Mantineo	OPS-CQ	Rosetta PI's	
M.Warhaut	OPS-OP		
J.Cande	TEC-QE	H.Scheuerle	DLR
		R.Willnecker	DLR
		D.Moura	CNES
		P.Kletzkine	SCI-PRL
		C.Berner	SCI-PRP
		W.Pinter Krainer	SCI-PRP
		M.Schwetterle	SCI-PRP
		M.Kasper	SCI-PRQ
		J.Salvignol	SCI-PRL
		M.Ranne	SCI-PMO
		F.Pedersen	SCI-PRP
		B.Hedley	SCI-PCO
		B.Gramkow	SCI-PRP

C H A N G E L O G

date	issue	revision	pages	reason for change
June 2004	1	0	ALL	Issue for the Preliminary MCRR

T A B L E O F C O N T E N T S

1	Introduction.....	1
2	POWER	2
2.1	Design principle	2
2.2	Lithium Ion batteries	2
2.2.1	Conclusion:.....	3
2.3	Solar cell generator.....	3
2.3.1	Solar generator wing deployment.....	3
2.3.2	Initial performance of the measurement strings	5
2.3.3	Initial operating point and wing power output performance	5
2.3.4	Conclusion:.....	7
2.4	Power Conditioning Unit (PCU).....	8
2.4.1	PCU unit power dissipation.....	8
2.4.1.1	Dissipation in BDR mode.....	8
2.4.1.2	Dissipation in APR mode	8
2.4.2	PCU module efficiency	8
2.4.2.1	Battery-Discharge –Regulator (BDR) efficiency and input current sharing	8
2.4.2.2	Battery-Charge-Regulator (BCR) efficiency.....	9
2.4.3	Array-Power-Regulator (APR) efficiency.....	9
2.4.4	Maximum-Power-Point-Tracker (MPPT) operation	10
2.4.5	Conclusion.....	12
2.5	Subsystem Power-Distribution-Unit (SS-PDU).....	13
2.5.1	SS-PDU unit power dissipation.....	13
2.5.2	Auxiliary power supplies.....	13
2.5.3	Pyro firings	13
2.5.4	Conclusion.....	22
2.6	Payload Power-Distribution-Unit (PL-PDU).....	23
2.6.1	PL-PDU unit power dissipation.....	23
2.6.2	Auxiliary power supplies.....	23
2.6.3	Pyro actuations	23
2.6.4	Conclusion.....	27
3	Thermal Control.....	28
3.1	Launch.....	28
3.2	Comparison Between Telemetry and Computed Temperatures	30
3.2.1	Lateral Panels	31
3.2.2	Other Internal Units	32
3.2.3	Top ‘+Z’ Payload Panel.....	33
3.2.4	Thrusters	34
3.2.5	HG Antenna Pointing Mechanism.....	35
3.3	TCS Performance Evaluation.....	37
3.3.1	Main Spacecraft Body	37
3.3.2	Stand-by Thrusters.....	37
3.3.3	Firing Thrusters	39

3.3.4	HG APM Operations	42
3.3.5	Heater Software Control	42
3.4	TCS References	43
4	OBDH Hardware	44
4.1	Design Principle	44
4.1.1	Architecture and Interfaces	44
4.2	Commissioning	44
4.2	Conclusion	46
5	System Software and Operations	47
5.1	System Software	47
5.2	Data Management System	47
5.2.1	Tele command reception, distribution and handling	47
5.2.2	Telemetry collection, formatting, storage, distribution and down link	47
5.2.3	Mission Time Line	48
5.2.4	On Board Control Procedures	48
5.2.5	On Board Monitoring of Telemetry Data	49
5.2.6	Failure Detection Isolation and Recovery (FDIR)	49
5.3	Attitude Orbit Control System	49
5.4	Solid State Mass Memory	50
5.5	Autonomous Star Tracker	50
5.6	Navigation Camera	51
5.7	Conclusion	52
6	TT&C	53
6.1	Design Principle	53
6.2	Initial Flight Data	54
6.3	Functional and Performance Data	54
6.4	Conclusions	56
7	Attitude and Orbit Control Subsystem (AOCS)	58
7.1	GENERAL DESCRIPTION	58
7.1.1	AOCS MODES	58
7.1.2	AOCS UNITS	61
7.1.3	AOCS FAILURE DETECTION ISOLATION AND RECOVERY	63
7.2	SUMMARY OF AOCS COMMISSIONING HIGHLIGHTS	63
7.3	AOCS IN-FLIGHT PERFORMANCES	64
7.3.1	AOCS UNIT PERFORMANCES	64
7.3.1.1	ACQUISITION INTERFACE UNIT	64
7.3.1.2	SUN ACQUISITION SENSORS	64
7.3.1.3	INERTIAL MEASUREMENT PACKAGES	65
7.3.1.4	STAR TRACKERS	67
7.3.1.4.1	ACQUISITION CAPABILITY	67
7.3.1.4.2	TRACKING PERFORMANCES	68
7.3.1.5	NAVCAM	69
7.3.1.6	REACTION WHEELS	69
7.3.2	DYNAMICS AND DISTURBANCE TORQUES	71
7.3.2.1	SPACECRAFT INERTIA IN-FLIGHT CALIBRATION	71

7.3.2.2	SA FLEXIBLE MODES FREQUENCY CALIBRATION	72
7.3.2.3	DISTURBANCES TORQUE	73
7.3.3	POINTING PERFORMANCES	73
7.3.3.1	SOLAR ARRAY POINTING ACCURACY.....	73
7.3.3.1.1	SUN ACQUISITION MODE	74
7.3.3.1.2	SUN KEEPING MODE.....	78
7.3.3.1.3	SAFE HOLD MODE	79
7.3.3.2	ABSOLUTE POINTING ERROR OF THE HGA.....	81
7.3.3.3	APE AND RPE FOR OPERATIONAL PHASES.....	84
7.3.3.4	DELTA-V ACCURACY.....	85
7.3.4	FUEL CONSUMPTION.....	87
7.4	LESSONS LEARNED.....	90
7.5	CONCLUSION	90
8	RCS.....	92
8.1	From Launch to Separation.....	92
8.2	LEOP Operations	93
8.3	First RCS Pressurisation	93
8.4	DSM1	96
8.4.1	Apparent Temperature Anomalies.....	97
8.5	First RCS Isolation.....	97
8.5.1	Apparent Pressure Anomalies	98
8.6	RCS REFERENCES	98
8.7	RCS ANNEX 1	98
9	EMC.....	99
10	Conclusion.....	100

1 INTRODUCTION

This report is part of the documentation for the Rosetta Mission Commissioning Results Review MCRR part 1.

It describes the status of the spacecraft from its successful launch (07:17:51 UTC on 2nd March 2004) up to the end of the first part of the commissioning and verification phase CCVP 7th June 2004. Due to the long duration from launch until the complete CCVP end of commissioning the MCRR will be held in two parts this document currently reflects what has been done during the first part; it will be updated after the second part for the final MCRR. Currently the spacecraft has performed its first Deep Space Manuver and has passed its first Perihelion with the Sun, while being operated according to operational needs to support payload commissioning, with no major problems. This report describes the performance of each of the S/C subsystems to the extent they have been used to date.

2 POWER

This part of the report describes the results of the performance analyses of the ROSETTA power subsystem including solar generator for the LEOP and early commissioning phase.

For power saving reasons the Solid State Mass Memory (SSMM) recorder was off during the launch, therefore no housekeeping telemetry is available between lift-off and in-orbit telemetry acquisition.

2.1 Design principle

The ROSETTA power subsystem comprises the Solar Array (SA) generator, the source of electrical energy during Sun phases, three Li-Ion batteries, one Power Conditioning Unit (PCU) providing a stable 28 volt main bus and battery charge and discharge modules and finally one Sub System Power distribution Unit (SS-PDU) and one Payload Power Distribution Unit (PL-PDU) providing switchable current limiters for bus support units and experimenters together with the necessary pyro channels.

2.2 Lithium Ion batteries

The three onboard Lithium Ion (Li-Ion) batteries have been fully charged, 100% State-of-Charge (SoC) during the launch preparation in the pre-launch mode. At H0-4hrs, at going to launch mode, the End-of-Charge voltage (EOCV) has been set to the LEOP in-orbit value of 89% SoC. The batteries had stable temperatures of 21 °C on the launch pad. At H0-13min the batteries started to deliver power to the spacecraft which had been set to internal power. Due to the satellite load of 108.9W about 1% of their capacity was delivered by each battery up to lift-off.

After acquisition of signal it could be observed that due to the spacecraft's (SC's) attitude some Sun incidence was present on the still undeployed -Y wing solar array leading to a varying degree of power support for the bus (approximately 23 to 88W). This further alleviated the power requested from the batteries until the -Y wing solar array took over the provision of power to the SC after its deployment in full. At this time, H0+144min, the battery recharge started with all three batteries immediately going into taper charge mode. This can be fully explained by the fact that the absolute minimum SoC reached was 88%, giving a calculated battery EMF of 24.6V volt, very close to the LEOP EOCV of 24.7volts. The taper charge currents fell below 1A first on battery (BTR) 1 after about 3 minutes and then for batteries 2 and 3 simultaneously after 4 minutes. With the tapered battery charge current falling to a level of C/100 (0.165A) the recharging was complete after 36.5 minutes for BTR1 and after 39 minutes for BTR2 and BTR3. The small and not concerning difference can be explained by the fact the BTR 1 discharge current has been seen to be slightly lower than the average even

before the launch. This led to a slightly less discharge state at the end of the battery usage in LEOP, with the difference being less than 1% SoC which is hardly detectable.

The batteries temperature evolved from a pre lift-off of about 21 °C to slightly higher than 22 Degr. C at the start of the recharge. This temperature evolution is well within the expected temperature increase range of 2 °C.

2.2.1 Conclusion:

The three ROSETTA on-board Lithium-Ion batteries supported the SC launch as expected. Their total capacity usage was 11% which is relatively small due to the fact that the launch took place at H01 without further delay and that the SC showed nominal performance with no unrecoverable power consumption, as was budgeted. All battery telemetry showed performance as predicted and gives good confidence in battery health and performance capabilities, for the commissioning phase as an emergency energy source and for the planned use during the Mars fly-by.

Note: All battery performance predictions have been made using the AEA Technology provided software tool BEAST2000 v3.

2.3 Solar cell generator

2.3.1 Solar generator wing deployment

The ROSETTA solar cell generator was deployed using the on-board automatic separation sequence commands. The -Y wing, the first to go, showed a 'deployed' telemetry status 3 minutes 58 seconds after the last nominal thermal knife (TK4A) started drawing current at 2004.062.09.59.56.152. The +Y wing deployment status changed to 'deployed' 4 minutes 8 seconds after the last nominal thermal knife (TK10A) started drawing current. This timing is well within the expected durations. The separation sequence automatically terminated the thermal knife firing after detection of the deployment status of the second wing. The redundant thermal knives -Y wing TK1B and TK2B had also been fired by that time. All activated thermal knives showed nominal current consumption.

About twenty minutes after their deployment and with a stable SC attitude each solar wing temperature had stabilised. The -Y wing to 67.7°C (T1 -Y0 Isc string), 69.2 °C (T2 -Y1 Voc string) and 73.9 °C (T3 -Y4 ops string), the +Y wing to 64.6 °C (T1 +Y0 Isc string), 69.2°C. (T2 +Y1 Voc string) and 70.8 °C (T3 +Y4 ops string). These measured temperatures match well with the predicted ones.

ROSETTA solar array thermal knife firing

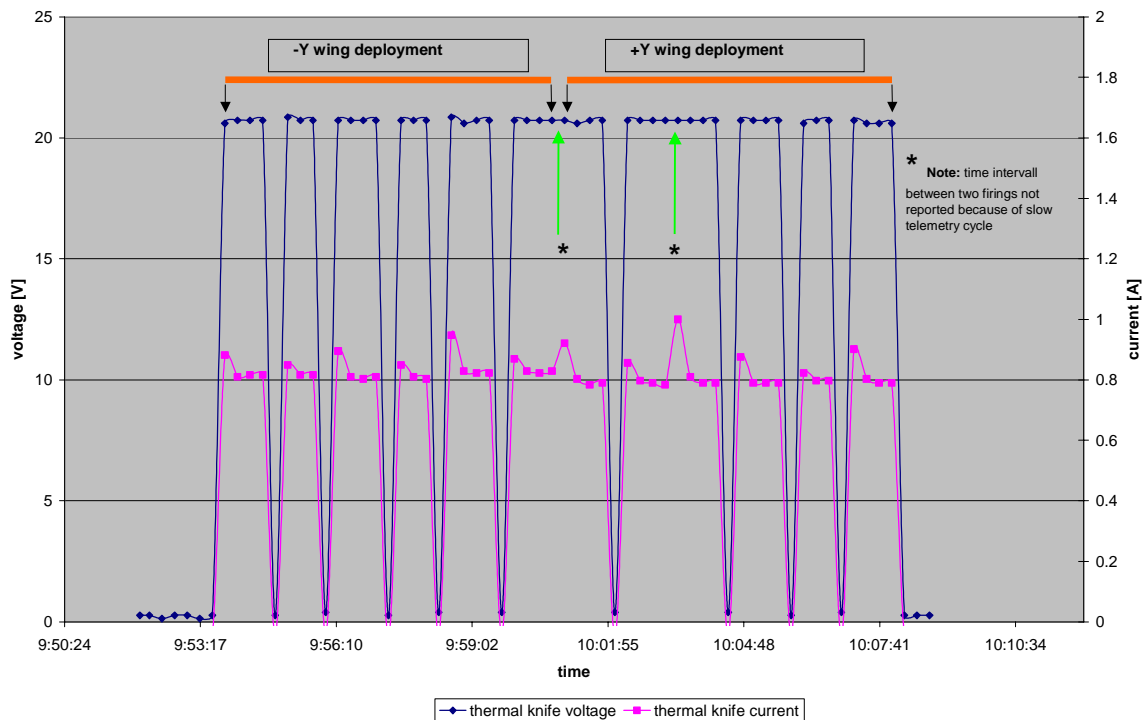


Figure: Solar array wing deployment, thermal knife voltages and currents

Note: The initial higher thermal knife current is nominal and due to the lower cold resistance of the knife at initial voltage application

2.3.2 Initial performance of the measurement strings

The initial measurement string readings after temperature stabilisation were as follows:

At 2004.062.10.23.58.148 the readings were:

Solar aspect angle	T1 -Y Isc string	Isc current	T2 -Y Voc string	Voc voltage
1.76 degree	67.7 °C	1.070 Amp	69.2 °C	2.790 V
Predicted	at 67.7 °C	1.027 Amp	at 69.2 °C	2.769 V
Delta :		+4.2%		+2.8%

Solar aspect angle	T1 +Y Isc string	Isc current	T2 -Y Voc string	Voc voltage
1.97 degree	64.6 °C	1.055 Amp	69.2 °C	2.774 V
Predicted	at 64.6 °C	1.026 Amp	at 69.2 °C	2.769 V
Delta :		+0.8%		+0.2%

Differences between predicted and measured values are below 1% for the open circuit voltages of both wings and therefore below the measurement accuracy. The measured short circuit current is 4% higher for the -Y wing and about 1% higher for the +Y wing. Based on similarity between the cells in the measurement strings and the cells in the operating sections one would expect also a slightly better performance of the complete solar generator.

Great care shall be taken in extrapolating the BOL near to Sun hot performance to the deep space conditions later in the mission where radiation damage and low temperature low Sun intensity conditions prevail.

Nevertheless these measurement results are the basis for some confidence that the solar array power in later mission phases will also have a good chance of meeting or exceeding the predicted in-orbit performance.

2.3.3 Initial operating point and wing power output performance

After temperature stabilisation, the operating points of the two solar array wings have been measured.

The operating points of the two wings at 2004.062.10.23.58.148 were:

- Y wing	Vops = 49.69 V	Iops = 2.46 A	T3 -Y ops string = 72.3 °C
+Y wing	Vops = 49.65 V	Iops = 2.49 A	T3 +Y ops string = 73.9 °C

A plot of the initial operating points versus the predicted output power of a wing in shown in figure below.

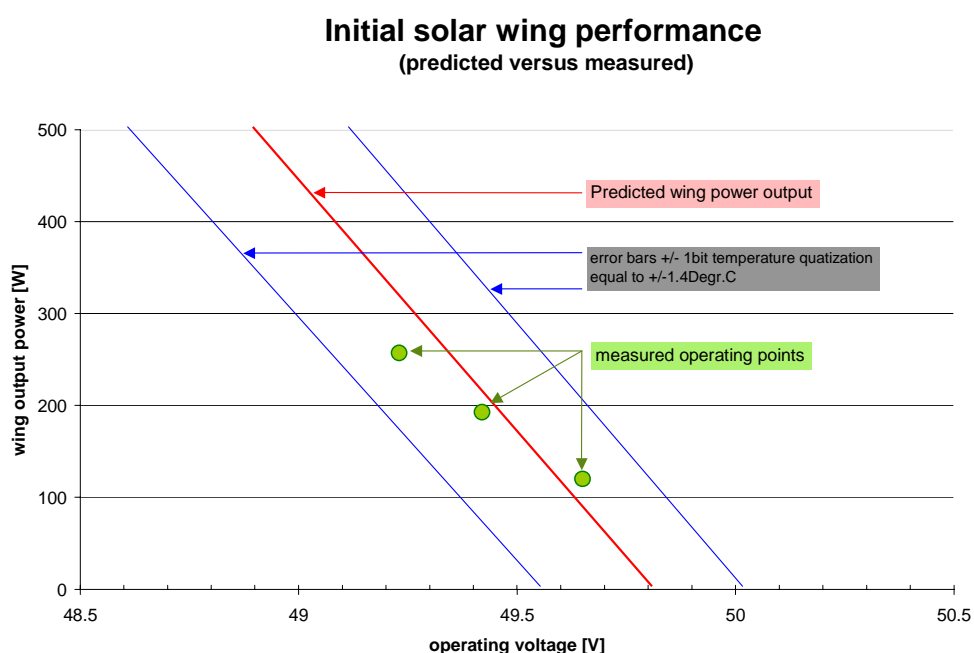


Figure: Initial solar array wing performance

Although the measured points are close to the predicted curve, suggesting that the wings delivers power as predicted, great caution shall be used in the interpretation of the data because:

- a) of uncertainties involved in the prediction of the wing performance very close to it's open circuit voltage, where uncertainties in the model used, increase
- b) of the large impact of the temperature measurement accuracy on the modelled power output at this operating point

At the present moment it seems more appropriate to concentrate on the measured performance of the measurement strings as shown in the paragraph 2.3.2

2.3.4 Conclusion:

Early telemetry analysis of the solar cell generator suggests nominal performance. Because the software prediction model shows increased uncertainties in the operating range of the early mission phases (operating point close to the open circuit voltage of the array) and a large influence of temperature measurement accuracies on predicted performance, no final accurate judgment is possible to date.

To confirm the solar array performance, it is suggested that further analysis of telemetry data, to be gathered during the satellite's journey through space, shall be conducted in good time.

Note: All solar cell and solar wing performance related predictions have been made using the DUTCH Space provided software tool 'POWERTOOL v5' adapted to the LEOP conditions (zero radiation damage, zero micrometeorite damage).

2.4 Power Conditioning Unit (PCU)

The ROSETTA PCU is the heart of the power subsystem and its input and output parameter performance at solar array wings, batteries and main bus level are closely interrelated, making a good performance analysis a demanding exercise. This is additionally complicated by the presence of the additional Maximum-Power-Point-Tracking (MPPT) control mode. Large amounts of machine-readable telemetry data were necessary to be able to depict and analyse the PCU performance.

The nominal output voltages and currents of the all PCB local auxiliary power converters have been verified. The measured voltages and currents have not drifted w.r.t. earlier AIV phase verification tests.

2.4.1 PCU unit power dissipation

2.4.1.1 Dissipation in Battery Discharge Regulator BDR mode

In-orbit, so far, the PCU has only been observed for a very short time being in BDR mode. This is explained by the fact that only data after separation and signal acquisition is available and the fact that even with undeployed solar arrays almost always some Sun was present on one of the outer panels.

For one of the observed BDR mode cases the main bus load was 190W, at which the unit dissipated 12.3W. The PCU internal temperature was 32°C.

2.4.1.2 Dissipation in Array Power Regulator APR mode

Two distinct power cases have been analysed, a lower power and a higher power mode. In both cases the APR input voltages were around 49 volts. In the first case the main bus load was 222.4W, here the PCU dissipated 20.3W giving an overall efficiency of 91.6%. In the second case the main bus load was 488.5W, here the PCU dissipated 28.1W giving an overall efficiency of 94.5%.

2.4.2 PCU module efficiency

2.4.2.1 Battery-Discharge –Regulator (BDR) efficiency and input current sharing

The highest in-orbit BDR input currents have so far been observed just before the start of the –Y wing solar array deployment. The PCU internal temperature was 32°C. The following picture was derived from the telemetry:

2004.062.09.56.14.147

	Battery discharge current	Battery voltage	Main bus current	efficiency
BDR 1	2.78 A	24.34 V	2.26 A	93.4 %
BDR 2	2.79 A	24.30 V	2.26 A	93.2 %
BDR 3	2.77 A	24.30 V	2.29 A	95.2 %

Although the analysed case shows an output module power of only 66W, which is outside the specification module output power window of $150W < P_{out} < 300W$, still all three BDR module meet the specification of $\eta > 93\%$.

The calculated BDR input current sharing spread is less than 0.4%, much better than the specified $\Delta I < 3\%$.

2.4.2.2 Battery-Charge-Regulator (BCR) efficiency

Because of the small total discharged capacity and the lower in-orbit commanded SoC all three batteries went into taper charge mode immediately after the start of recharging. The PCU internal temperature was 32°C. The first telemetry sample received after -Y wing solar array started to deploy showed the following picture:

Time: 2004.062.10.00.14.147

	Battery charge current	Battery voltage	Main bus current	efficiency
BCR 1	2.42 A	24.75 V	2.21 A	96.9%
BCR 2	2.57 A	24.73 V	2.34 A	97.1%
BCR 3	2.48 A	24.72 V	2.25 A	97.4%

The calculated module efficiency values compare very favourable with the specification of $\eta > 94\%$.

2.4.3 Array-Power-Regulator (APR) efficiency

The maximum in-orbit total SC input power through the APR's has been measured as 518W so far. The PCU was in APR mode, the internal temperature was 24°C. Analysis of recorded telemetry has given the following picture:

Time: 2004.067.00.13.54.255

	Array input current	Array input voltage	Main bus current	efficiency
APR A1	1.76 A	48.88 V	2.91 A	94.6%
APR A2	1.74 A	48.87 V	2.89 A	95.1%
APR A3	1.77 A	48.85 V	2.92 A	95.6%
APR B1	1.75 A	48.99 V	2.90 A	94.6%
APR B2	1.76 A	48.96 V	2.92 A	94.8 %
APR B3	1.76 A	48.95 V	2.92 A	94.8 %

The calculated module efficiency values compare favourable with the specification of $\eta > 94\%$.

All APR's show better than specified output current sharing ($\Delta I < 1\%$ measured, versus a specification of $\Delta I < 3\%$)

2.4.4 Maximum-Power-Point-Tracker (MPPT) operation

The MPPT was in operation three times, just before the deployment of the first solar array wing. Due to the fact that the SC was with a switched off attitude control system slowly rotating around the SC x-axis, allowing some Sun on the outer panels of the still undeployed array wings, the MPPT operated as expected, sometimes with very low power available. As low as 23W at $V_{sa} = 55V$ resulting in 140mA, or 3.9W to main bus per APR module, were extracted from the solar array at that point. The observed behavior was expected, as each module is known to operate perfectly down to 100mA.

Also the situation where one wing operates in MPPT mode while the other in APR mode is present. In this case only one APR section regulates the main bus, while the other obtains whatever power is available on that wing.

The observed MPPT operation was as expected and fully nominal.

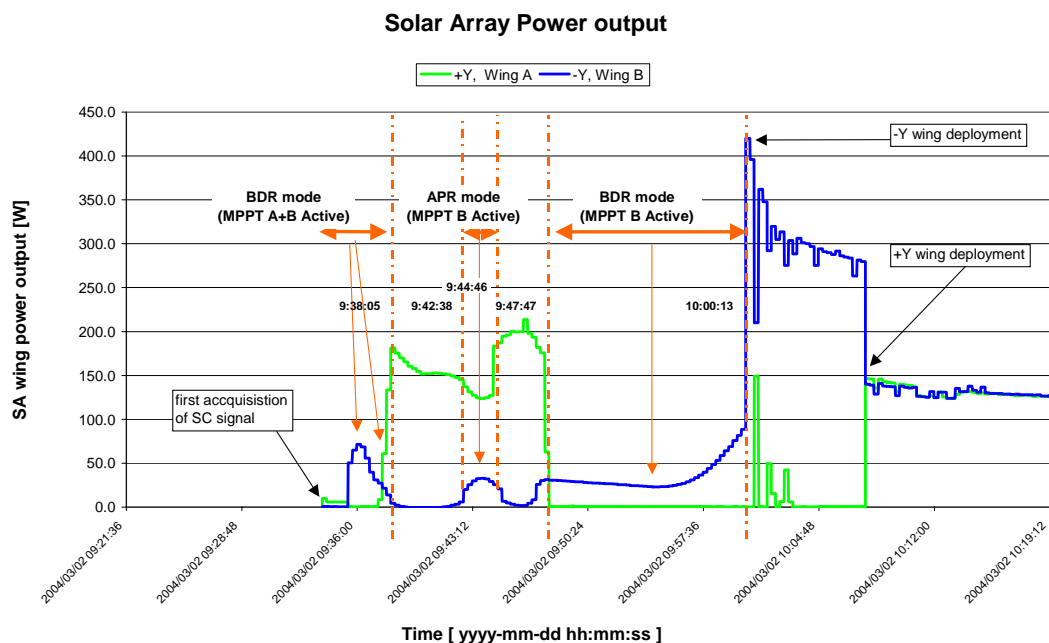


Figure: Solar array wing power output during first LEOP phase

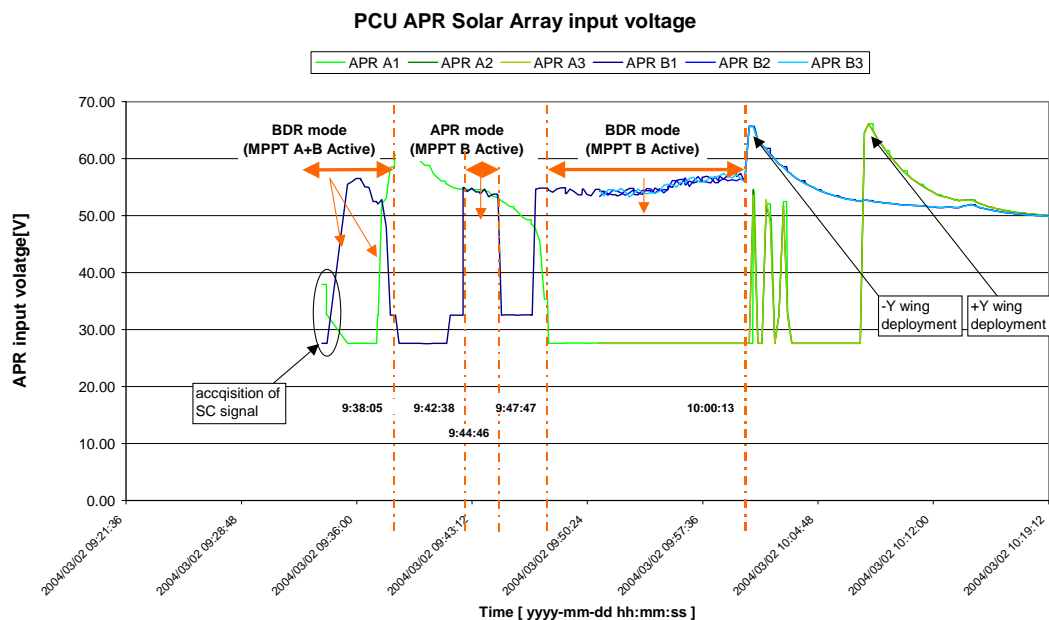


Figure: APR input voltage during first LEOP phase

2.4.5 Conclusion

The PCU, including the maximum power point tracker operation, performed as expected. Where applicable, specifications were met and often largely exceeded.

2.5 Subsystem Power-Distribution-Unit (SS-PDU)

2.5.1 SS-PDU unit power dissipation

Two distinct power cases have been analysed, a lower power and a higher power mode.

In the low power case ($P_{out}=103W$) the following data has been analysed:

I main bus	ΣI FCL's	ΣI LCL's	$I_{mb}-(I_{FCL's}+I_{LCL's})$	SS-PDU dissipation
4.016 A	1.824 A	1.837 A	0.335 A	$P_{diss} = 9.36 W$

In the high power case ($P_{in}=386W$) the following data has been analysed:

I main bus	ΣI FCL's	ΣI LCL's	$I_{mb}-(I_{FCL's}+I_{LCL's})$	SS-PDU dissipation
14.345 A	1.894 A	11.905 A	0.546 A	$P_{diss} = 15.29W$

Although for these in-orbit load cases there is no directly comparable specification value, the data is plausible and is considered nominal.

2.5.2 Auxiliary power supplies

Secondary voltages and primary input currents of the PCU auxiliary power supply are found to be nominal.

2.5.3 Pyro firings

The SS-PDU was used to supply the firing current to the following item:

- Reaction Control System (RCS) priming
- Lander NEA release
- High Gain Antenna (HGA) deployment
- RCS first pressurisation
- RCS Isolation

All firings were nominal.

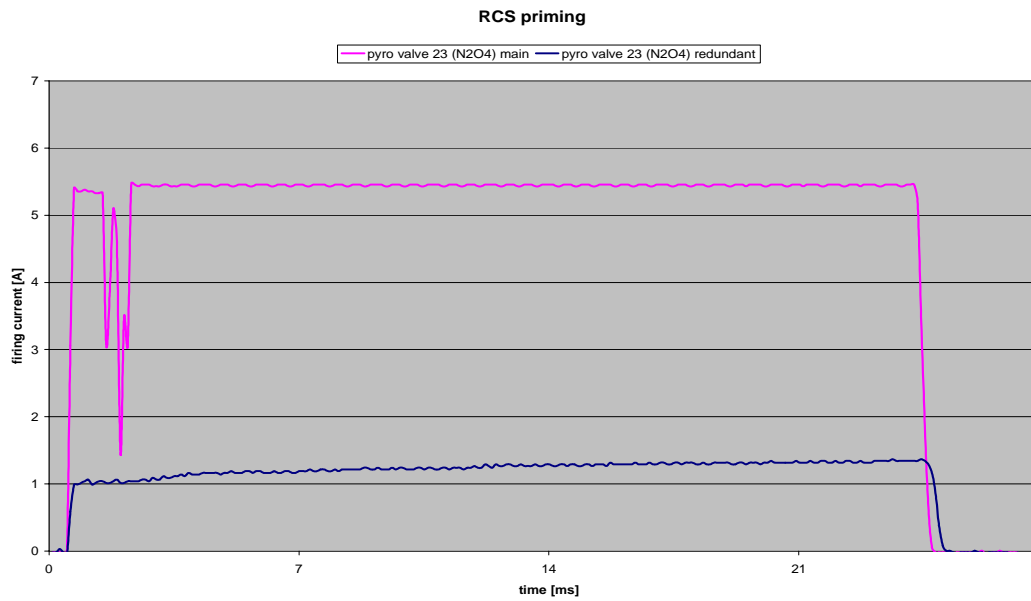


Figure: RCS priming, N₂O₄ pyro valve 23 main and redundant firing currents

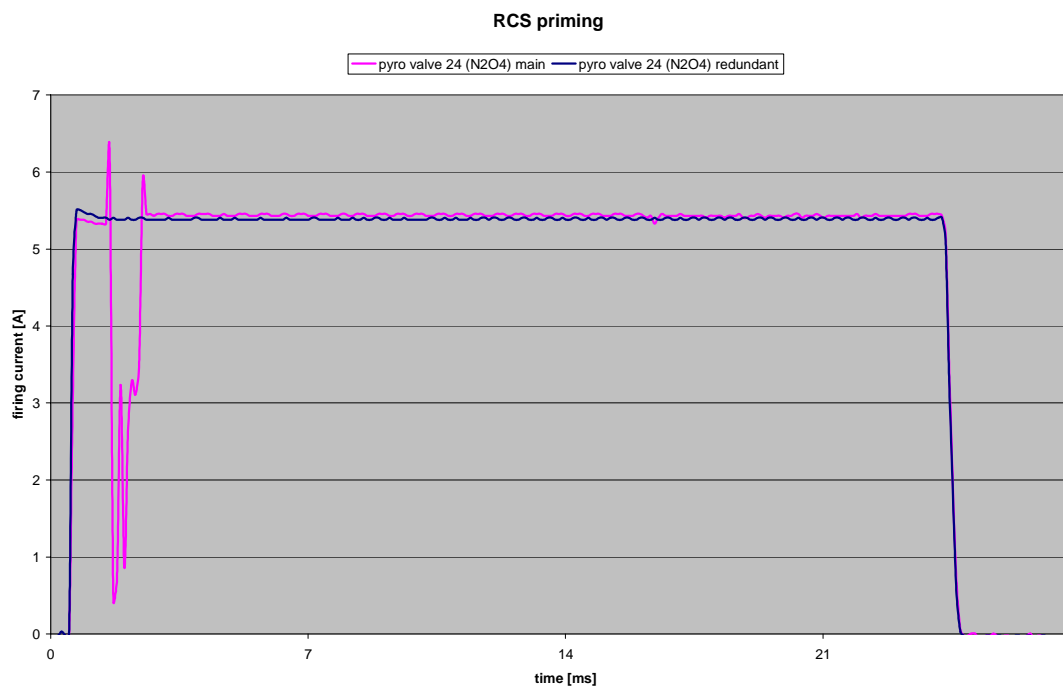


Figure: RCS priming, N₂O₄ pyro valve 24 main and redundant firing currents

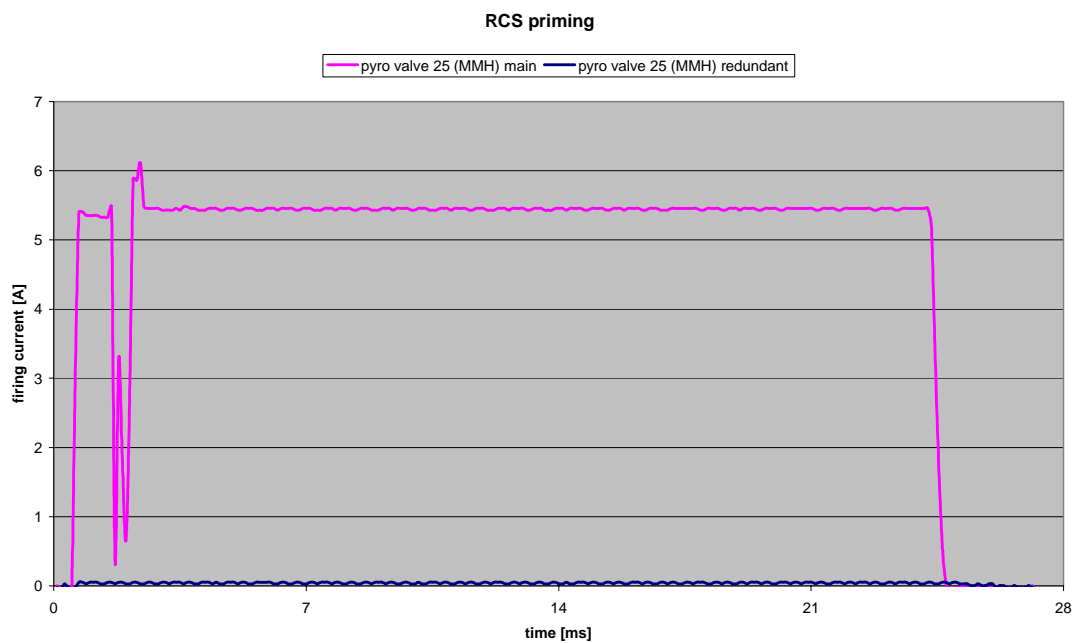


Figure: RCS priming, MMH pyro valve 25 main and redundant firing currents

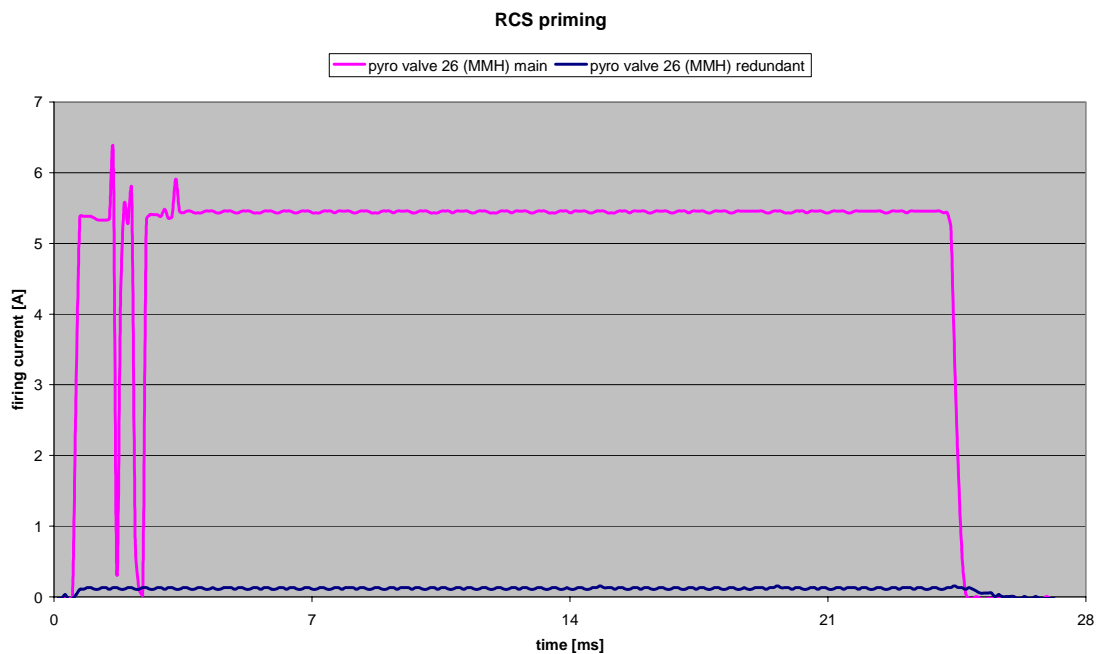


Figure: RCS priming, MMH pyro valve 26 main and redundant firing currents

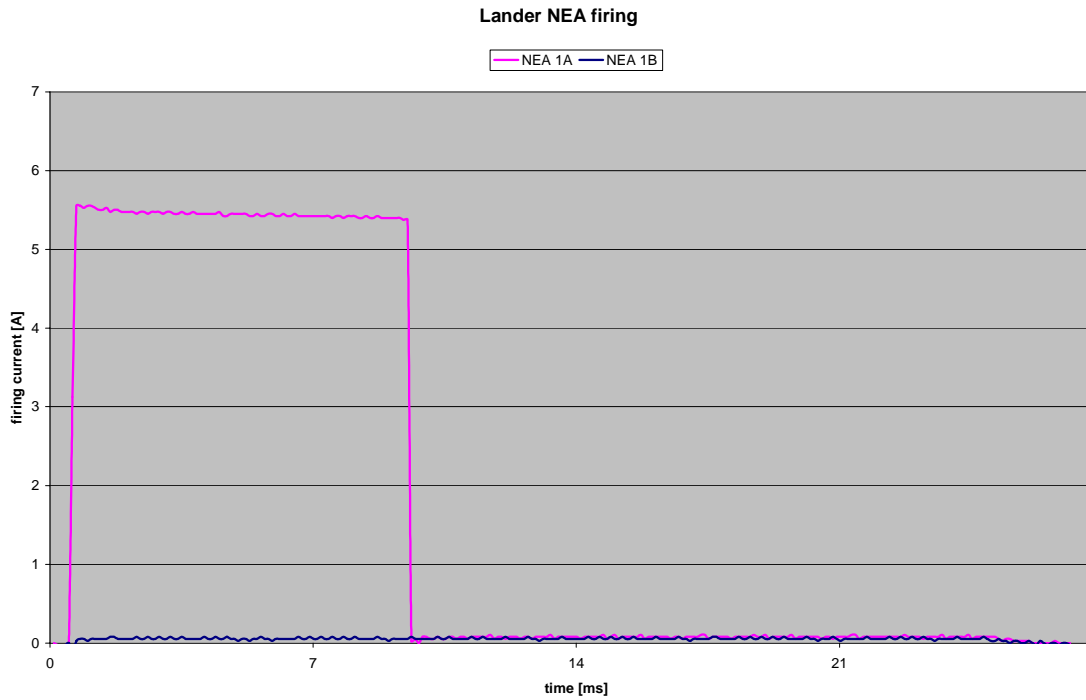


Figure: Lander NEA 1A & 1B firing

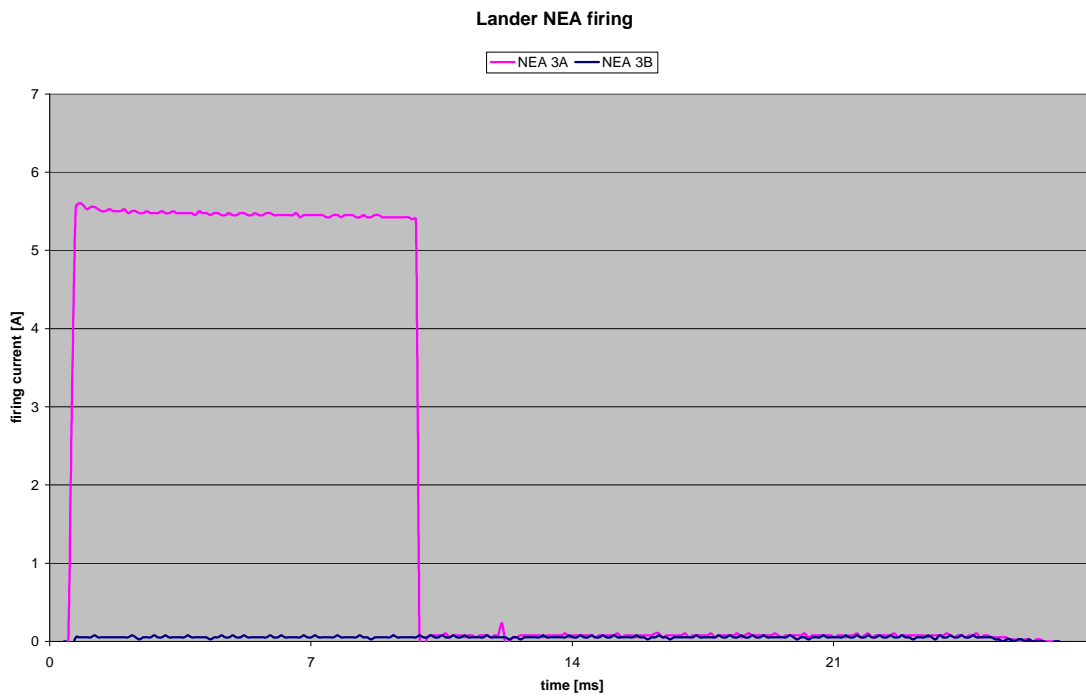


Figure: Lander NEA 3A & 3B firing

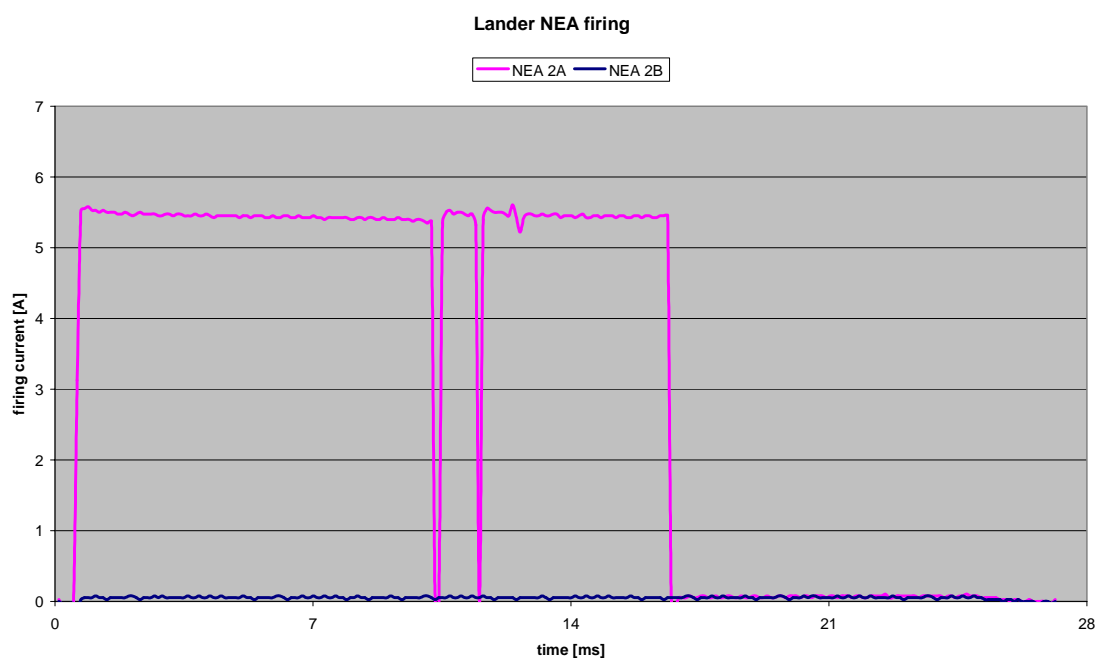


Figure: Lander NEA 2A & 2B firing

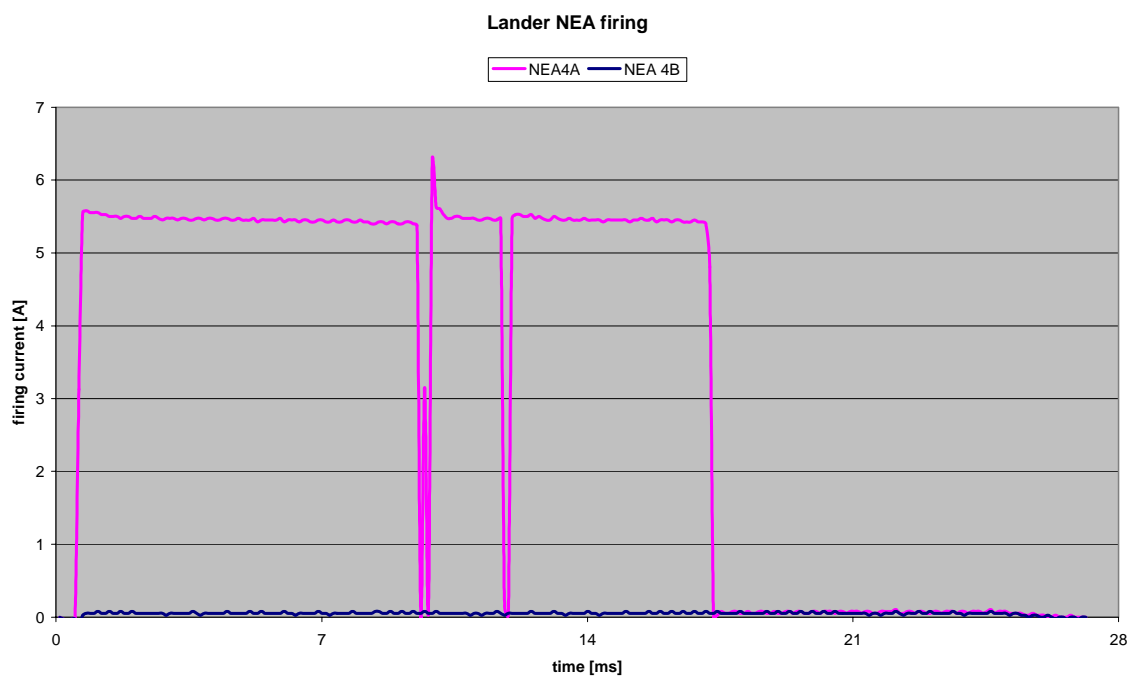


Figure: Lander NEA 4A & 4B firing

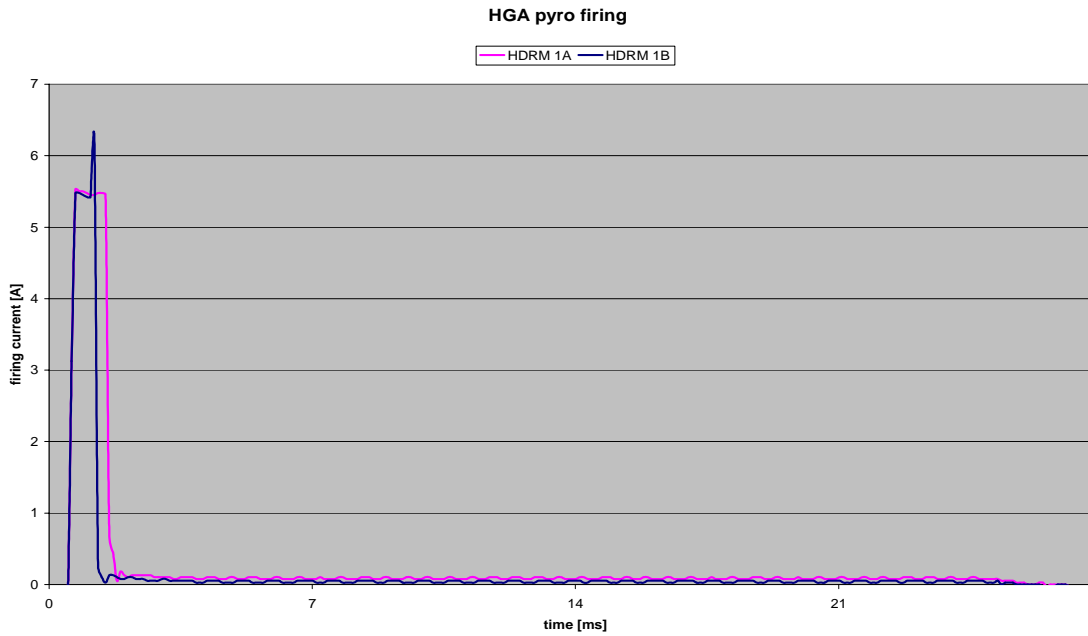


Figure: HGA pyro firing currents HDRM1A & HDRM 1B

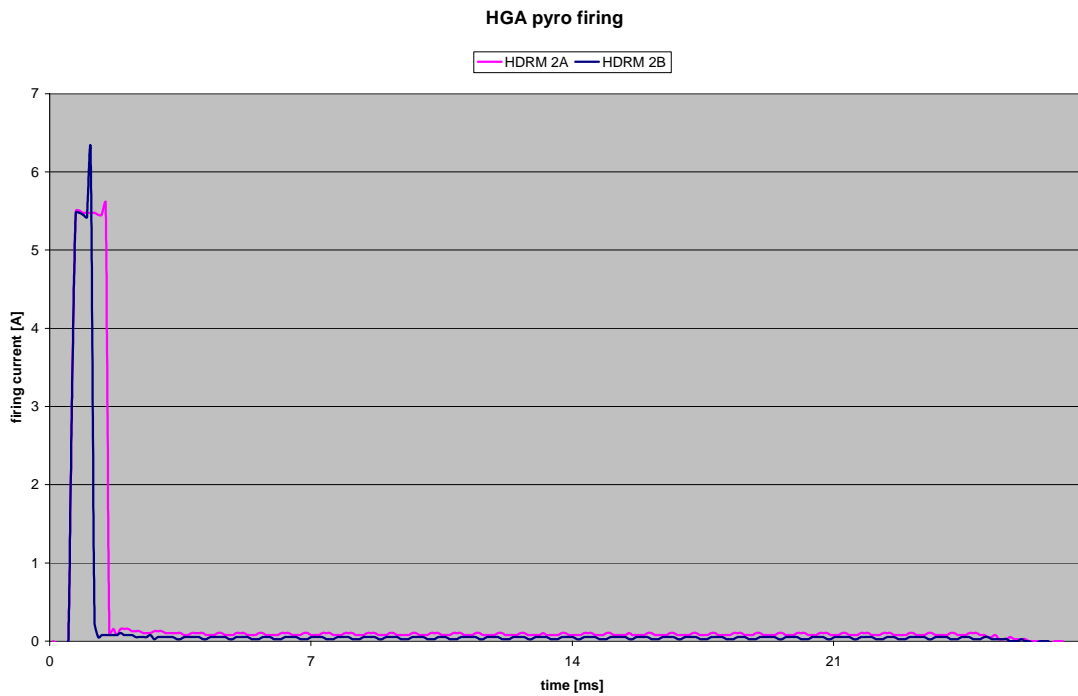


Figure: HGA pyro firing currents HDRM 2A & HDRM 2B

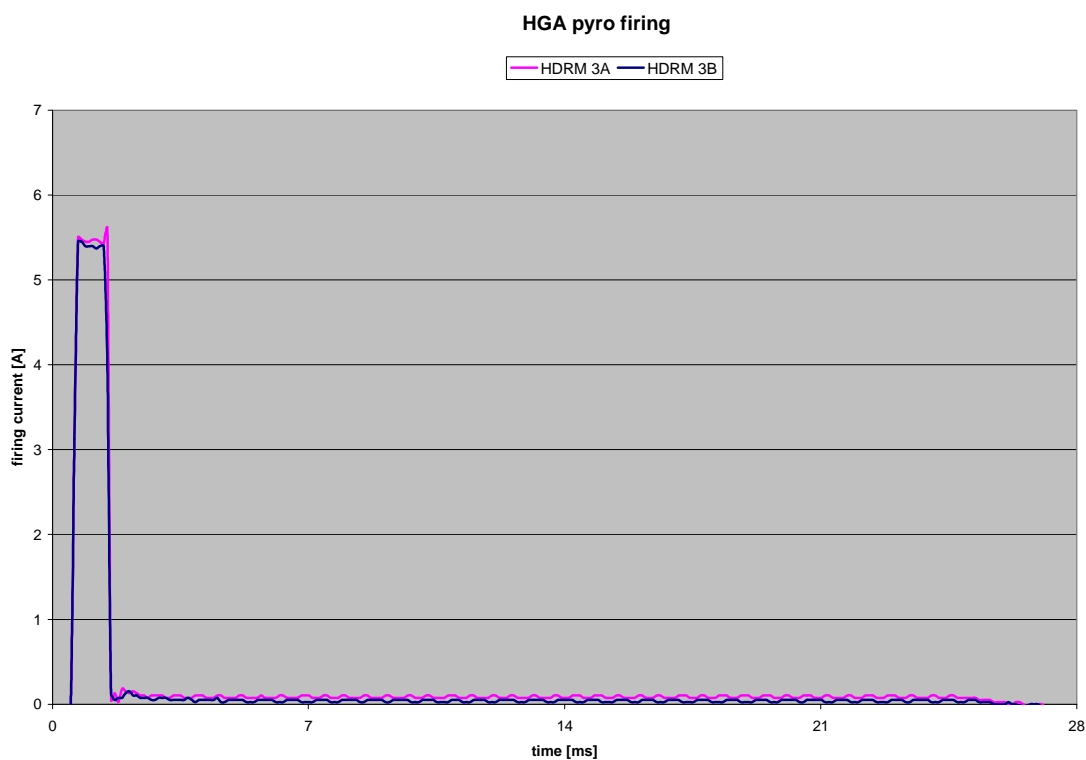


Figure: HGA pyro firing currents HDRM 3A & HDRM 3B

RCS 1st pressurisation, DOY 127, 2004 N₂O₄ tank 1, MMH tank 1

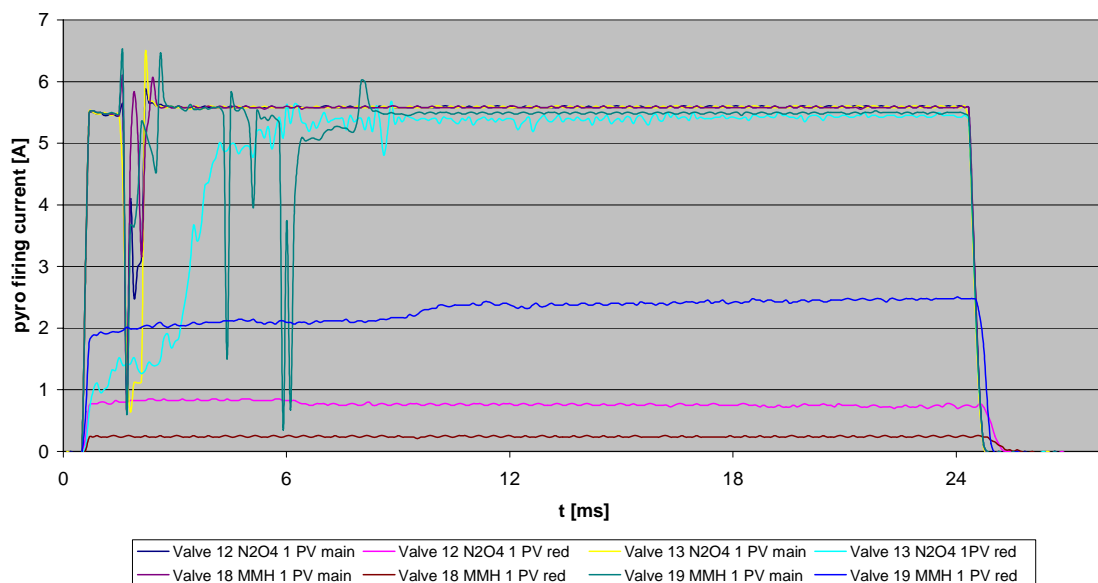


Figure: RCS 1st pressurisation, N₂O₄ and MMH tank

RCS 1st pressurisation, DOY 127, 2004
Helium tank 1

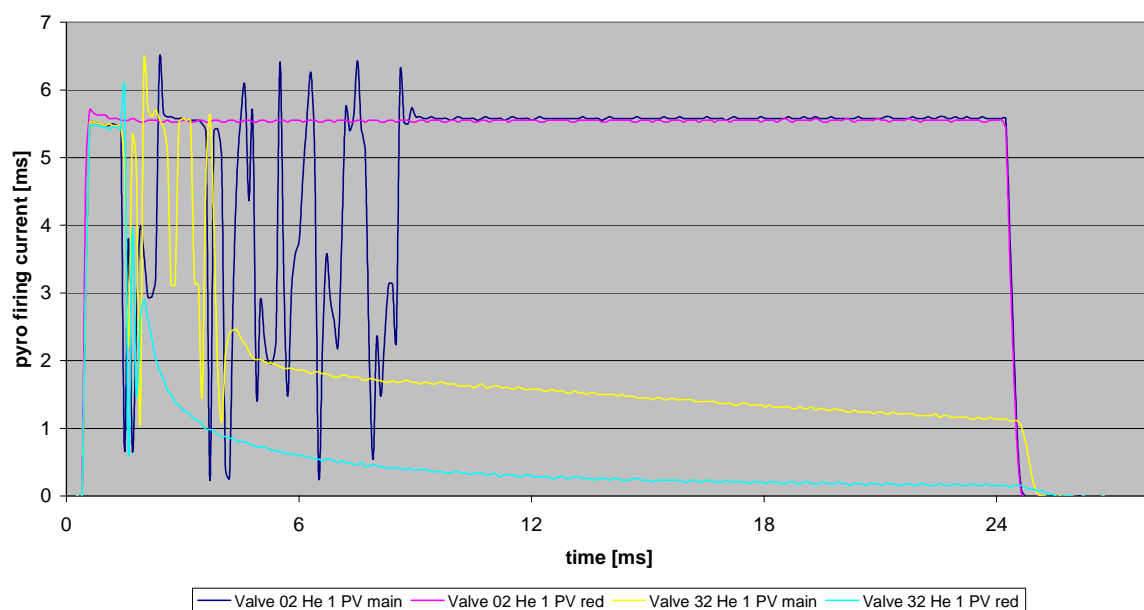


Figure: RCS 1st pressurisation, helium tank

RCS first isolation
Helium tank

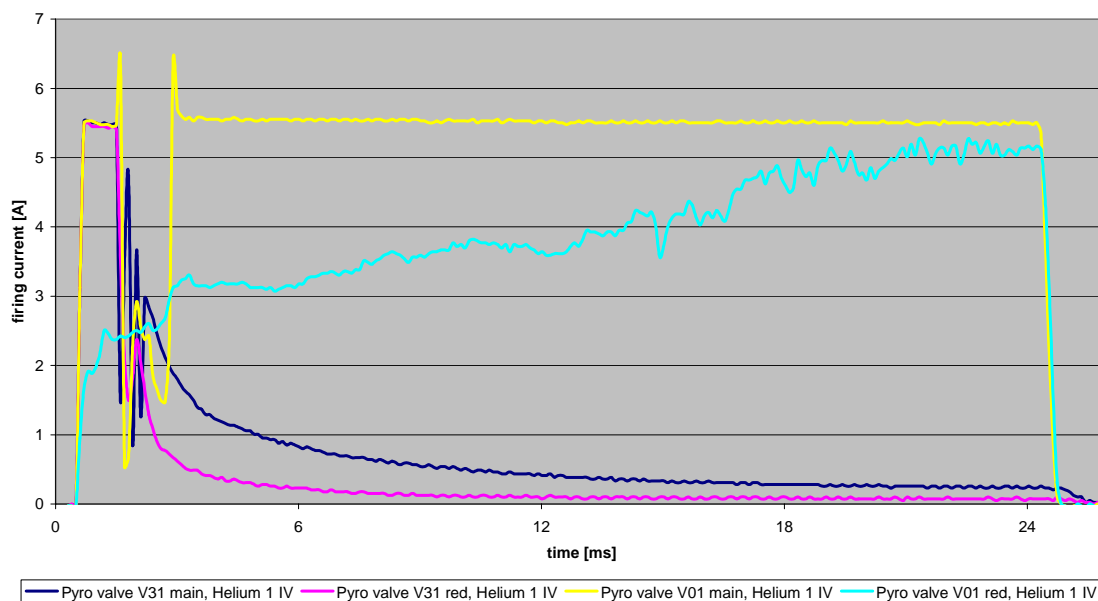


Figure: RCS first isolation Helium tank

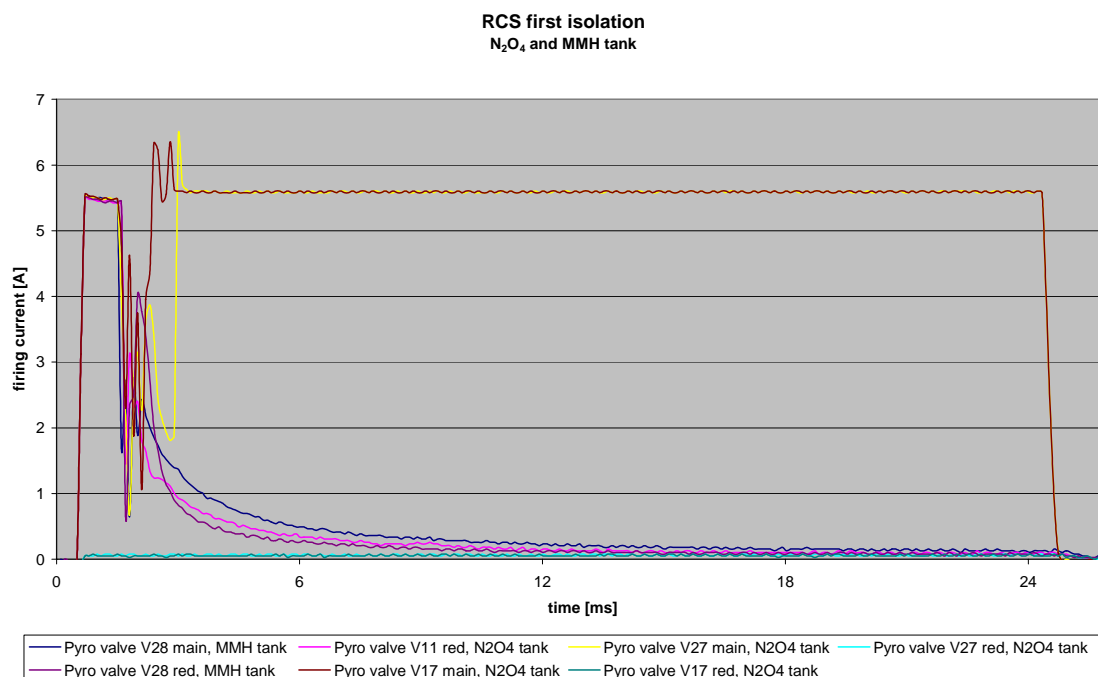


Figure: RCS first isolation N₂O₄ and MMH tank

Note: It is a nominal mode for a pyro to show either high or low resistance after powder ignition, as well as any intermediate state. This is specifically true for a pyro already fired. For the used pyros the redundant input has a separate ignition bridge wire, but shares the explosive chamber. In this case the redundant pyro charge ignites at the time of prime pyro firing. Carbon deposits nevertheless often allow an arc of variable current to develop during redundant pyro firing. This is visible in the previous graphs, where a current of about 5.5A represents the pyro source limitation current within the 24 ms firing window. Even if pyro devices go open circuit during firing the correct firing signal during firing signal application can be verified by the about 80mA flowing through the 330 Ohm anticharge resistor located in the harness close to the pyro interface connector.

The Lander Non-Explosive-Actuators (NEA's) are fuse wires imbedded in wax, but are connected to the standard pyro interface. For these types of actuators, it is imperative to see the current going to the 80mA residual value to be able to confirm successful operation. All four main NEA's have shown nominal operation.

2.5.4 Conclusion

The SS-PDU LEOP operation was without any problems. All analysed individual functions show nominal performance.

2.6 Payload Power-Distribution-Unit (PL-PDU)

2.6.1 PL-PDU unit power dissipation

Two distinct power cases have been analysed, a lower power and a higher power mode.

In the low power case ($P_{out}=0W$) the following data has been analysed:

I main bus	ΣI LCL's	I _{mb} - I LCL's	SS-PDU dissipation
0.447 A	0.0 A	0.447 A	P _{diss} = 12.5W

Although for this in-orbit load case there is no directly comparable specification value, the data is plausible and is considered nominal.

In the high power case the following data has been analysed:

I main bus	ΣI LCL's	I _{mb} - I LCL's	SS-PDU dissipation
3.885 A	3.336 A	0.549 A	P _{diss} = 15.4W

The calculated dissipation compares well with the specified $P_{diss} < 16W$ and the on-ground measured value of 15.45W for this load condition.

2.6.2 Auxiliary power supplies

Secondary voltages and primary input currents of the PCU auxiliary power supply are found to be nominal.

2.6.3 Pyro actuations

All payload related pyro firings went well with the exception of the ALICE detector door prime pyro. After a first firing, no door movement could be confirmed. An investigation launched revealed that a nominal 24ms pyro pulse with limiting pyro current amplitude of 5.4A had been delivered from the PL-PDU pyro board. The pyro current buffer stores current samples every 100.14 μ s starting three counts before pyro current is allowed to flow until 30 counts after nominal pyro current termination. An in-depth design and ground verification investigation also showed that there is no reason to believe the SC was part of the ALICE pyro problem. A second unsuccessful prime pyro firing was performed, which showed again a 24ms, 5.4A pyro pulse, but no detector door opening. A slight SC attitude change further increased the ALICE temperature before the redundant pyro was fired successfully, opening the important detector door.

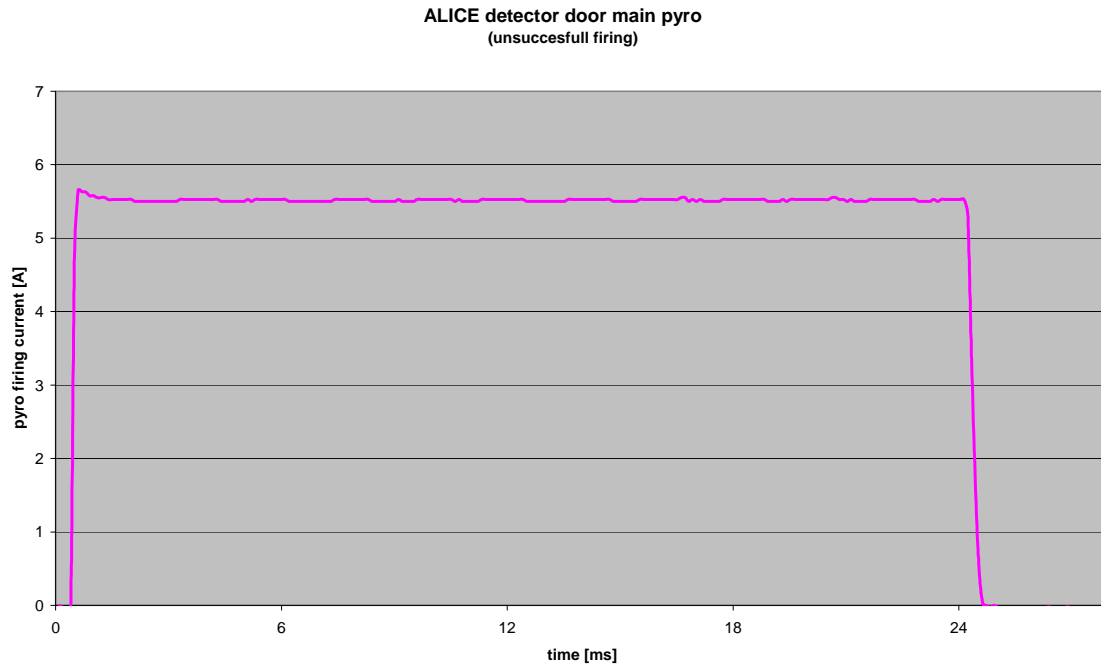


Figure: ALICE detector door unsuccessful main pyro firing

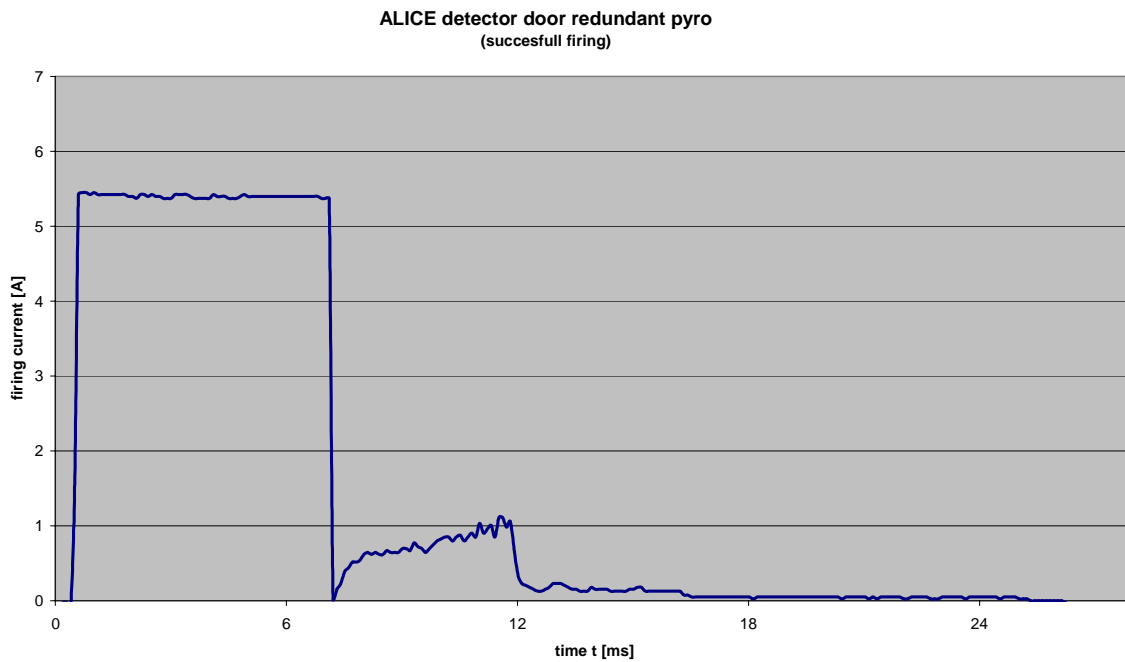


Figure: ALICE detector door successful redundant pyro firing

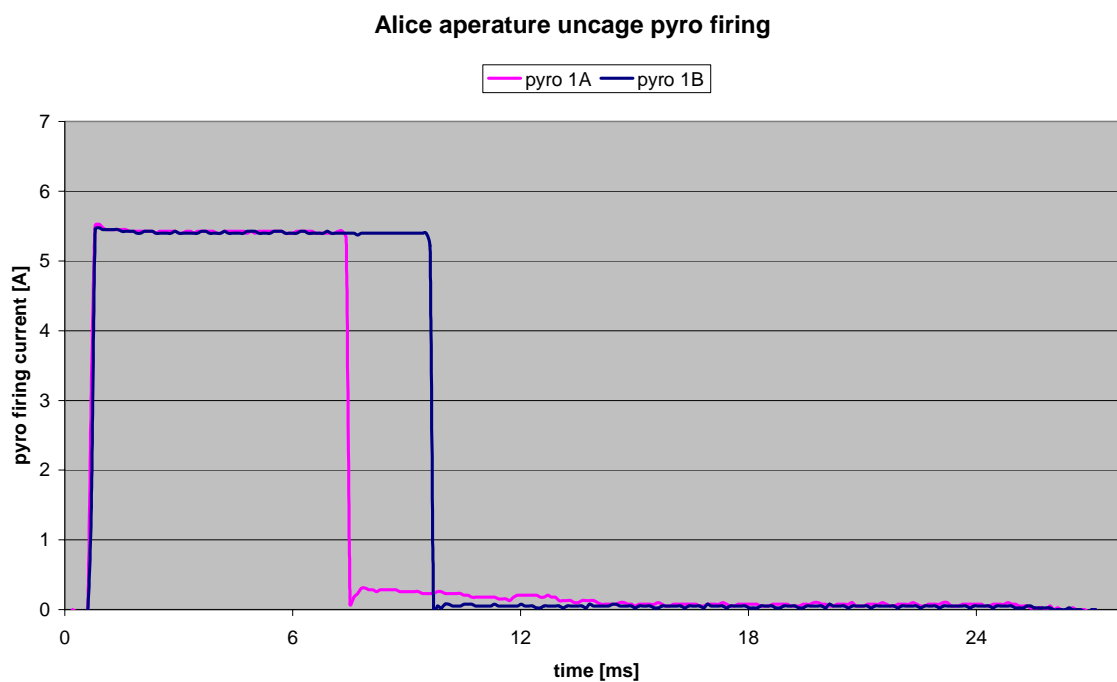


Figure: ALICE aperture uncage pyro firing

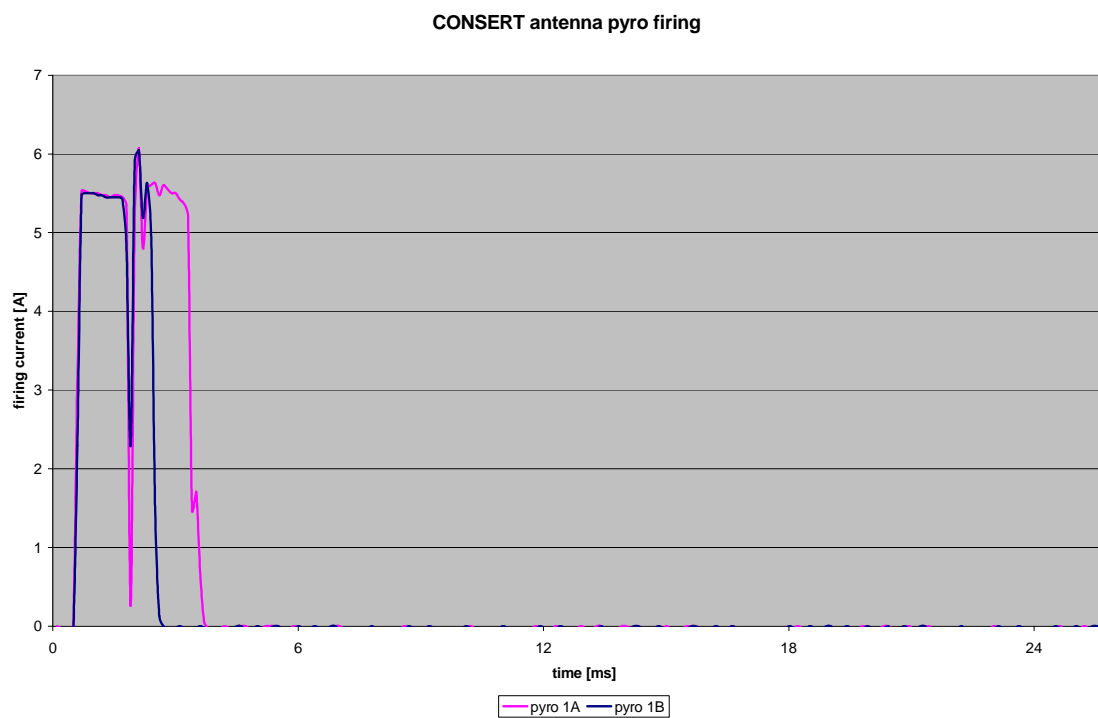


Figure: CONSERT antenna pyro 1A & 1B firing current

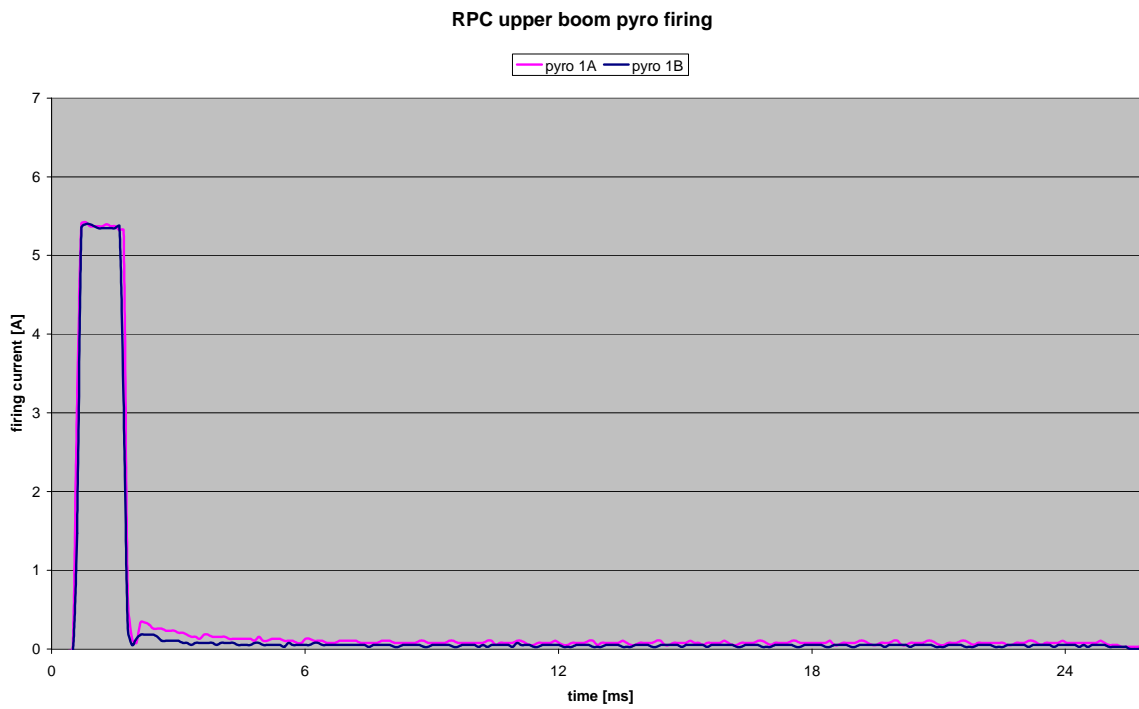


Figure: RCS upper boom pyro 1A & 1B firing currents

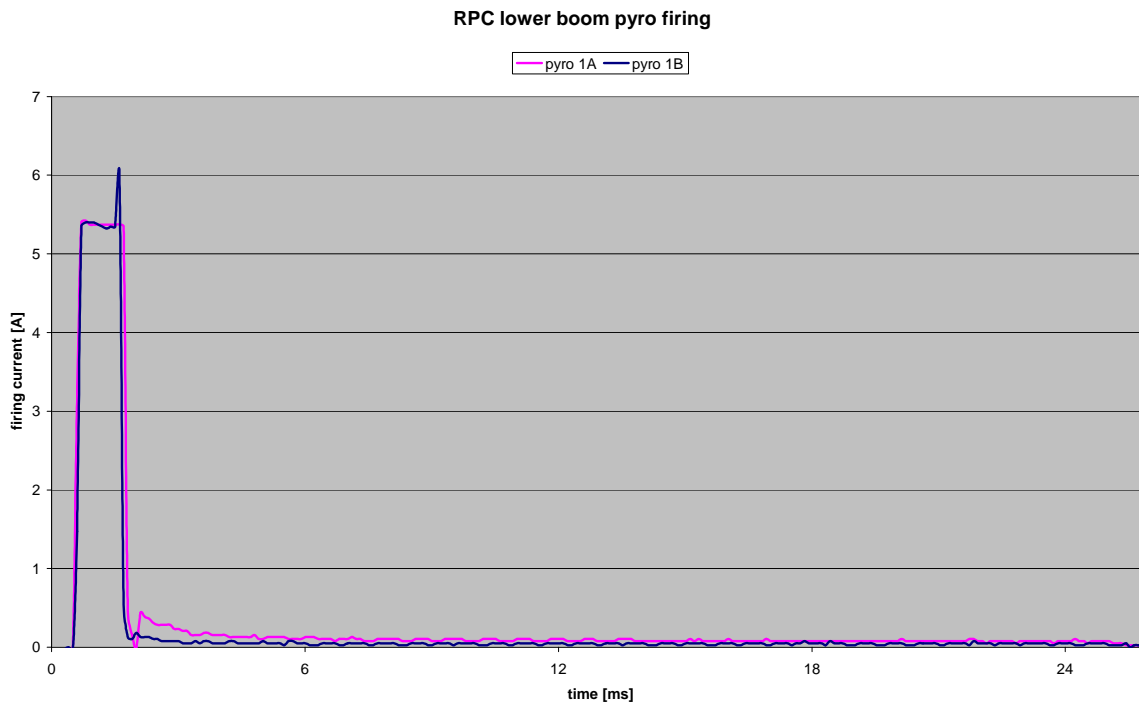


Figure: RCS lower boom pyro 1A & 1B firing currents

2.6.4 Conclusion

The PL-PDU LEOP and early commissioning operation was without any problems with the exception of the known problem as reported in RO-ALS-NC-9125 (faulty reading of redundant KAL converter LCL current through main PDU TM/TC board).

All other analysed individual functions show nominal performance.

3 THERMAL CONTROL

This part of the report describes the thermal behaviour of the spacecraft as revealed by the first in-flight results and the temperature problems that have been detected.

3.1 Launch

The main thermal constraints for the S/C at launch were imposed by the propellant tanks and by the batteries. At launch, the maximum allowable pressure in the tanks was limited to 14.7 bar and the tanks were pressurized close to their maximum allowable limit, i.e. 14.5 bar when in equilibrium at 24°C ambient temperature of the filling hall. To make sure that the tank pressure was below its launch limit of 14.7 bar with a reasonable margin, the temperature of the tanks had to be kept at 22°C or lower. The other limit was imposed by the batteries that had to be kept as close as possible to 20°C at launch. This temperature insured maximum performance during about 2.25 hours discharge occurring between launch and S/C separation. The above temperatures had to be attained considering that the total internal dissipation of the S/C was 120 W and that the S/C is completely insulated with MLI blankets with the exception of relatively small louvered radiators.

The under-fairing environment was improved by the night launch that excluded the fairing heating by the Sun. A mass flow rate of 3,500 m³/h of air at 13°C inlet temperature was specified to achieve the required temperatures. This was confirmed by the recorded data shown in table 1 where the temperatures computed with the S/C convective model are reported as well.

	Measured Temp. [oC]	Predicted Temp. [oC]
Panel -Y		
Battery 1	20.0	20.2
Battery 2	20.7	19.8
Battery 3	20.7	19.6
PCU	28.6	26.7
SS PDU	23.6	23.7
Panel +Y		
SSMM	22.9	22.6
TRSP 1	25.0	28.4
TRSP 2	25.7	26.7
CDMU 1	23.6	26.6
CDMU 2	25.0	26.6
Tanks		
MMH	21.4	22.0
NTO	21.4	22.0
He -Y	20.7	19.8
He +Y	21.4	19.9

Tab. 1 – Temperatures of tanks and dissipating units at launch (recorded before the first launch attempt). In the table above, the tanks were not in a steady-state condition and their temperature continued to cool down to about 20°C when the cryogenic fuel was loaded and the launch finally took place.

Before launch, the heater system was brought in its nominal launch configuration where the LCL's of the nominal H/W heaters were switched 'off'¹ and the LCL's of the redundant H/W heaters were powered-on². The heaters, however, were kept switched off by their 'cold-guard' thermostats that are open at ambient temperature. All the S/W heaters were disabled³. For a detailed heater setting see ref. 1.

The timeline of the main flight events is reported in table 2 (approximate, for information).

¹ Exceptions were Boom hinges for which also the nominal LCL was powered on.

² Exceptions were ROSINA DFMS and RPC IES that had also their redundant LCL powered off.

³ Exceptions were APM and thrusters that had the redundant LCL's powered 'on', but their heaters were kept powered off by 'cold guard' thermostats.

	Ignition of main stage engine
+ 7.0 s	Ignition of solid boosters
+ 7.3 s	Lift -off
+ 2 mn 19 s	Jettisoning of solid boosters
+ 3 mn 09 s	Jettisoning of fairing
+ 9 mn 57 s	Beginning of ballistic phase
+ 1 h 56 mn 57 s	Delayed ignition of 2nd stage
+ 2 h 13 mn 30 s	Separation

Tab. 2 – Main launch events. Note the delayed ignition of the 2nd stage after the ballistic phase that lasted about 1 hour and 47 min. Part of the ballistic phase was in eclipse.

To protect the external P/L, appendages and thrusters from unexpected cooling, the redundant H/W heater circuits were left powered so that the ‘cold guard’ thermostats could have had switched on the heaters in case of need. When the telemetry signals were acquired at separation, the spacecraft status was as expected. None of the heaters were activated and the temperatures of the spacecraft were similar to the ones recorded before launch. This was also thanks to the spinning performed during the ballistic phase that ‘barbequed’ the S/C under the Sun.

3.2 Comparison Between Telemetry and Computed Temperatures

To assess the status of the S/C from a thermal point of view, temperatures of the telemetry will be compared with the results of the thermal mathematical model that was adapted to mimic to the maximum extent the conditions experienced in flight. Data of two steady states with different SAA are reported. Figure 3.1 illustrates the definition used for the SAA.

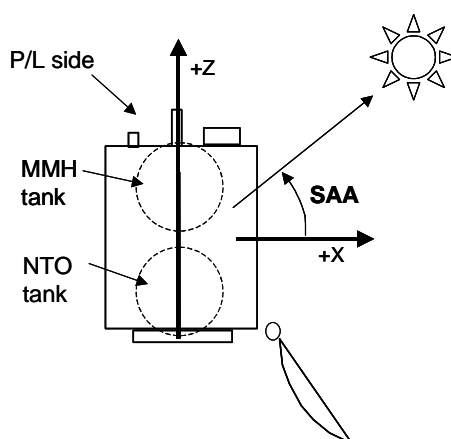


Fig. 3.1 – Definition of the SAA and items mainly affected by it

With the heaters configured nominally according to ref. 1, the reported data refer to data recorded on March 10th, at 23:15 z (SAA = 0°) and on March 11th, at 0:28 z (SAA = 50°). For these cases, the distance from Sun was about 0.975 AU and the correspondent solar flux was 1441 W/m². The computer runs for the two cases were performed by Astrium Ltd. once the telemetry data were made available to them. No special adaptations of the thermal models were introduced with the exception of the solar flux, SAA and power dissipations that were updated to the best knowledge of their actual values.

3.2.1 Lateral Panels

The temperatures of the equipment installed on the lateral ‘+/-Y’ panels are reported in tables 3 and 4.

	SAA = 0 deg			SAA = 50 deg		
	Measured T [oC]	Predicted T [oC]	DT	Measured T [oC]	Predicted T [oC]	DT
Panel -Y						
Battery 1	20.7	18.8	1.9	16.7	16.4	0.3
Battery 2	18.3	16.6	1.7	14.5	15.2	-0.7
Battery 3	18.3	16.5	1.8	14.5	15.6	-1.1
PCU	21.4	18.3	3.1	18.9	17.5	1.4
SS PDU	18.3	15.6	2.7	16.7	14.3	2.4
PL PDU	20.7	16.7	4.0	22.1	20.1	2.0
IMU 1	24.3	26.5	-2.2	18.9	21.6	-2.7
IMU 2	24.3	26.9	-2.6	11.0	10.6	0.4
IMU 3	16.1	16.0	0.1	11.5	11.0	0.5
APME	12.5	12.7	-0.2	8.5	11.5	-3.0
SADE	20.0	15.1	4.9	18.3	13.0	5.3
SSTE 1	10.0	11.2	-1.2	11.0	13.2	-2.2
SSTE 2	5.0	5.2	-0.2	7.5	8.6	-1.1
VIRTIS EL	5.4	5.2	0.2	9.6	11.1	-1.5
CONS EL	5.0	3.9	1.1	11.5	11.7	-0.2
Avrg T	16.0	15.0	1.0	14.1	14.1	0.0

Tab. 3 – Results for the ‘-Y’ panel units (predictions with no uncertainties)

Overall, as discussed below, the average of the temperatures and the interior bulk temperature of the spacecraft is found to be in line with thermal model results for the analysed conditions. The largest individual discrepancies can be related to various causes as: quality of the steady-state, knowledge of the actual dissipated power, accuracy of the equipment thermal models and the actual sensor position with respect to the thermal nodes where the power is applied.

	SAA = 0 deg			SAA = 50 deg		
	Measured T [oC]	Predicted T [oC]	DT	Measured T [oC]	Predicted T [oC]	DT
Panel +Y						
SSMM	29.3	29.1	0.2	30.0	33.8	-3.8
TRSP 1	18.9	22.4	-3.5	17.8	22.0	-4.2
TRSP 2	24.3	24.4	-0.1	24.3	24.2	0.1
EPC 1	18.3	21.2	-2.9	16.1	21.0	-4.9
EPC 2	33.0	27.8	5.2	32.0	28.4	3.6
TWT 1	23.6	26.6	-3.0	19.4	26.0	-6.6
TWT 2	48.3	43.5	4.8	46.7	42.1	4.6
WDE	22.1	27.0	-4.9	19.4	26.3	-6.9
CDMU 1	17.2	17.9	-0.7	16.1	18.5	-2.4
CDMU 2	20.0	20.7	-0.7	20.0	21.5	-1.5
SS RTU	15.6	19.9	-4.3	14.5	20.8	-6.3
PL RTU	16.1	15.4	0.7	18.9	23.5	-4.6
AIU	18.3	18.4	-0.1	16.7	18.7	-2.0
RSI USO	28.6	26.7	1.9	27.9	31.4	-3.5
RDFU	23.6	22.7	0.9	24.3	28.0	-3.7
RPC PIU	19.4	16.2	3.2	20.7	23.1	-2.4
MIR ME	8.3	6.6	1.7	10.0	14.6	-4.6
MIR USO	7.1	5.3	1.8	10.5	14.3	-3.8
Avg T	21.8	21.8	0.0	21.4	24.3	-2.9

Tab. 4 - Results for the '+Y' panel units (predictions with no uncertainties)

The WDE in tab. 4 (Wheel Drive Electronics) and the RWA's (Reaction Wheels) are powered via the same LCL. In this case, as in some other cases, the total power delivered by this LCL is known by the telemetry but the split between the various items is affected by some uncertainty. An example that illustrates the effect of the model accuracy is given by the TWT (Traveling Wave Tube), tab. 4, where its very high power density causes temperature gradients between the various parts of the unit. The average temperature of the various nodes of the model of this unit is therefore considered in the table for comparison with the telemetry read-out. In this case, the accuracy of the comparison between read-out and model results is then affected by the actual location of the sensor. When the model uncertainties for hot cases are added to the predicted temperatures, only few units (e.g. the SADE, Solar Array Drive Electronics) display temperatures hotter than predicted by few degrees (about 1.1 °C).

3.2.2 Other Internal Units

The units reported in table 5 are located inside the spacecraft but not directly connected to the radiator panels. The largest deviation here occurs with the MMH tank that is located on the upper illuminated part of the S/C at 50°C SAA. It must be noted that the model over-predicts the temperature of this item and is then to be considered conservative for hot cases predictions.

	SAA = 0 deg			SAA = 50 deg		
	Measured T [oC]	Predicted T [oC]	DT	Measured T [oC]	Predicted T [oC]	DT
Tanks						
MMH	21.1	22.1	-1.0	21.7	28.6	-6.9
NTO	19.0	22.0	-3.0	19.3	19.9	-0.6
He -Y	20.7	18.4	2.3	17.8	20.1	-2.3
He +Y	25.7	22.9	2.8	23.6	25.9	-2.3
R. wheels						
RW 1	25.7	22.1	3.6	25.5	25.8	-0.3
RW 2	23.6	20.6	3.0	22.9	23.8	-0.9
RW 3	27.1	23.5	3.6	25.3	24.3	1.0
RW 4	25.0	21.2	3.8	22.5	21.6	0.9

Tab 5 – Propellant tanks, pressurant tanks and reaction wheels (predictions with no uncertainties)

An indication of the ability of the model to predict the average temperature level of the environment inside the S/C is revealed by the helium pressurant tanks temperatures. These are in fact black non-heated items that find their equilibrium at the equivalent environment temperature.

Other important items such as the NAVCAM's and STR's cycled their temperatures between the limits imposed by the software control. This is the behaviour that is also predicted by the thermal model.

3.2.3 Top '+Z' Payload Panel

The '+Z' panel supports most of the Rosetta payload/sensor heads units (see fig. 3.1). Their thermal control is mainly achieved by conductive coupling with the panel, complete MLI wrapping and addition of heaters for the cold hibernation cases or for when the units are not powered. The coupling with the panel spreads by conduction the dissipated heat and the external absorbed Sun loads. The presence of sensor apertures, the 'irregular' geometry of the sensor heads and the small dimension of the MLI pieces make an accurate temperature prediction more difficult here. Results for some of these P/L units are reported in table 6. Temperature discrepancies for several P/L can also be induced by their configuration in the early flight phase (P/L were still stowed and with closed covers at the time of the analysed cases). The configuration implemented in the thermal model, that is typically set-up for analyses of later cold mission phases, is instead with all P/L deployed and with open covers.

	SAA = 0 deg			SAA = 50 deg		
	Measured T [°C]	Predicted T [°C]	DT	Measured T [°C]	Predicted T [°C]	DT
Panel +Z						
MIDAS	20.0	16.4	3.6	23.6	27.3	-3.7
COSIMA	11.0	13.3	-2.3	9.6	18.8	-9.2
GIADA	7.0	0.0	7.0	20.0	19.5	0.5
COPS	11.0	7.8	3.2	27.9	28.0	-0.1
VIRTIS	-5.3	-1.7	-3.6	1.5	9.0	-7.5
ALICE	-3.9	-1.8	-2.1	10.5	16.9	-6.4
MIRO	9.2	2.0	7.2	12.0	4.6	7.4
SREM	14.5	17.1	-2.6	21.4	29.4	-8.0
RPC ICA	9.2	14.9	-5.7	20.0	30.4	-10.4
RPC IES	25.7	16.6	9.1	31.0	24.6	6.4
Avrg T	9.8	8.5	1.4	17.8	20.9	-3.1

Tab. 6 – Results of the '+Z' P/L units (predictions with no uncertainties)

Overall, the average level of the '+Z' units is satisfactory although the scatter of individual units is larger than that occurring for the lateral panels. The scattering is similar to that obtained from the results of the TB phases performed during the system TV test. For the SAA = 50° case, most of the units are predicted hotter than what they actually are (exceptions: MIRO and RPC IES). This is attributed to a certain degree of conservativeness of the model that assumes MLI performances worse than actual under Sun illumination.

OSIRIS cameras that are not reported above, cycled their heaters under software control as predicted by the model.

3.2.4 Thrusters

For the analyzed Sun distances, all thruster valves were within their upper limit of 60°C in their pre-firing condition. However, the Sun-exposed thrusters on the '+X' side of the spacecraft (Thrusters 2, 4, 5, 7) are 10°C to 15°C hotter than expected (see tab. 7). The other not illuminated thrusters have temperatures that are in line with the model predictions either in steady-state conditions or when their heaters cycle under the control of the software. From tab 7, it is clear that there is a strong effect of the SAA on the thruster temperatures. The indication that the Sun-illuminated thrusters could run at high temperature at close distance from the Sun was already given by the TV test of the S/C but the obtained results were compatible with the temperature limit of the thrusters. The new mission introduced phases with spacecraft activity at solar distances smaller than the old ones and the possibilities for trimming down the temperature was very limited due to the hard constraint on the heater power imposed by the power budget of the cold hibernation phase. In fact, modifications that could cold-bias the thrusters implied also an increase of heater power demand in the cold cases. After the TB/TV test modifications were introduced aimed at reflecting the solar input without increasing the I.R. heat rejection. Eventually, the modification did not have the effect that was anticipated by the analysis and the recorded temperatures are closer to the ones predicted without any modification. The thrusters temperatures evolved with changing

Sun distance and eventually 65°C were reached at perihelion distance as discussed in the next chapter.

	SAA = 0 deg			SAA = 50 deg		
	Measured	Predicted	DT	Measured	Predicted	DT
	T [oC]	T [oC]		T [oC]	T [oC]	
Thrusters						
2 Valve A	46.7	39.9	6.8	42.5	36.6	5.9
2 Valve B	46.7	39.9	6.8	41.3	37.2	4.1
4 Valve A	51.7	43.7	8.0	26.4	34.4	-8.0
4 Valve B	51.7	43.6	8.1	27.9	35.2	-7.3
5 Valve A	50.0	36.9	13.1	28.0	34.8	-6.8
5 Valve B	51.7	37.0	14.7	30.0	34.9	-4.9
7 Valve A	51.7	39.8	11.9	45.0	44.7	0.3
7 Valve B	51.7	40.2	11.5	45.0	44.6	0.4
Avrg T	50.2	40.1	10.1	35.8	37.8	-2.0

Tab. 7 – Results for the '+X' Sun-illuminated thrusters (predictions with no uncertainties)

3.2.5 HG Antenna Pointing Mechanism APM

During the first days of the mission cruising at Sun distances below 1.0 AU, the APM reached its temperature limit of 70°C in operational condition and had to be switched off.

The thermal testing on the APM unit showed that the FM APM has been TV cycled up to 76°C (at housing, where the flight thermistors are located) without any performance degradation, while during the life time thermal testing of the QM the housing temperatures were driven up to 90°C. As the temperature difference between housing and encoder has been verified only via analysis and the encoder itself has been tested to 80°C (at encoder level), the above 70°C temperature limit for the thermistors reading was confirmed as a maximum limit (10°C temperature difference between encoder and housing have been estimated by analysis).

The complete temperature increase with the APM motors 'on' could not be observed because the limitation of 70°C has been reached after 8 hours.

As a consequence of this problem, the thermal mathematical model of the APM has been completely revised and correlated with the observed in-flight results, see tab. 8 and ref. 2 for more details. In particular, ref. 2 reports other correlation cases that are derived from the TVTB system test and that were considered to include also cold cases in the correlation exercise.

			Flight Measured	Correlated Version	Delta	Within 5°C	Within 10°C
Flight	SAA = 50	EDU Housing	46,7	50,4	3,7	yes	yes
	Xband ON	ADU Housing	46,7	50,7	4,0	yes	yes
	APM OFF	Wave Guide	75,0	79,4	4,4	yes	yes
	SAA = 0	EDU Housing	53,3	52,8	-0,5	yes	yes
	Xband ON	ADU Housing	57,5	55,4	-2,1	yes	yes
	APM OFF	Wave Guide	80,0	81,3	1,3	yes	yes
	SAA = 50	EDU Housing	46,7	49,2	2,5	yes	yes
	Xband OFF	ADU Housing	46,7	47,9	1,2	yes	yes
	APM OFF	Wave Guide	72,5	71,3	-1,2	yes	yes

Tab. 8 – APM correlation with in-flight results

The new model indicates that the striping modification (see Fig. 3.2) that was introduced for the new mission resulted in a temperature reduction of 15°C compared with the original configuration. This reduction could be achieved due to the low insulation characteristic of the MLI (6-layers only). However, this was not enough to eliminate any constraint at close distance to the Sun.



Fig. 3.2 – Modified APM – The APM MLI was modified by application of 30% flexible solar reflective stripes on the Sun facing sides. The modification reduced the temperature of the APM because the MLI does not have high insulation properties.

It was also found that the main reasons causing the overheating of the APM and that were not captured by the old model, were:

- +X S/C side heats up under direct Sun light and re-irradiates heat to the APM;
- The antenna dish that interfaces with the APM reaches high temperatures under the Sun and heats up the APM by conduction and radiation;
- The light-weight MLI (6 layers only with many seams) that was used to insulate the APM has poorer performance under Sun-light than anticipated.

These factors were taken into account during the post launch correlation (table 8).

3.3 TCS Performance Evaluation

3.3.1 Main Spacecraft Body

From the comparison between the telemetry data and computed temperatures, it was shown in the previous paragraphs 3.2.1, 3.2.2 and 3.2.3 that the model predicts temperatures for the units mounted inside or on the top floor of the spacecraft with acceptable deviations. This gives confidence that the thermal design will provide acceptable temperatures also in other mission phases. Larger deviations were observed for Sun exposed items and are discussed below. All items are well within their acceptance temperature limits. The thrusters and the APM are kept below 70°C by SAA and operation constraints. Temperatures of solar arrays are reported in chapter 2.3.

3.3.2 Stand-by Thrusters

Thrusters that are under direct Sun-light show temperatures higher than expected and this is a strong function of the Sun distance and of the SAA. This means that also other thrusters that are presently not illuminated can show temperature problems if brought under Sun light. The practicable SAA range is then limited to small negative angles at close Sun distances to avoid that the '-Z' thrusters reach too high temperatures.

On May 24th, the spacecraft reached its closest distance to Sun of 0.886 AU (corresponding to a solar flux of 1,745 W/m²). At this point, the thruster valves achieved the maximum temperatures (with a SAA of about 0° to 18°) reported in tab. 9.

Thruster	Temperature [°C]	Remarks
2	60.0	+X thrusters, steady-state
4	53.3	“
5	53.3	“
7	65.0	“
1	2.5 to 26	-X thrusters, heater cycling
3	4.2 to 5.8	-X thrusters, steady-state, heater off
6	2.5 to 26	-X thrusters, heater cycling
8	2.5 to 26	-X thrusters, heater cycling
9	20.7 to 21.4	-Z thrusters, steady-state, heater off
10	30 to 31	-Z thrusters, steady-state, heater off
11	30 to 31	-Z thrusters, steady-state, heater off
12	18 to 22	-Z thrusters, steady-state, heater off

Tab. 9 – Maximum thruster temperatures at perihelion (0.886 AU)

The thrusters that are at a critical level are the numbers 2 and 7 where the thermal design did not manage to keep the valves below 60°C. To assess the level of criticality, it can be noted that the thruster qualification programme included:

- Thermal cycling test covering a temperature range from -5° to 85° C with non-operating excursions up to 120° C;
- Hot start firing (steady-state and pulse mode) with thruster and propellant both at 60° C;
- Hot re-start firing (worse case pulse modes) with propellant at 60° C and thruster temperature from 58° C to 112° C.

Therefore it can be concluded that the attained levels for the thrusters 2 and 7 can still be tolerated.

Thrusters 7 reached the temperature limit of 60° C around the April 13th when the Sun distance was 0.97 AU ($1,456 \text{ W/m}^2$). The same distance will be reached again on August 1st. For larger distances, the temperature will go down as demonstrated by the results already given in tab 7 that correspond to a distance of 0.975 AU.

3.3.3 Firing Thrusters

When thrusters fire continuously (or almost continuously), the temperature increase of their valves is limited to less than 20°C as illustrated in the graph of fig. 3.3 that reports the temperature for a continuous firing of several minutes.

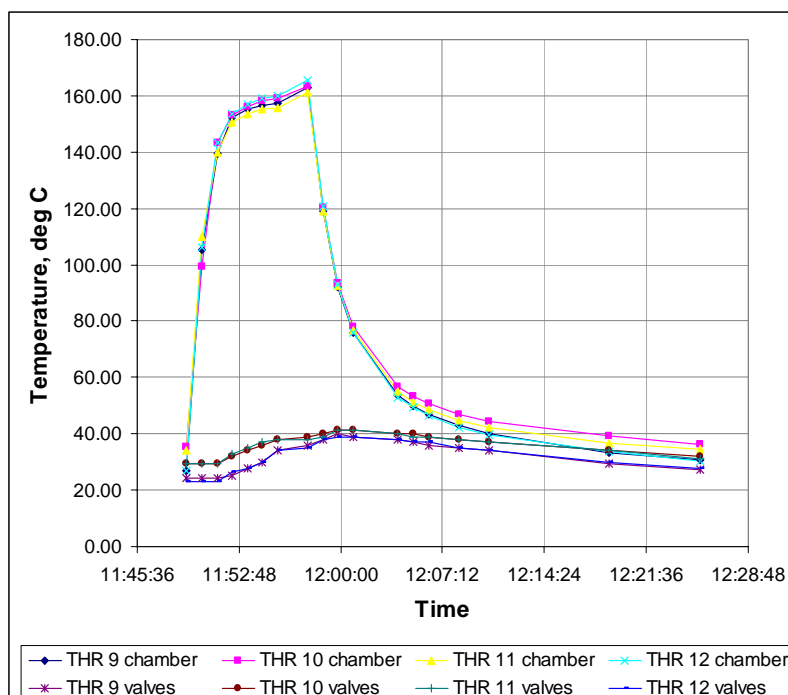


Fig. 3.3 – Recorded temperatures during thrusters firing in off-modulated mode, -Z thrusters

This behaviour for a long firing was also confirmed by the long delta-V (about 3.5 hours) manoeuvre performed between May 10th and 11th and reported in fig. 3.4a and 3.4b.

Figure 3.4a reports the temperature response of the FCV's of thruster 12 that was one of the four used to provide the impulse for the delta-V. Here, it is possible to note the following:

- Three plots of three sensors are reported: two monitoring the FCV of the nominal thruster that actually fired and one monitoring the FCV of the redundant thruster that was not used.
- All sensors started at the same temperature and started to rise when the nominal thruster began firing.
- After the initial 'ramp-up' (first gradual pulse modulated firing) where the temperature increased, the temperature of the firing thruster levelled out because

of the cooling of the continuous flow of the fuel, while the redundant one continued to rise due to the heat conducted from the firing thruster.

- When the fuel flow stopped, the nominal thrusters valves raised their temperature due to the heat conducted from the hot parts of the thruster and its temperature plot joined the one of the other thruster during the cool-down.
- The largest soak-back effect was 20°C and was experienced by the non-firing thruster.

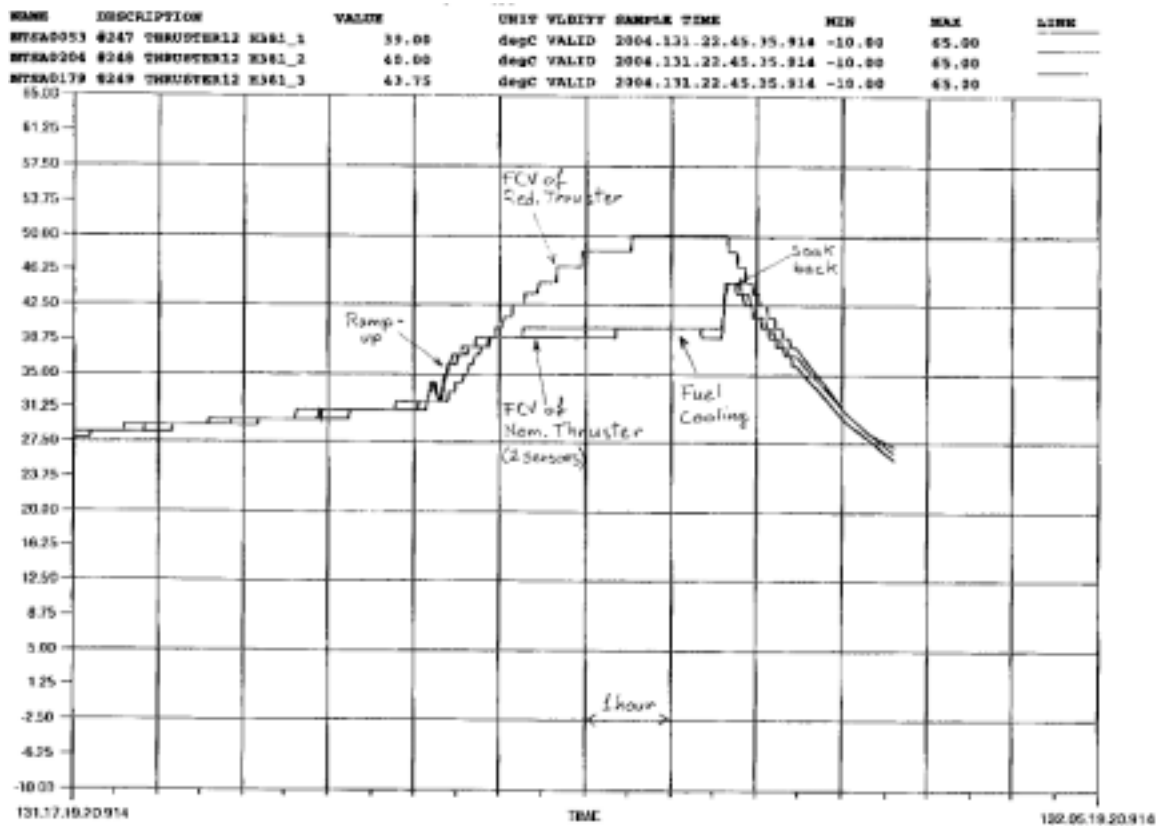


Fig. 3.4a – Temperature response of thruster 12 during continuous long firing (about 3.5 hours). Temperatures of FCV's of nominal and redundant thrusters are reported.

Figure 3.4b reports the temperature response of the FCV's of thrusters 5 that was one of the four used to control the attitude around the Z-axis of the S/C during the delta-V manoeuvre (pulse modulated firing). Here, it is possible to note the following:

- As before, three plots of three sensors are reported: two monitoring the FCV of the nominal thruster that actually fired and one monitoring the FCV of the redundant thruster that was not used.
- All sensors started at the same temperature that in this case was higher (53.75°C and 57.50°C) because these thrusters were heated by the Sun.
- When the nominal thruster started to fire, the temperature went down due to the cooling of the fuel that overcame the heating of the Sun while the non-used thruster remained on a constant level.
- Subsequently, the temperature of the FCV's of the nominal thruster varied as a result of the variable flow rate of the fuel.
- When the fuel flow stopped, the nominal thrusters valves raised their temperature due to the heat conducted from the hot parts of the thrusters.

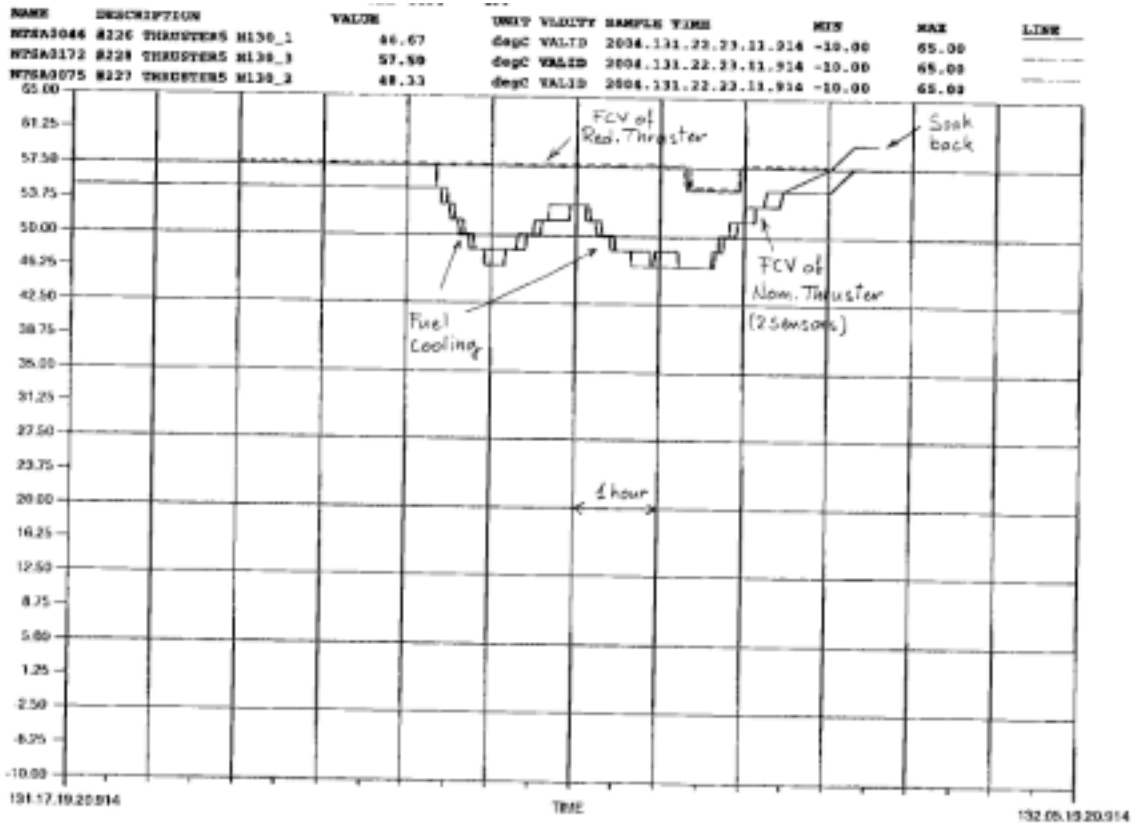


Fig. 3.4b – Temperature response of thrusters 5 in pulse modulated mode used for attitude correction during a delta-V manoeuvre. Temperatures of the FCV's of nominal and redundant thrusters are reported.

3.3.4 HG APM Operations

Because of the temperature problem reported in paragraph 2.2.5, the APM cannot be kept switched on for long periods when close to the Sun. During Earth pointing cruise phases the APM can be kept off without operational constraints. But when the S/C is Sun-pointing an operational scenario with intermediate APM operation for re-pointing had to be established. Practically, the motor is switched ‘on’ only for short periods to allow re-pointing the antenna to the Earth and subsequently is switched off and allowed to cool down. The analyses performed with the newly correlated model indicate that safe operations of the APM in all attitudes will be possible from 1.1AU onwards. The detailed results are contained in ref. 2 and a summary charts are presented in fig. 3.5.

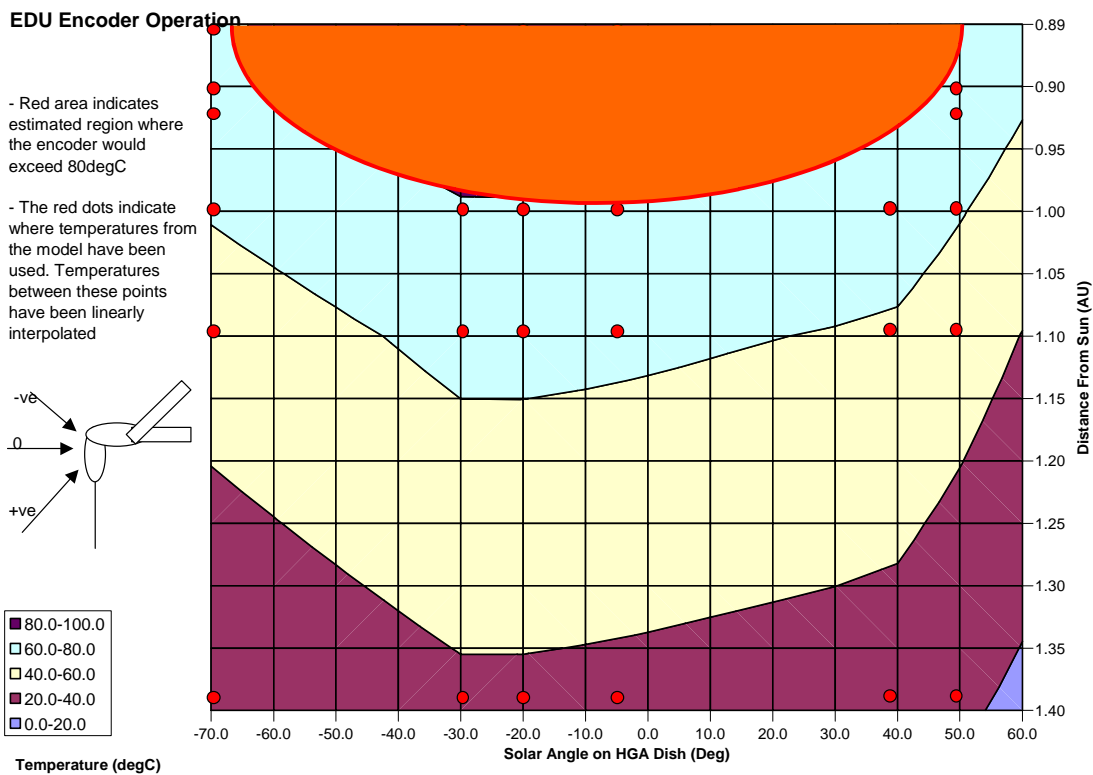


Fig. 3.5 – Conditions for safe usage of APM. Within the blue area, the encoder temperature ranges from 60° to 80°C when kept continuously ‘on’. Housing temperature is 10°C colder.

3.3.5 Heater Software Control

On March 3rd, the thermal control software for heater control was enabled. The software performs the switching of the heaters that are installed on:

- RWA's, STRs, Nav-Cam's, batteries, SADM (S/S PDU lines);
- APM and thrusters valves (P/L PDU lines).

The software keeps cycling the items between pre-assigned temperature thresholds. In addition, the software tries to identify a possible failure on a heater line and switches to the redundant lines if necessary. The software performs its functions as expected, however a number of modifications of the temperature thresholds were deemed necessary in order to let the software to operate smoothly.

Problems were encountered when an item temperature is driven outside the temperature thresholds by the effect of the environment. A typical example is given by the hot thrusters and explained below:

- The Sun-illuminated thrusters are driven by the Sun input to a temperature that is higher than their switch-off threshold.
- The software keeps trying to switch-off the relevant heaters (that are already-off after the first attempt) until the number of allowable attempts is expired (cooling filter, see ref. 1 for details).
- The software interprets this as a heater line failure and switches the control on the redundant heater line issuing an anomaly report.
- The same problem described above occurs with the redundant line and the software issues a second anomaly report.

The above chain of events necessitated a case-by-case evaluation of the problem and a new thresholds definition and uploading. This behaviour was already detected during the TBTV system test and it was considered normal.

3.4 TCS References

- 1 FCP-SY0370, Thermal Control Management, Issue 3, dated 22-07-03
- 2 RO-DSS-TN-1210, APM In-Flight Thermal Verification and Operation Rules, Issue 2, dated 17-05-04

4 OBDH HARDWARE

4.1 Design Principle

The standard OBDH Bus architecture is the base adopted for the Data Management System (DMS) that has been enhanced with the addition of High Speed IEEE 1355 serial data links to speed the internal data traffic and also interface the Mass Memory Unit (SSMM), the Star Tracker (STR) and the Navigation Camera (CAM).

The core of the DMS is the CDMU that contains the Processor Modules and manages the acquisition of TM data, the acceptance and distribution of commands, the broadcast of time synchronisation as well as a high redundant reconfiguration capability (4 Reconfiguration modules) and associated Safeguard Memorys (SGM).

There are two physically independent CDMU in the DMS, each containing 2 processors that can individually be allocated to Data Handling or AOCS tasks.

Subsystem and payload experiments are interfaced via dedicated RTUs, one for payload and one for S/S, for data gathering and distribution of timing and commands.

The DMS features a massive memory unit (SSMM) capable of storing up to 25 Gigabits of random memory with direct high speed links to the 4 processors, the TM format generators, to the VIRTIS and OSIRIS payloads and to the Navigation Camera. The software resident in the SSMM provides the ability to compress data either lossy or lossless.

4.1.1 Architecture and Interfaces

(TO BE ADDED IN next issue)

4.2 Commissioning

Early from the initial contact with the Rosetta S/C the DMS Hardware behaved completely NOMINAL as expected.

CDMU:

The CDMU was initially configured with:

PM 1 in charge of the AOCMS

PM 2 in charge of the DMS Handling
Reconfiguration and Master Clock in RM #4
OBDH Bus B
Input / Output A selected
Format Generator TFG B
Command Module HPCM-B

In case of reconfiguration the following modules are allocated:

PM 2 reserve for DMS
PM 3 reserve for AOCMS
Reconfiguration and Master Clock in RM #2
OBDH Bus A
I/O B
TFG A

The observed clock stability and related time correlation are well within expectations.
The content of the Safeguard Memories (SGM) were dumped and found correct.

- Mainly two TM bit rates were used 2Kbps and 22Kbps. Various TC uplink bit rates were tried, specially the lowest (required for emergency and safety) of 7.8 bps as well as the highest of 2000 bps.
- EDAC counters showed the expected jumps due to a known SW bug this will be corrected in the next issue of the SW see section 5.
- There were two commands rejected on-board, just at the beginning of the first pass, that were reported as "dirty" by the on-board processing. The event coincided with an abnormal reading of the FCL current of the active Receiver #2. No further rejects were seen afterwards.

The commissioning of the CDMU was successfully completed during LEOP 3.

SSMM:

The separation sequence was in charge of commanding the SSMM from standby into operational mode and this took place as foreseen. Two days later the unit was fully configured around Memory Controller A in ON Status and B OFF, the three Memory Modules ON and being used (except 3 banks in MM3)
The SSMM is being extensively used since commissioning and is providing satisfactory services to all the units using it.

RTU:

Both RTU S/S and RTU P/L are configured to nominal (Core A ON / B OFF) from the beginning and no problems have been reported. Core B are not yet used.
Operational parameters are nominal.

4.2 Conclusion

The hardware items of the DMS are, from the very beginning of the mission, providing continuous and reliable TM and TC services to the mission. The behaviour is solid and highly predictable. It must be said though that the High Speed Links together with the SSMM have not yet seen a case of maximum demand this will be seen in CVP part 2.

5 SYSTEM SOFTWARE AND OPERATIONS

5.1 System Software

The system software is contained within the avionics subsystem of Rosetta, in five major units:

- Data Management System (DMS)
- Attitude Orbit Control System (AOCS)
- Solid State Mass Memory (SSMM)
- Autonomous Star Tracker (STR)
- Navigation Camera (CAM)

All software supports the ESA packet standards (TM&TC) and implements those parts of the Packet Utilisation Standard needed for the Rosetta mission

5.2 Data Management System

This software can run in any one of the four 31750 processors located in the two CDMUs, it performs the following tasks:

5.2.1 Tele command reception, distribution and handling

Commands can be received from a number of sources; from Ground via the decoder, and from on-board via the Mission Time Line, Backup Mission Time Line, System Init Table, Onboard Control Procedures, Application Programs, FDIR monitors, command requests from the AOCS, and different types of files held in the SSMM. In order to overcome the limitation of the packet tele command standard regarding deep space missions, commands can be up-linked via a file transfer protocol, stored as a file in the SSMM and then executed as required.

Commands are distributed according to their Packet Identifiers to internal tasks or other users via the OBDH bus or 1355 links. Also commands for none packet users are stripped of the packet protocol and sent as discreet commands with timing delays being respected.

Internally the DMS has buffers and queues to handle the above command tasks; these have been sized so no commands should be lost during the handling process.

5.2.2 Telemetry collection, formatting, storage, distribution and down link

Telemetry packets are collected from all other units via the OBDH bus or 1355 links; discreet telemetry from non-packet users is also formatted into standard packets for further handling.

Telemetry data is stored onboard in the SSMM and in an internal data pool for onboard processing/monitoring; telemetry from this data pool can be formatted into standard house keeping packets whose frequency and content can be changed by tele-command. Via this data pool data from one unit can be distributed to other units by request telecommand.

Telemetry packets can be routed to the real time downlink via Virtual Channel 0 or the SSMM for storage in packet stores.

5.2.3 Mission Time Line MTL

The mission time line is the prime source of commands for controlling normal operations. The MTL stack can hold up to 3000 time tagged commands in time order with a time resolution of 1 second. When the time matches the spacecraft lapsed time (SCET) the command is processed by the command handler. Commands can be added, edited and deleted by ground command at any time, also the processing of the stack can be enabled or disabled by ground. To enable the MTL to hold up to 3000 commands they are held in files on the SSMM and fetched to a cache in the DMS as required. Should the SSMM not be available a reduced MTL of 117 commands is available for operations internally in the DMS. Both of these MTLs are for normal operations they are lost if a soft or hard reboot of the DMS is performed. Additionally a backup MTL is available, this is for critical commands that would still need to be executed at a certain time even if a reboot of the DMS has occurred.

5.2.4 On Board Control Procedures OBCPs

On board control procedures replace the man in the loop for real time operations, they are used for simple procedures that will be executed many times during the mission e.g. unit turn on/off and mode change, and can also be used for real time contingency actions. They can issue tele commands, wait for responses or time outs, and make decisions on telemetry or parameter values. The DMS can execute up to 20 in parallel via a simple time slice executive. Each procedure is self-standing, written in a spacecraft control language and is interpreted on board; this means that any error in a procedure cannot propagate to other parts of the DMS software. This means that any changes to a procedure only require local testing and no regression testing of other elements of the software, and that the spacecraft operations team can identify, implement and uplink any change in a very quick maintenance cycle. OBCPs are stored in the SSMM with critical ones also being stored in the DMS image so they can be used even when the SSMM is not available. More complex tasks needed for operations are implemented in the natural machine language and are imbedded in the software code, these are table driven where possible in order to improve maintainability.

5.2.5 On Board Monitoring of Telemetry Data

Telemetry data located in the data pool from subsystems and payloads can be monitored against a pre-defined limit set or status. When this test has triggered a number of consecutive times, a pre-defined command is executed. The monitoring is table driven and parameters can be enabled, disabled or updated by command.

5.2.6 Failure Detection Isolation and Recovery (FDIR)

FDIR is implemented in the DMS to monitor the status of lower level equipments and reconfigure to redundant when required.

5.3 Attitude Orbit Control System

This software can run in any one of the four 31750 processors located in the two CDMUs. It interfaces with the DMS software and through it to the ground. It manages all the AOCS sensors and actuators directly through the AOCS Interface Unit (AIU) for functional data acquisitions and commands. For equipment configuration through the RTU, it routes the commands to the DMS SW. The AOCS software consists of an elementary chain of functions to be performed, which begins with the acquisitions of sensor information and ends with the emission of commands to the actuators. This is linked with complementary functions as command ability to operate the space craft, data collection for both on board processing and to provide operability from ground, FDIR to cope with failure detection and autonomous recovery, autonomy to perform complete sequences without ground action.

The AOCS software implements the following application functions

- Estimation algorithms
- Control algorithms
- Ephemeris propagation algorithms
- Functional AOCS monitoring
- Sensors and actuators processing
- Sensors and actuators monitoring algorithms
- Sensors and actuators configuration procedures
- Reconfiguration procedures necessary for FDIR

To achieve the Rosetta mission ten AOCS modes are managed by the AOCS SW

- Stand-By (SBM)
- Sun Acquisition (SAM)
- Sun-Keeping (SKM)
- Safe/Hold (SHM)
- Normal (NM)
- Thruster Transition (TTM)
- Spin-Up (SPM)
- Orbit Control (OCM)

- Asteroid Fly-by (AFM)
- Near Sun Hibernation (NSH)

5.4 Solid State Mass Memory

The SSMM software runs on one of two DSP processors contained within the unit. The main objective of the SSMM software is to implement a file system in the mass memory where on board data can be stored in files depending on source and/or packet ID. The files can, when commanded by the DMS, be sent to other users on board or down linked to the ground. Both lossless (RICE) and lossy (Wavelet) compression of stored files is possible when commanded.

The SSMM software is also responsible for handling all interfaces with the unit:

- IEEE 1355 links with DMS, VIRTIS, OSIRIS, CAM
- Transfer Frame Generator
- Mass memory bus supporting redundant memory controllers

The software can support simultaneous storage and retrieval of data over all 1355 links and down link of data from selected files, together with data compression, command handling, normal file structure handling and FDIR. One of the features is that should the software be rebooted or the processors switched over the data stored in the mass memory is not lost.

5.5 Autonomous Star Tracker

The STR software runs in one of two units on a DSP processor, one feature of the overall system is that both can be on at the same time giving a more real time back up. The software supports seven functional modes:

- Stand by
- Autonomous Acquisition and Coarse Attitude Determination
- Autonomous Tracking and Fine Attitude Determination
- Cartography
- Commanded Star Tracking
- CCD health status analysis
- Self test

The main operational modes are:

- Autonomous Acquisition and Coarse Attitude Determination

The STR determines the coarse attitude describing the orientation of its reference frame in any position in the celestial sphere using an on board star catalogue. When it has identified the star field present in its field of view it switches to Autonomous Tracking mode. In case the STR cannot perform autonomously e.g. to

many bright objects or a comet dust environment, it can accept a coarse attitude command from the AOCS. This also makes it very resilient to SEUs in its CCD.

- **Autonomous Tracking and Fine Attitude Determination**

The STR continuously provides accurate information describing the orientation of its reference frame by collecting and processing images of limited portions of the CCD that are located around known positions of stars in its FOV. The STR refines its attitude and rate measurements.

- **Cartography**

The STR provides the AOCS with position and magnitude measurements of the ten brightest stars in its FOV.

- **Commanded Star Tracking**

The STR accepts the initial position and rate of upto five stars, and then performs tracking of these.

5.6 Navigation Camera

The CAM software runs in one of two units on a DSP processor. The software supports five functional modes:

- Stand by
- Imaging
- Point target tracking
- Asteroid tracking
- Self test

The main operational modes are:

- **Imaging**

This mode is planned to be used for asteroid or comet detection at far distances or mapping the comet nucleus at close distances, these images are sent over the 1355 high speed link to the SSMM for down link to the ground. No further processing is done on board.

- **Point target tracking**

The CAM will simultaneously track up to five point sources while they are in the FOV.

- **Asteroid tracking**

The CAM will image and track the designated asteroid while in the field of view and pass the information to the AOCS, which will maintain the spacecraft pointing to the asteroid.

5.7 Conclusion

As with any large complex software system using more than one processor communicating with others there were some known bugs before launch, and operational work around solutions were available. Apart from specific functionality required for mission phase in the future e.g. asteroid fly by or comet mapping; all of the above functionality has been used without major problems found in this first commissioning phase. A number of small anomalies have been reported. All have been investigated with the problem being found quickly and some are still under investigation. The most important of these is that the star tracker sometimes loses stars for short periods, the system can handle this, and the problem has been traced to a few stars being wrong in the on board catalogue and possibly one line of code being missing from a procedure. Resolution of both is expected soon and may already be available before this report is issued.

Already the software maintenance procedures have been shown to work, see the APM problem reported in section 3 of this report.

As stated above some bugs “features” were known before launch and already a decision was taken to correct them with a new software issue planned for upload after launch together with some of the problems found during this last commissioning phase. This new issue has been under test by industry and ESOC for almost two months now and it is currently planned to be up-linked some time in July.

6 TT&C

6.1 Design Principle

The Tracking, Telemetry and Command (TT&C) subsystem is specially suited for Deep Space communications and is built around a mission specific designed Transponder able to receive and transmit in both S and X Bands.

In nominal mission conditions both Uplink and Downlink are established via X-Band links, however the S-Band receive capability was retained to ensure command access to the S/C in case of emergency at distances beyond the reach of the existing X-Band ground transmitters

There are two physically independent Transponders on board, each featuring two transmitters (S and X) and two receivers (S and X). The design is such that there are **always** two receivers working in hot redundancy.

Transmission in S-Band uses a 5 Watt solid state amplifier whereas TWTA's are used to boost the X-Band signal as provided by the Transponders. A full set of 5 antennas, (2LGA, 2 MGA and 1HGA) guarantee access from Earth for command in all mission scenarios and downlink telemetry from the S/C for nominal mission cases.

The TT&C subsystem is designed to interface with the ESA ground segment and with the NASA ground segment.

A block diagram as in Fig. ---- shows the configuration adopted to link the various units composing the whole subsystem. All items are shortly described below:

(TO BE ADDED IN LATER ISSUE in next issue)

6.2 Initial Flight Data

One minute after S/C separation the ESA Kourou Station acquired the first RF/TM signal and soon followed the first Uplink Sweep that succeeded in locking the S-Band receiver via LGA-rear. First Commands were uplinked and accepted at 10:34, one hour after separation.

New Norcia ground station made contact with Rosetta for the first time just 13 hours after separation. Receive, Transmit and Ranging were nominally working from this early contact and have continued to perform satisfactorily since.

The HGA was deployed within day 1 of launch and its commissioning started a day later with S-Band trials; the HGA being fully commissioned upon completion of X-Band planned tests on day 5 of the mission.

The nominal configuration adopted since then is:

- X-Band downlink via HGA, Transmitter 2 – TM 22 Kbps
- X-Band uplink via HGA – Receiver 2 – 2000 bps
- Back-up Receiver #1 in S-Band via LGA-rear at 7.8 bps

It is important to mention here that most of the problems encountered during integration and system testing of the Rosetta S/C prior to launch, reported as “false” and / or “unwanted” locking, **are no longer a cause of concern for the daily operation** of the S/C. The ESOC team mastered thoroughly the peculiarities of the Transponders and their extreme sensitivity and produced Operational Procedures well tailored to cope with them.

None of these “deficiencies” have surfaced or troubled the daily contacts since the beginning of the mission.

6.3 Functional and Performance Data

The planned commissioning of the TT&C subsystem made provisions for both **functional testing** of the various items in the S/S and **performance testing** of selected parameters.

Functional testing covered the following cases:

- 1- Transponder 1 Uplink and Downlink via LGA front in S-Band
- 2- Transponder 1 Uplink and Downlink via HGA in S-Band
- 3- Transponder 1 Uplink and Downlink via HGA in X-Band
- 4- Transponder 2 Uplink and Downlink via LGA rear in S-Band
- 5- Transponder 2 Uplink and Downlink via HGA in X-Band
- 6- Transponder 2 Uplink and Downlink via HGA in S-Band
- 7- RFDU switches 1 to 5
- 8- WIU switches 6 and 7
- 9- USO on /off. USO warming. USO muted/Un-muted
- 10- S and X-Band ranging

For details on the date and time as well as the sequence when the above were performed refer to ESOC report RO-ESC-RP-5910.

Both TWTA 1 and TWTA 2 were used during functional checks.

All cases above were done as per plan and resulted in confirming **NOMINAL** operation as expected.

Performance testing focussed on the following:

- a. Link Budget
- b. HGA Pattern calibration
- c. LGA Threshold
- d. Ranging
- e. USO reference for RSI payload

Link Budgets:

Using the On-board receiver AGC as parameter to estimate how accurate the link predictions were in the Link Budget Tables, the only conclusive statement is that for the uplink via LGA's there is a positive margin of 4 to 6 dBm in excess of worst case predictions. This is easily explainable when considering the irregularities of the pattern of the omnidirectional antenna assembly made by the two LGA-rear and LGA-front.

Figures measured in X-Band uplink using the HGA were felt to be 1 to 2 dBm short in comparison to predictions, however there is a need to repeat the pattern calibration exercise made with the HGA for a suspected minor offset in its mounting on-board.

Assessment of the downlink budget figures requires a credible correlation between the measured AGC value at the IFMS and the antenna input in the Ground Station. There is a proposal to further characterize / verify this downlink as mentioned in the ESOC report.

HGA Pattern Calibration:

Three fixed HGA positions were calibrated while slewing the S/C in spiral around each position. As a result an offset of 0.43 deg in Azimuth and of 0.15 deg in Elevation was attributed to the mounting of the HGA on-board. Accordingly a bias was introduced in the software controlling the drives and an increase of 3.6 dB was observed in the strength of the downlink signal. A further calibration will be done in the next commissioning part.

LGA Threshold:

An attempt to perform this test on the 2nd of June failed to determine at what level of S-Band input commands were not accepted. The problem was the Ground Station not being able to provide a sufficiently low signal radiated towards the S/C. The test will be to be repeated later, perhaps close to perigee by end of August.

Ranging:

Results obtained during X and S band ranging (performed during the night of 6 to 7 March) did not provide a consistent set of values that could be correlated with previous ground measurements. This is mainly caused by the lack of adequate System and Unit level test data prior to launch. The discrepancy reported in X-Band, when comparing delta values between Transponder 1 and Transponder 2, has been subject of due clarifications and is now resolved. There is still to be explained a lower delay value obtained at X-Band when compared with S-Band. Further test campaigns for ranging are planned before the next commissioning phase ends.

The HGA calibration, LGA threshold and Ranging need to be performed when the spacecraft is further from the Earth.

USO frequency source:

The USO was connected to the transponders as driving frequency source during the two sessions for commissioning of the RSI payload. Some concern was raised on the phase noise after initial assessment. The second RSI campaign produced much better and satisfactory results.

6.4 Conclusions

Apart from the outstanding commissioning of the two Medium Gain Antennas: MGA-S and MGA-X, all units in the TT&C subsystem have been tested and proven to deliver

the functions as expected. Further characterisations for fine-tuning, as mentioned above, would require additional field trials to be accommodated in the planning.

7 ATTITUDE AND ORBIT CONTROL SUBSYSTEM (AOCS)

7.1 GENERAL DESCRIPTION

The AOCS is in charge of attitude and orbit measurement and control with sensors and actuators for autonomous attitude determination and control as well as pre-programmed manoeuvring. AOCS subsystem is built around the AOCS Interface Unit (AIU), which is used by the AOCS software to exchange functional data with a complete set of sensors and actuators: Inertial Measurement Package (IMP), Star Trackers (STR) and Navigation Cameras (CAM), Sun Acquisition Sensors (SAS), Reaction Wheel Assembly (RWA), Reaction Control System (RCS).

7.1.1 AOCS MODES

In order to perform all of the operational tasks required, the AOCS subsystem consists of 10 software-operating modes of three different types: survival, operational and hibernation. Most of these modes are further divided into several phases, which are in charge of well-defined specific activities.

The **Stand-By Mode (SBM)** is used in Pre-launch and Launch Modes for general check supervision. Only the DMS functions are activated. However, It is possible to command thrusters through the AIU for RCS Priming and Venting.

SAFE MODES

The **Sun Acquisition Mode (SAM)** performs the first attitude acquisition after launch and then again after solar array deployment to enable the solar arrays to be pointed towards the Sun. The mode is also used as a second level backup mode. SAM uses first the gyros and thrusters to reduce the potential spacecraft rate to less than 0.25 deg/s on each axis. It then ensures a permanent 2-axes stabilisation of the Spacecraft, before entering in Safe Hold Mode and completing the 3 axes stabilisation. A slow spin motion around the Sun direction is achieved. The Autonomous Attitude Acquisition is commanded to the star tracker (outside the control loop). Once a 3-axis attitude is provided by the star tracker, its consistency with the Sun direction measured in spacecraft frame and computed from on-board ephemeris is tested, enabling transition to the next phase.

The **Sun Keeping Mode (SKM)** is the first level backup mode when a major attitude failure is detected and continuation of the current operational mode is no longer feasible. It is equivalent to the SAM, except that the control is based on the 2 SAS mounted on the solar arrays, instead of body mounted SAS. This mode is implemented to perform, in case of failure, a transition to SHM without losing the solar array

orientation towards the Sun (reacquisition without battery). At the end of SKM, the Star Acquisition Phase is performed: Autonomous Attitude Acquisition is commanded to the star tracker. Once a 3-axis attitude is provided by the star tracker, its consistency with the Sun direction measured in spacecraft frame and computed from the on-board ephemeris is tested, enabling transition to the SHM.

If the automatic SKM to SHM transition is impossible, the **Earth Strobing sub-Mode (ESM)** is started. Its aim is to allow the ground to recover the communications. The general principle is to implement a rotation of the Spacecraft around the Sun direction, while keeping the solar arrays Sun pointed, and to ensure that the Medium Gain Antenna (MGA), whose boresight points towards the spacecraft +X axis, describes a cone defined by the Sun-Spacecraft-Earth angle, providing a periodic link with the Earth (carrier signal only), once per revolution. In order to achieve the (along mission variable) adequate angle between the Sun direction and the MGA, the Sun sensors implemented on the Solar Arrays are used, and the Solar Arrays are rotated. The Spacecraft attitude is then controlled with these Sun sensors, in Solar Array axes, as in SKM. The duration between two consecutive links with the ground being sufficiently stable, the ground computes then the right instant to send a “stop strobing” TC, which leads the spacecraft to a 3-axis stabilised attitude with the +X axis Earth pointed and the SA perpendicular to the Sun.

The **Safe Hold Mode (SHM)** completes the sequence initiated by the Sun Acquisition Mode or the Sun Keeping Mode aiming to reach a safe permanent attitude with X-axis pointing towards the Earth and the solar arrays towards the Sun. To reach the final SHM attitude three sequential slew manoeuvres are therefore performed with thruster control, keeping the solar arrays facing permanently toward the Sun. The guidance is commuted to stabilisation on ephemerides and the HGA control is enabled. Provided the ground has enabled the reaction wheels switch-on, the wheels are then spun up to a predefined rate before they can be used for attitude control. Once the commanded rates have been reached, actuation capability is autonomously transferred to reaction wheels.

OPERATIONAL MODES

The **Normal Mode (NM)** is designed for most of the mission operational phases. Attitude control in Normal Mode is based on reaction wheels, gyros and star trackers. The gyroless estimation is reserved to Earth/Sun pointing quiet cruise phases. The spacecraft commanded attitude could be either processed autonomously on board or on ground. Solar array orientation towards the Sun and High Gain Antenna orientation towards the Earth are respectively commanded to the mechanisms. Reaction wheel off-loading is performed autonomously with thrusters, as soon as the on-board measured wheel rate is higher than an upper threshold, or lower than a lower threshold. By this way, wheel rate saturation and zero crossing are avoided. As soon as the wheel rate reaches a warning threshold (which is lower than the reaction threshold), a warning message is downlinked. Then the ground can decide to manage the wheel off-loading, for instance through proper orientation of the solar arrays (using solar pressure torque as

off-loading control torque), and to avoid the use of thrusters. For very small orbit manoeuvres, it is authorized that the Ground directly commands short thruster impulses in Wheel Controlled Damping Phase. This avoids to transit by the Thrusters Transition Mode where the use of thrusters for the control could disturb the Orbit Manoeuvre accuracy.

The **Orbit Control Mode (OCM)** is specifically intended to perform orbit manoeuvres and corrections. For large manoeuvres the Spacecraft Z axis is orientated to the proper direction, and then a thrust is generated along the Z-axis. X and Y axis attitude control is performed by off-modulation, and Z-axis control by on-modulation of complementary thrusters. During some time critical mission phases (asteroid final approach, comet approach and comet orbit phases), a 3 axis “vectored thrust” can be generated in any direction without turning the spacecraft, the 3-axis attitude control being realised by thruster on-modulation. The exact length of the thrust is autonomously controlled on board using either integrated measured accelerations provided by accelerometers, or integrated on-times commanded to the thrusters.

The **Thruster Transition Mode (TTM)** ensures a smooth two-way transition between the Normal Mode, designed with reaction wheels control, and the orbit control mode, the spin-up mode and the near Sun hibernation mode, which are designed with thrusters control.

The **Asteroid Fly-by Mode (AFM)** is designed to point the asteroid optical center along the payload Z-axis in order to track the asteroid visible part in the field of view of the scientific instruments. The attitude guidance and control is based on closed-loop tracking of the asteroid body using navigation camera angular measurements with respect to the asteroid optical center. This phase lasts a few hours and is particularly critical during the few tens of minutes around closest approach when Rosetta has to rotate very fast (0.3 de/s) and guarantee accurate and stable asteroid observations

HIBERNATION MODES

Two hibernation modes are provided in order to preserve resources and minimise ground contact during the long cruise phases between critical events. The objective of the **Near Sun Hibernation Mode (NSHM)** is to maintain the Solar Arrays pointed towards the Sun, and optionally an antenna pointed towards the Earth to enable communications, while minimising the fuel consumption and the number of thruster cycles. It uses a thruster adaptive pulse width control algorithm, in order to achieve whenever possible a one-sided limit cycle which uses the external disturbance torque as a propellant in one direction. The thruster control must keep the spacecraft Earth/Sun pointed attitude within a programmable attitude limit cycle in the range $\pm 15^\circ$.

The **Spin-Up Mode (SPM)** is used to enter the Deep Space Hibernation phase of the mission. Its goal is to spin-stabilise the Spacecraft around 4°/s about a given inertial direction, such that the principal axis of inertia remains inertially fixed during the whole

hibernation phase. When entering this mode, the Spacecraft is three-axis stabilised with its estimated principal axis towards a commanded inertial direction, which is typically 20° away from the Sun direction. The final spacecraft dynamic state shall be unambiguously checked on-board for authorising the shut down of AOCS and transition to Hibernation. The Spacecraft will remain in this state for about 2 years around the 5.2AU aphelion.

7.1.2 AOCS UNITS

The Spacecraft carries four coarse **Sun Acquisition Sensors (SAS)**. Two of these sensors are situated on the main body and together generate more than hemispheric coverage providing measurements to enable initial Sun acquisition. A further unit is situated on each solar array allowing for fast recovery of the Sun on the solar arrays in case a serious Sun pointing failure has occurred.

The two redundant autonomous **Star TRackers (STR)**, which provide the spacecraft inertial attitude without any ground intervention are each capable of tracking up to nine stars between magnitudes 2 and 5.5 and can determine autonomously from those coordinates the star tracker quaternion in inertial space. Each STR consists of two separate units, an optical head and a processing unit that is shared with the Navigation Camera. These STR have been designed to operate even while the spacecraft is within the cometary dust cloud. This significant achievement is described in a separate paper. The Rosetta Spacecraft is also equipped with two redundant **Navigation CAMeras (CAM)** with electronics common to the STR. These will detect the asteroids at long range and will be used to control the spacecraft pointing during the very fast flybys. They will also be used to detect the comet some months before the encounter to allow accurate determination of its orbit for the precise planning of the various rendezvous manoeuvres and mapping of the comet for selection of the landing site.

The avionics sensor suite finally includes three **Inertial Measurement Packages (IMP)** composed of a set of three mutually orthogonal high performance Ring Laser Gyros. Each package is also equipped with three accelerometers for monitoring and controlling the orbit correction manoeuvres. The 2 first packages are mounted in a skewed configuration, which allows the AOCS to use any combination of 3 gyros among the 6, to calculate a 3 axes attitude. The third unit is an ultimate alternative used by the AOCS, when it is not able to identify 3 safe gyros among the 6 first ones.

The AOCS includes four **Reaction Wheels Units (RWU)** of which three are normally to be used. Each reaction wheel has a 40Nms momentum capacity and can deliver 0.2Nm torque. Additionally they are equipped with a high-resolution wheel speed monitor. During the asteroid flybys all four reaction wheels may need to be used simultaneously in order to meet the pointing requirements during the fast observation slew.

The coarse attitude control and orbit manoeuvres are performed with the **Reaction Control System (RCS)**, which is composed of two redundant sets of 12 bi-propellant thrusters of 10N. Two sets of four parallel thrusters are available for all the major orbital manoeuvres and the two sets of eight remaining thrusters are configured to generate force free attitude control torques during orbit manoeuvres, coarse pointing modes and wheel-off loading. Each thruster features individual flow control valves and latch valves so that it can be isolated in case of failure.

The AOCS is also in charge of monitoring and steering the HGA towards Earth and the solar array towards the Sun using respectively the **HGA Pointing Mechanism (HGAPM)** and the **Solar Array Drive Mechanism (SADM)**. For this purpose Sun and Earth ephemerides are generated on-board using Chebyshev polynomials for which coefficients are regularly updated from the ground to cover the different sequence of the mission phases.

	AIU	IMP	SAS	STR	CAM	RWU	RCS	SADM	HGAPM
SUN ACQUISITION MODE									
RRP	1	2					1	HOLD	
SCP	1	2	2				1	OFF/2	
SAP	1	2	2				1	OFF/2	
SPP	1	2	1+(2)				1	OFF/2	
SUN KEEPING MODE									
RRP	1	2					1	HOLD	
SAP	1	2	1/2				1	HOLD	
STAP	1	2	1/2	(1)			1	HOLD	OFF/1
SAFE HOLD MODE									
EAP	1	2	(2)	1			1	2	OFF/1
EPIP	1	2	(2)	1		3	1	2	OFF/1
EPP	1	2	(2)	1		3		2	OFF/1
WOLP	1	2	(2)	1		3	1	2	OFF/1
NORMAL MODE									
GLEP	1		(2)	1		3		2	1
WOLP	1	2/1	(2)	1		3	1	2	1
Other Phases	1	2/1/OFF	(2)	1		3		2	1
THRUSTER TRANSITION MODE									
	1	2/1	(2)	1		OFF/3	1	2	1
ORBIT CONTROL MODE									
	1	2	(2)	1		OFF/3	1	2	1
ASTEROID FLY-BY MODE									
	1	2		1+(1)	1+(1)	4		2	1
NEAR SUN HIBERNATION MODE									
	1		(2)	1			1		
SPIN-UP MODE									
	1	2	(2)				1		1

Table 1: AOCS Modes versus Units

7.1.3 AOCS FAILURE DETECTION ISOLATION AND RECOVERY

Owing to the complex mission requirements and the high communications return trip time the spacecraft needs a high level of autonomy, both for operations and for contingency cases. The ground control centre cannot exert any real-time control because of the long signal roundtrip time, occultations and hibernation periods, when the control centre is not manned for cost reasons. Rosetta has to resolve any critical problems autonomously and therefore an elaborate FDIR service has been implemented. While most spacecraft cannot perform automatic recovery for more than one failure, Rosetta can keep the solar arrays pointed towards the Sun and its HGA to Earth in the event of multiple independent failures. The complexity of such a design was one of the major drivers in the ROSETTA AOCS development.

7.2 SUMMARY OF AOCS COMMISSIONING HIGHLIGHTS

The first months of ROSETTA operations have included a number of AOCS events and minor anomalies that are summarized in the following Table. Following star trackers switch ON at 13:15 UTC on DOY 062, spacecraft entered SHM at 13:51 UTC and reaction wheels were switched ON at 14:23 UTC. Spacecraft entered NM at 14:47 UTC and throughout the rest of mission was mostly commanded either in GSEP or FPAP.

EVENT	DATE	COMMENT
Normal Mode Entry	DOY 062	Commanded into Normal Mode at 14:47 UTC.
First Wheel Off-Loading	DOY 062	First Reaction Wheel Off-Loading at 20:00 UTC.
HGA Deployment	DOY 063	High Gain Antenna deployed at 00:34 UTC.
TCM Manoeuvre	DOY 063	First test delta-V manoeuvre of 1 m/s.
APM Switched OFF	DOY 064	Decided to keep the APM off as normal status. APM will be operated once a day to re-point the HGA to avoid temperature increasing.
SAS Parameters Update	DOY 065	SAS luminance thresholds for post-LEOP were uplinked as planned.
RW Friction Test	DOY 066	Characterization of friction torques over operational range.
RW 4 Switched ON	DOY 066	Configuration with 4 wheels decided to allow easier momentum management in presence of higher than expected friction torques.
STR B Switched ON and OFF	DOY 069	Slew to +X Sun pointing and test of star acquisition and tracking.
SA Flexible Modes Calibration	DOY 070	SA flexible modes calibration via three reaction wheel offloading
SAS Misalignment Calibration	DOY 070	Sun Sensors misalignment calibration including slews to both extremes of the MGA strobing angles (-70 and +50 deg)
Spurious Attitude Errors	DOY 080	In two occasions STR registered spurious attitude errors most likely due to stars ID 1717 and ID 1856 entering FOV that are incorrectly treated in the catalogue.
STR B Switched ON	DOY 090	Star Tracker B activated and kept in Tracking mode
STR Software Patch	DOY 090	STR software patch required allowing operation of both STRs in parallel (i.e. AIU multiplexing) uplinked to both STRs.
AOCS RAM Software Patch	DOY 091	Software patch uploaded to remove commands to switch ON APM substitution heater every time the APM is switched off. Bias values to the APME pointing algorithm uplinked.
Pointing Performance Preliminary Evaluation	DOY 091	During MIRO operations high frequency attitude measurements to allow detailed evaluation of the spacecraft pointing performance.
Spurious Attitude Errors	DOY 091	Another occasion of spurious spike in attitude determination detected during MIRO pointing profile. Problem was again caused by star 1856.
STR CCD Health Check	DOY 094	A CCD health check has been performed on STR A. During this

		period attitude determination has been switched over to STR B.
STR A Alignment Parameters Update	DOY 098	The alignment parameters of STR A have been updated on to correct a typo in a command uplinked after launch.
STR B switched OFF	DOY 113	-
STR A Loss of Stars	DOY 111	During period of inertial pointing to enable ALICE warm attitude STR A reported only 6 stars tracked.
High Thruster Temperature	DOY 115	Emergency slew back to GSEP commanded to react to high temperatures on thruster modules exposed to the Sun.
STR A Loss of Stars	DOY 116	STR reported loss of all stars and went out of tracking. AOCS commanded STR A back into tracking and no anomalous effect observed.
IMP B Switched ON	DOY 122	In preparation for the deep-space manoeuvre.
DSM Manoeuvre	DOY 131	Deep Space Manoeuvre of 152.80m/sec.
DSM Touch-Up Manoeuvre	DOY 137	Deep-space manoeuvre touch-up of 4.989 m/s
STR Large Object in FOV	DOY 135	The object disappeared after 32 sec and no impact on the attitude measurement was observed.
IMP-B Switched ON	DOY 145	After end of DSM-1 activities.
AOCS EEPROM Software Patch	DOY 146	Ensure that in case of APM switch OFF substitution heaters are also kept OFF. Deep-Space flag was set in AOCS software

Table 2: Summary of AOCS Highlights

7.3 AOCS IN-FLIGHT PERFORMANCES

7.3.1 AOCS UNIT PERFORMANCES

7.3.1.1 ACQUISITION INTERFACE UNIT

AOCS Interface Unit (AIU) enabled correct commanding of AOCS actuators and acquisition of both digital and analog data from AOCS sensors. However noise level on -15V power supply was reported higher than expected. It is possible that a revision of the FDIR thresholds associated to these parameters may be needed in the future. The AIU -15V was observed to be stable but as a precaution the recovery action of its surveillance was disabled during the HGA deployment and re-enabled immediately after. The problem is currently being investigated.

7.3.1.2 SUN ACQUISITION SENSORS

On DOY 070, spacecraft was commanded to slew around Y_{SC} axis with SA articulations between $+70^\circ$ and -50° . The difference between Sun direction derived from SAS measurements and predicted direction extrapolated from both STR quaternion and ephemerides enabled characterisation of SAS over their complete operational ranges. The preliminary results of SAS alignment calibration including the average and root mean square of the difference between the measured and the predicted Sun angle are listed in the following Table.

ACM	SAS	Angle	Mean	1 σ
A	plus Y SA	around SAS Y axis	0.092	0.013
A	plus Y SA	around SAS X axis	-0.123	0.033
A	minus Y SA	around SAS Y axis	-0.127	0.015
A	minus Y SA	around SAS X axis	-0.001	0.038
A	fictitious	around SAS Y axis	0.196	0.010
A	fictitious	around SAS X axis	-0.064	0.034
B	plus Y SA	around SAS Y axis	0.183	0.013
B	plus Y SA	around SAS X axis	-0.182	0.032
B	minus Y SA	around SAS Y axis	-0.184	0.014
B	minus Y SA	around SAS X axis	0.115	0.039
B	fictitious	around SAS Y axis	0.163	0.012
B	fictitious	around SAS X axis	-0.159	0.035

The conclusion from this calibration is that no SAS misalignment update was required.

7.3.1.3 INERTIAL MEASUREMENT PACKAGES

The three gyros health status has been periodically checked through the Laser Intensity Monitors (LIM). LIM are characterized by a stable or slightly increasing value over a long period of time. There is thus no fall off or trend observed as a possible indication that performance problems could occur.

	IMP X Axis NACA6200	IMP Y Axis NACA6201	IMP Z Axis NACA6202
DOY 063	1.44802	1.45168	1.48279
DOY 143	1.31528	1.26124	1.33322

Table 3: Average of Gyro Laser Intensity IMP A

In general, we have found that gyro performances have been very stable over time. Figure 7.1 exemplifies this impression. This is a rather long-term history plot of gyro bias as estimated on-board. The short-term variations corresponding to spacecraft slews or perhaps thermal shifts are hardly noticeable. The bias estimation drops observed successively on DOY 090 and DOY 094 are due to attitude determination temporarily switched over from STR A to STR B for maintenance operations. Indeed it is perfectly nominal to have both STR and gyro misalignment errors completely transmitted through gyro-stellar filter. The spikes observed on the maximum innovation are due to corrupted stars entering STR A field of view and will be discussed in next section.

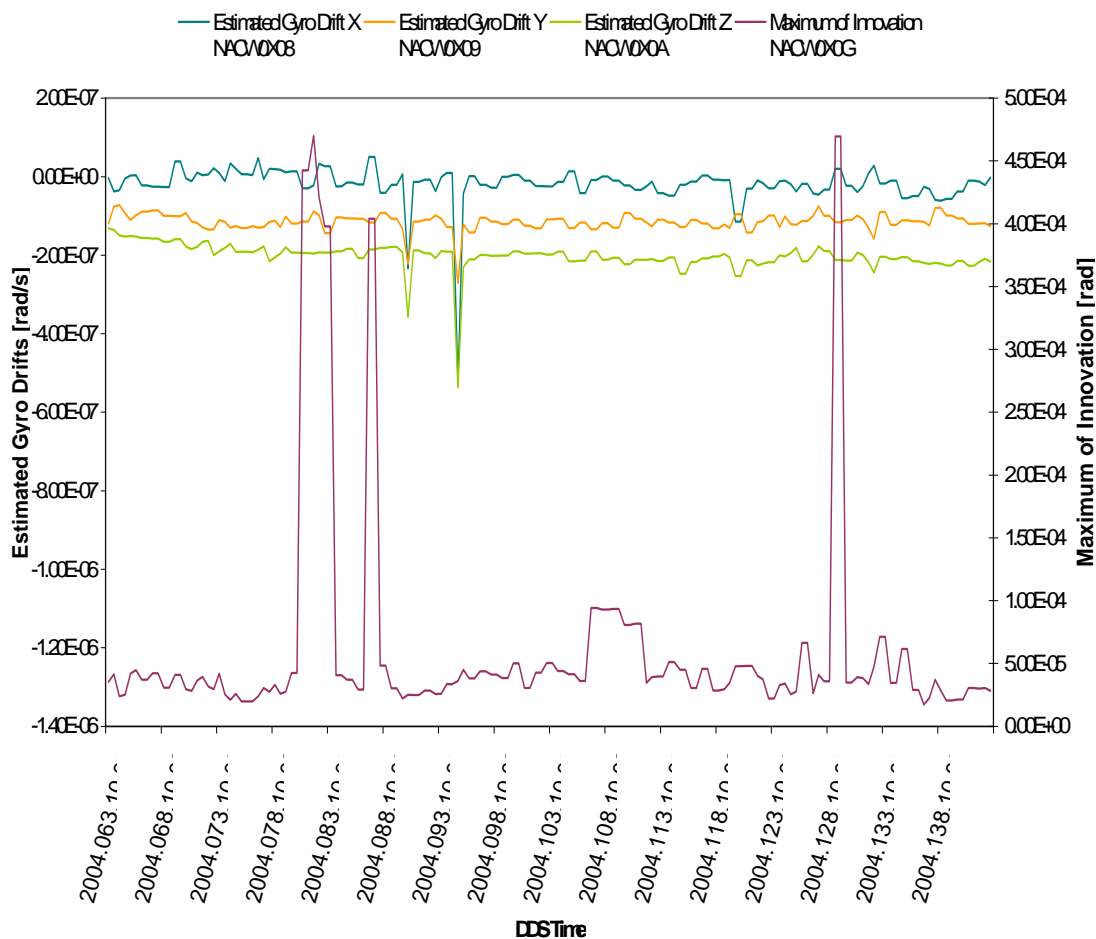


Figure 7.1: Estimated Gyro Drift and Innovation Histories

The estimated gyro drift mean and its associated standard deviation have been computed over the first month of the ROSETTA mission and are listed in the hereafter Table. It has first to be noted that the gyro drift estimation means are very consistent with the STR orientation inducing higher star measurement noise around spacecraft X axis.

Estimation Drift Errors [rad/s]		X	Y	Z
Estimation Observed	Mean	-1.90E-08	-1.15E-07	-2.02E-07
	1σ	5.06E-08	2.14E-08	3.61E-08
Estimation Simulated	1σ	1.05E-07	4.88E-08	6.08E-08
Margin	%	-52	-56	-41
RPE Required ⁽¹⁾	1σ	5.20E-06	5.20E-06	5.20E-06

Margin	%	-99	-100	-99
⁽¹⁾ Comet Observation: RPE of payload 3.00E-04° over 1 second, half cone at 95% confidence level				

Table 4: On-Board Estimated Drift Errors

The Relative Pointing Requirement shall obviously also include the contributions from attitude guidance and control errors as well as drift estimation error and as such could not be compared too straightforwardly to the on-board estimation of gyro drift. However, the observed estimate is rather impressively two orders of magnitude lower than the most stringent RPE requirement.

Due to the star tracker measurement noise, the gyro angular random walk and the bias stability contribute to final estimator performance, it is actually difficult to derive or isolate actual IMP performances out of the telemetry data. However it is clear from the previous figures that gyros in collaboration with star tracker are extremely good.

The on-board estimation of gyro drift has been also monitored during spacecraft GSP slews and it has to be noted that in good accordance with the prediction there has been no significant degradations of gyro drift estimation due to the spacecraft dynamics.

According to Avionics Requirements Specification (RO-DSS-RS-2001), the gyro-stellar estimator performances have to be compatible with an absolute pointing error lower than 0.15° during target detection phases and lower than 0.03° during the comet observation phase. Since the attitude pointing requirement is clearly a combination of several different contributions (e.g. attitude guidance, estimation and control errors), the allocation for attitude estimation error was then limited to 0.05 deg (i.e. 8.710^{-4} rad) during the target detection phase and 0.01 deg (1.710^{-4} rad) during the comet observation phase. The estimation error observed on gyro drift already indicates that a similar excellent performance is also expected on the attitude reconstruction.

The accelerometers in the IMP units consistently with gyro measurements have been found to measure the first test delta-V of 1 m/s with an accuracy of better than 0.5 % compared to the simultaneously performed Doppler measurement.

IMP C was not operated during commissioning period.

7.3.1.4 STAR TRACKERS

7.3.1.4.1 ACQUISITION CAPABILITY

Several Autonomous Acquisitions and Coarse Attitude Determinations (AA&CAD) have been exercised on both STR A and B during the commissioning period. On DOY 062, the two STR were switched on at 11:25 (SAM/STAP) and again at 13:15 (SKM/ESP). Upon first switching on, STR A failed to acquire tracking (as expected), but STR B attained AT&FAD and tracked 9 stars. After completing Solar Array

rotation, both STR units had successful AA&CAD before entering AT&FAD. Since LEOP few others Autonomous Acquisition have been commanded to both STR A and B, however on DOY 069 during STR software patch, it was required to permit operation of both STRs in parallel. The pattern recognition capability and the associated acquisition performances of ROSETTA STR are very satisfactory.

Despite the absence of STR patches in order to decrease STR CCD matrix sensitivity against parasitic straylight effect following MEX in-flight anomalies, the different acquisition problems observed on MEX were not reproduced (as expected). This correct behaviour of ROSETTA STR during acquisition is essentially due to the fact that both Sun and Earth avoidance angles were strictly respected. The acquisition problem encountered by MEX STR during wheel off-loading phases due to some high accelerations pushing the tracked stars outside their respective tracking windows has apparently not affected ROSETTA operations either. In any case, should ROSETTA experience high acceleration during WOLP, STR dust software modification which has been specifically developed for ROSETTA would enable immediate re-entry into tracking mode commanded by AOCS.

7.3.1.4.2 TRACKING PERFORMANCES

Although the STR is providing excellent accuracy and operating very well in general, it has experienced several “loss of track” problems that have still to be fully diagnosed. Normally STR locks on to 9 stars and tracks them as long as they remain in the FOV. On DOY 111, during period of inertial pointing of ALICE payload to warmer attitude to heat up the ALICE cover, STR A reported only 6 stars tracked. On DOY 116, STR even reported loss of all stars and went out of tracking.

On at least two separate occasions as illustrated in Figure from previous section, a relatively important increase in maximum innovation has been observed. On all cases the sudden jump of the innovation value associated with slight degradation of attitude estimate were identified while some specific stars were entering STR field of view; in particular stars referenced in a on-board catalogue ID 1717 and ID 1856. The observed maximum pointing error was 0.1deg. Although the consequence on gyro-stellar estimation seemed very similar, the investigations of star ID 1717 and ID 1856 anomalies has led to slightly different causes:

- In the case of ID 1717, it has been identified that the definition of the on-board catalogue was the source of the problem. In the current catalogue stars under certain angular distance threshold are merged into one, which is then incorporated in the on-board catalogue. Star ID 1717 is for instance resulting from the merge of three different stars. The problem is that the faintest star signal in ID 1717 cluster is exactly matching the detection limit of STR CCD resulting in strange toggling behaviour and degradation of single star measurement accuracy. The straightforward

corrective action will be to reduce the distance threshold and to uplink a newly generated catalogue.

- In what concern ID 1856, Flight Dynamic Team spotted that STR had actually confused ID 1856 in its on-board catalogue with another star referenced 79072 in the Hipparcos catalogue. Early investigation indicates that distortion compensation of star position on the CCD has not been correctly implemented within the STR software leading to possible incorrect selection of stars to be tracked. It has however to be noted that this problem only affects the star cluster filtering function and that once stars selection and linking is performed then correct distortion compensation is applied to compute STR quaternion.

Although investigations are still on-going, the STR measurement outages (including STR glitch observed on LEOP pass 5) could most likely be linked to the erroneous matching of star ID 1856. This minor deficiency of STR could most likely be solved by STR software patch including modification of both triad and star catalogues. In any case in has to be born in mind that in the vast majority of tracked stars, there is very good agreement between measured error position and performance analysis.

The measured magnitude accuracy has not been fully characterised during the commissioning period but it is deemed to not appreciably affect the STR performances, as the algorithms have been designed so that the magnitude check is used only as a filter out check, but not strictly used for attitude measurement or pattern matching.

In conclusion, both STR AA&CAD and AT&FAD modes have worked very well. STR acquisition capability and detection limit has not been degraded due to stray light effects. The preliminary evaluations of STR A and B performances have shown that single star accuracy requirements both in terms of position and magnitude are met. From a pure operational point of view, successful uplinking of STR software patch on DOY 090 has enabled the correct multiplexing on the interface bus with AIU rending thus possible to operate both STRs in parallel.

7.3.1.5 NAVCAM

NAVCAM A and B were not operated during this commissioning period CVP part 1. It is planned in part 2.

7.3.1.6 REACTION WHEELS

Following transition to SHM on DOY 062, RWs were spun up and a higher than expected friction torque (but still within limit) was observed. This trend was again observed over the whole LEOP phase where RWs friction torque was confirmed to be unexpectedly high. This high friction torques of the Rosetta wheels was a problem for the spacecraft for its AOCs FDIR, which, amongst others, checks the reaction wheel

friction torques and commands transition to a different wheel configuration or to safe mode if 0.05 Nm friction torque level is exceeded. A specific RWAs friction torque characterisation was then decided on DOY 066.

This test consisted in gradually increasing speed levels on the four wheels (fourth wheel spun-up but not yet in AOCS loop) and to explore the friction torque over most of the wheels operational range. After each commanded step in speed levels, the friction torque magnitudes showed, after a short drop, a corresponding jump and then a slow decrease. The magnitude of friction torque was increasing slightly less than linear with angular momentum for all 4 wheels. The results from this RWAs friction torque characterization are summarized in the following Table.

	Friction Torque	Updated Operational Limit ⁽¹⁾
RW 1	-0.030 Nm @ 35 Nms	35 Nms
RW 2	0.030 Nm @ -31Nms	31 Nms
RW 3	0.035 Nm @ -31 Nms	31 Nms
RW 4	-0.030 Nm @ 24 Nms	24 Nms

⁽¹⁾ RW operated below 0.039Nm below angular momentum limit.

Table 5: Friction Torque Characterisation

In perfect accordance with acceptance test results, RW 1 showed the best performance while RW 4 that was also expected to have relatively low friction torque was actually quite high due to the fact that this RW was just switched on before characterization test.

The operational range for RW 2 and RW 4 was then further extended to 36Nms. Several trend analysis carried out after several weeks of run has demonstrated a satisfactory and consistent convergence of the friction torque towards levels observed during acceptance testing of the respective four wheels as depicted in the following Figure. Ultimately limitation on RW speeds was waived on all four wheels due to consistent decreasing of friction torque.

	Inertia [kgm ²]	Coulomb Torque [Nm]		Viscous Coefficient [Nm/rad]	
		Specification	Acceptance	Specification	Acceptance
RW 1	0.09385	0.005	0.004	0.0000800	0.0000595
RW 2	0.09347	0.005	0.004	0.0000800	0.0000941
RW 3	0.09473	0.005	0.003	0.0000800	0.0000739
RW 4	0.09410	0.005	0.003	0.0000800	0.0000596

Table 6: RWAs Specification and Acceptance Data

Finally it is worth adding that most of the RWAs friction torque monitoring was made under very stable thermal conditions with the RW base plate around 25deg.

In conclusion, the high friction torque observed at the beginning of the ROSETTA mission although unexpectedly high could be retrospectively explained by settling of lubrication system and had no implication on performances of ROSETTA AOCS apart from temporarily increasing the frequency of Wheel Off-Loading in order to alleviate the limitation in RWs speed ranges.

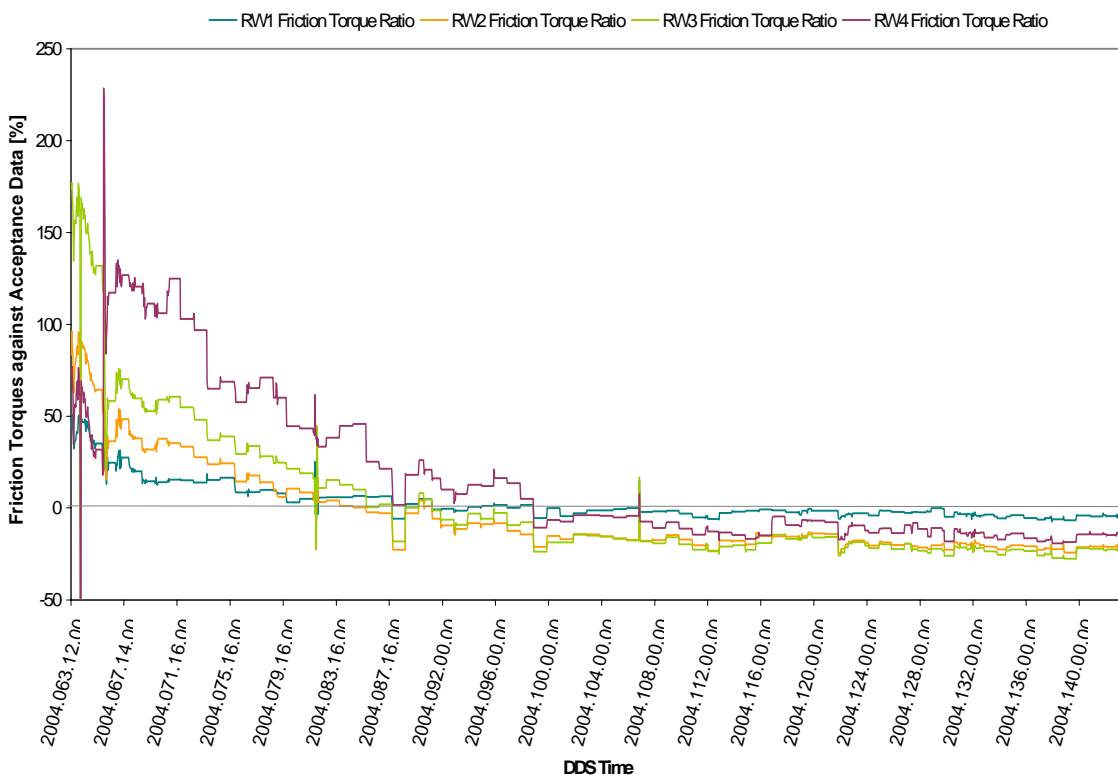


Figure 7.2: Friction Torque Evolution Against Acceptance Level

7.3.2 DYNAMICS AND DISTURBANCE TORQUES

7.3.2.1 SPACECRAFT INERTIA IN-FLIGHT CALIBRATION

During the current mission phase, the pointing requirements are less stringent and the on-ground prediction of the spacecraft moments of inertia is largely sufficient to ensure adequate AOCS pointing performances. Furthermore the presence of a large amount of fuel inside the tanks would prevent an accurate in-flight calibration of the spacecraft moments of inertia in those phases. Consequently in-flight calibration of spacecraft inertia has not been performed during the commissioning period.

7.3.2.2 SA FLEXIBLE MODES FREQUENCY CALIBRATION

On DOY 070 calibration of solar arrays flexible mode characteristics, i.e. the free-free frequencies and the free-free damping ratios, was conducted. This calibration is of interest, because if these free-free frequencies turned out to be quite different from the expected ones, there could have been an impact on the controller tuning and on the performances of all AOCS modes. Furthermore this calibration could confirm that the solar arrays deployment has been successfully performed with no hinge failure. The following Table summarized results extrapolated from telemetry retrieval.

	Free-Free Frequency (Hz)		Free-Free Damping Ratio	
	Predicted	Observed	Predicted	Observed
1 st Out-Of-Plane	[0.17..0.22]	0.19	7.5e-3	1.27e-2
2 nd Out-Of-Plane	[0.43..0.51]	0.5	-	-
1 st In-Plane	[0.60..0.96]	0.81	-	3.5e-3
1 st Torsion Mode	[0.51..0.60]	0.59	2.5e-3	4.1e-3

Table 7: Solar Arrays Flexible Mode Characteristics

The 1st Out-Of-Plane mode free-free damping ratio is higher than predicted free-free damping ratio however it was expected since the predicted free-free damping ratio has been computed from a worst-case minimum Cantilever damping ratio of 2.5e-3. The real cantilever damping ratio of the 1st Out-Of-plane seems to be around 4.2e-3

The free-free frequency in-plane mode is sufficiently high to ensure that there will be no resonance between this in-plane flexible mode and the OCM thruster actuation frequency (0.667Hz). It is not necessary to set OCM thruster actuation frequency to 1Hz.

The free-free damping ratio is lower than the predicted free-free damping ratio at 6.4e-3Hz. This was not expected, and means that the cantilever damping ratio of this in-plane flexible mode is around 1.36e-3, i.e. lower than the assumed worst-case minimum cantilever damping ratio at 2.5e-3Hz. This result is surprising, but will have no effect on the behaviour of the AOCS. PID controllers used in NM and OCM (the in-plane free-free frequency being always much higher than the cut-off frequencies).

The free-free damping ratio for the torsion mode is higher than the predicted free-free damping ratio at 2.5e-3Hz. The real cantilever damping ratio for this torsion mode seems to be around 4.14e-3Hz, i.e. higher than the worst-case minimum cantilever damping ratio of 2.5e-3Hz, and similar to the out-of-plane flexible mode cantilever damping ratio at 4.2e-3Hz.

All SA flexible mode characteristics are as expected with the exception of the cantilever damping ratio for in-plane flexible mode, but this has no consequence on the AOCS

controllers. Since the in-plane free-free frequency is as expected, it was not necessary to modify the OCM thruster actuation frequency.

7.3.2.3 DISTURBANCES TORQUE

The external torques and their evolution during the first week have been monitored rather closely and related data, recorded at beginning and completion of LEOP phase are recalled in the following Table.

		X	Y	Z
Observed Disturbance Torque on DOY 063	[μ Nm]	-28.0	76.4	21.4
Observed Disturbance Torque on DOY 066	[μ Nm]	-5.0	64.4	4.0
Predicted Max Disturbance Torque ⁽¹⁾	[μ Nm]	59	232	190
Predicted Max Momentum Loading	[Nms/day]	5.1	20.1	16.5

⁽¹⁾ Maximum solar disturbance at 1AU extracted from RO-DSS-TN-1028

Table 8: External Disturbance Torque

The disturbance torques were also observed higher in the Sun-biased attitude, which was the current baseline attitude, than in the +X_{SC} Sun pointing attitude (previous baseline) resulting in consumption of fuel increase from 50g/week instead of 10g/week. In any case these torques remained lower than predicted maximum values.

About 4 days after launch the spacecraft had largely stopped outgassing and one may expect that the latest values will remain valid as long as the Sun-spacecraft distance does not significantly increase. The large T_Y component is entirely due the high gain antenna being rotated to about -50 deg elevation and -180 deg azimuth, i.e. largely looking under the spacecraft and thereby creating a substantial Sun radiation pressure torque around the spacecraft y-axis.

7.3.3 POINTING PERFORMANCES

7.3.3.1 SOLAR ARRAY POINTING ACCURACY

There is no currently available detailed evaluation of SA pointing accuracy including APE of SA rotation and SA rotation control errors. However ROSETTA early operations have shown that the array pointing accuracy met system requirements and is in particular compatible with spacecraft power requirements. SA pointing performance was nevertheless the opportunity to address performances of AOCS safe modes.

Absolute Pointing Error between the Sun and the selected SAS bore-sight axis in both SAM and SKM has been within specification. SHM has enabled correct stars acquisition of both STR A and B and flawless transfer from thruster based AOCS to RWAs actuation. Actual convergence of the solar arrays within 20° was 250s very much below the required duration.

7.3.3.1.1 SUN ACQUISITION MODE

After separation from the AR5 launcher, the Spacecraft remained in SBM for 20 seconds while angular rate exchanges between axes leading to higher angular rates were observed. Following the automated sequence after separation and RCS priming, rate reduction phase was correctly entered at 9:45:53UTC.

SC Angular Rates [°/s]		X	Y	Z
@ 09:44:33 UTC	First IMP-A TM Packet	0.568568	0.604101	-0.185055
@ 09:45:53 UTC	Initial RRP	0.471121	0.676621	-0.212999

There were no over-rates observed nor triggering of FDIR related surveillance due to the impact of liquid sloshing as anticipated in RO.MMT.TN.2193. These angular rates were then successfully reduced after 40 sec. Then, in SCP phase a rate bias of 1°/s (0.017rad/s) about X_{SC} axis was commanded and Sun position was first detected at 09:46:55 UTC.

Sun Direction in X SAS Frame [°]		Azimuth	Elevation	Sun Aspect Angle
@ 09:46:55 UTC	First Detection in SCP	19.08	-17.85	TBC

When the Sun entered its capture zone (XZ SAS is illuminated), the rate bias was then cancelled and transition to SAP phase was performed. In SAP, a rate bias of 1.3°/s (0.023rad/s) about Y_{SC} axis was then commanded to capture the Sun close to the X_{SC} axis. During this rotation, rate biases of 0.15°/s (0.0026rad/s) were commanded about X_{SC} and Z_{SC} axes to prevent the Sun from getting too far away from the XZ plane. When the Sun was close enough from X_{SC} axis (X SAS illuminated), the rate bias about Y_{SC} axis was cancelled and transition to SPP phase was performed. SPP ensured a satisfactory pointing of X_{SC} axis towards the Sun. In BPP phase, the spacecraft was commanded to point X_{SC} axis at 45° away from the Sun. BPP convergence occurred after only 192 sec and Spacecraft autonomously switched back to SBM at 09:52:54.

Duration [s]		Predicted		Required	Observed
Entry	Phase	Mean	1 σ		
@ 09:45:53 UTC	RPP	53	11		40
@ 09:46:33 UTC	SCP	135	81	-	100
@ 09:48:13 UTC	SAP	102	30	-	76
@ 09:49:29 UTC	SPP	12	5	-	10
@ 09:49:39 UTC	BPP	174	1.8	-	192
	SAM	476	87	900	418

The SAM actual duration was therefore significantly lower than requirement.

SC Angular Rates [°/s]	X	Y	Z	Required
Final in RPP	-0.98820	0.009182	-0.00175	0.25
Final in SCP	-0.00507	0.004534	0.00289	0.10
Final in SAP	-0.00254	-0.00682	-0.00118	0.10
Final in SPP	-0.00045	-0.02432	0.002417	0.10 (0.017 around X _{SC})
Final in BPP	0.00203	0.01752	0.003562	0.02

X SAS Pointing Error in SAS Frame [°]	Azimuth	Elevation	Sun Aspect Angle	Required
Final in SAP	0.1636	-0.6154	TBC	-
Final in BPP	18.3770	-0.6994	TBC	45±4 Az and SAA 4 EI

After successful deployment of the Solar Arrays, SAM was correctly re-entered at 10:10:09 UTC and second Rate Reduction Phase meant to dump SA flexible mode motions was completed in 20 sec. Initial rates at RRP entry were the following:

SC Angular Rates [°/s]		X	Y	Z
@ 10:10:09 UTC	Initial RRP	-0.0216242	0.0135883	0.0092097

Then, in SCP phase a rate bias about X_{SC} axis was again commanded. In SAP, a rate bias about Y_{SC} axis was commanded to capture the Sun close to the X_{SC} axis. When the Sun was close enough from X_{SC} axis and with low residual rates, the rate bias about Y_{SC} axis was cancelled and transition to StAP phase was performed. SAs were also commanded to rotate to their canonical position, i.e. pointing SA normal towards +X_{SC} axis. StAP enabled the Star Tracker to perform the star acquisition and the attitude estimator to initialise before entry into the SHM. SKM transition occurred at 12:05:05 UTC.

Duration [s]		Predicted		Required	Observed
Entry	Phase	Mean	1 σ		
@ 10:10:09 UTC	RPP	230	126	-	20
@ 10:11:29 UTC	SCP	251	107	-	96
@ 10:13:05 UTC	SAP	144	53	-	108
@ 10:14:53 UTC	StAP	229 ⁽¹⁾	101	-	6594
	SAM	-	-	900 ⁽²⁾	6818

⁽¹⁾ Duration of StAP_CONV

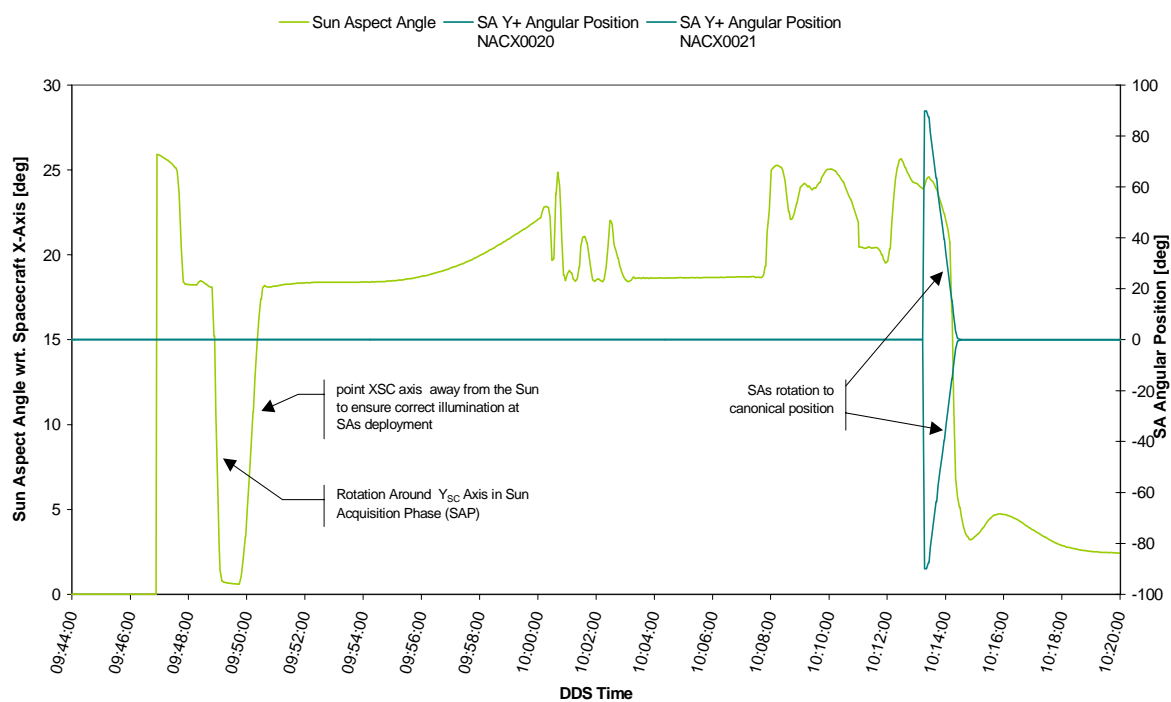
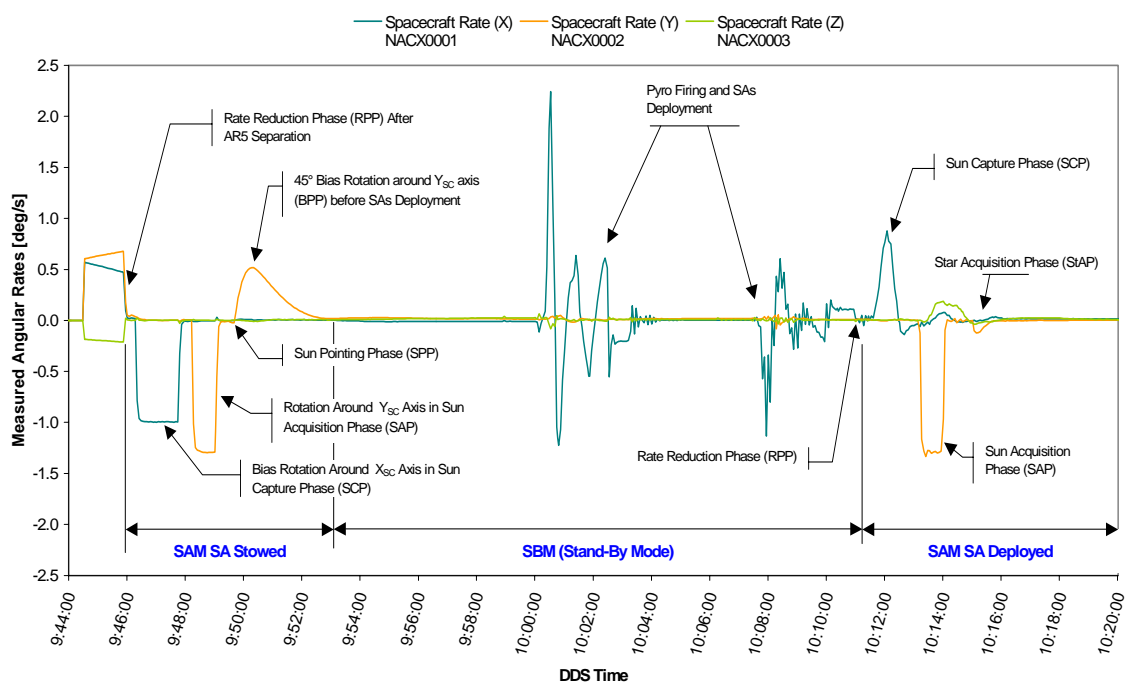
⁽²⁾ Duration specified to fulfil all StAP exit conditions including STR convergence under normal operations, which were obviously different from followed LEO sequence

SC Angular Rates [°/s]	X	Y	Z	Required
Final in RPP	0.000403	0.012009	0.003975	0.25
Final in SCP	-0.0394	0.003138	-0.00224	0.10
Final in SAP	-0.00491	-0.00553	-0.0014	0.10
Final in StAP	0.0125	-0.00094	-0.00087	0.05

SA Convergence [s] (SAA ≤ 20°)	Predicted		Observed	Required
	Mean	1 σ		
First Solar Array	525	215	250	-
Second Solar Array	525	219	250	-

Pointing Error of X SAS in SAS Frame [°]	Azimuth	Elevation	Sun Aspect Angle	Required
Final in SAP	0.9547	-2.865	TBC	-
Final in StAP	-1.9503	1.5031	TBC	5

Star acquisition was then first commanded to STR-A at 11:25:01UTC. But when STR-A was switched on it was apparently blinded by the Earth and could not perform acquisition as predicted from the MEX experience. It was therefore replaced temporarily by STR-B, which successfully acquired stars and entered autonomous tracking mode.



7.3.3.1.2 SUN KEEPING MODE

The Spacecraft was commanded to SBM at 12:05:05 UTC and entered SKM at 12:05:09 UTC. As the SHM entry was not allowed, after StAP phase the transition to MGA. The rate bias around the Sun line along $+Z_{SAS}$ of $0.017^\circ/s$ was still applied and SAs were commanded to rotate to reach their commanded position. When both SAs had reached their commanded position, transition to ESM was further performed. StAP was exited at 12:07:40 UTC and SKM/ESM to SHM transition was commanded at 13:52:15 UTC directly by enabling the SHM Entry Flag. There was no need to stop the strobing motion first.

Duration [s]		Predicted		Required	Observed
Entry	Phase	Mean	1 σ		
@ 12:05:09 UTC	SAP	144	53	-	84
@ 12:06:33 UTC	StAP	229	101	-	67

Duration [s]		Predicted		Required	Observed
Entry	Phase	Mean	1 σ		
@ 12:07:40 UTC	SAR	2205	700	-	1413
@ 12:31:13 UTC	ESM	7452 ⁽¹⁾	2597	-	4862
	SKM	-	-	-	6426

⁽¹⁾ Including EAH Phase

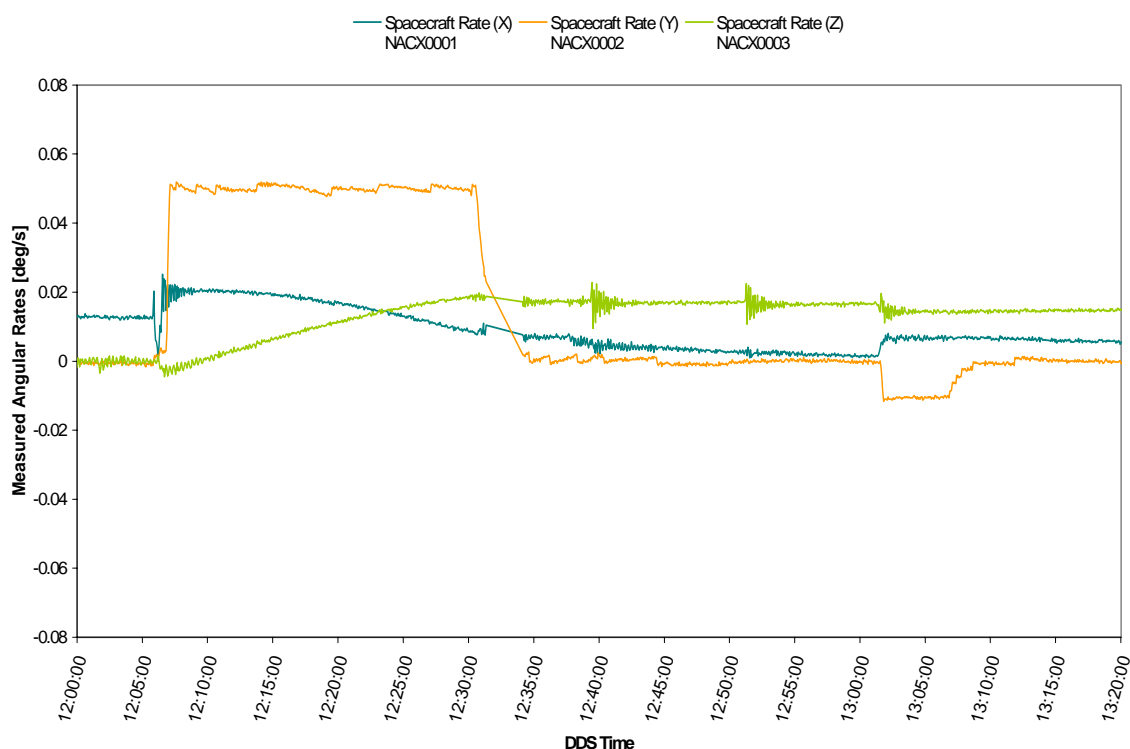
In SAR, the solar arrays angular rate to reach their commanded position was $0.05^\circ/s$. As the selected SAS was commanded to point the Sun, the spacecraft rotated around Y_{SC} . The SAR maximum angular rate about Y_{SC} axis was reached at entry in SAR during the transient period. In SAR, the commanded bias around Z_{SAS} axis remained $0.017^\circ/s$. The maximum angular rates about X_{SC} and Z_{SC} axes resulted from flexible mode excitation when thrusts are fired to control the central body attitude.

In ESM, the commanded bias about the Z_{SAS} axis was kept to $0.017^\circ/s$. In EAH, rates are commanded to zero. Maximum angular rates are reached at entry in EAH, when the bias about the Z_{SAS} axis was cancelled.

Max SC Angular Rates [$^\circ/s$]	X	Y	Z	Required
SAP	0.02520118	0.00232744	-0.00230623	-
StAP	0.01739588	0.05192144	-0.00214329	-

Max SC Angular Rates [$^\circ/s$]	X	Y	Z	Required
SAR	0.00865842	0.02471129	0.01771223	-
ESM	0.00592379	-0.00156537	0.01615640	-

Pointing Error of X SAS in SAS Frame [°]	Azimuth	Elevation	Sun Aspect Angle	Required
Final in SAP	-1.872	1.472	TBC	-
Final in StAP	0.205	1.326	TBC	5



7.3.3.1.3 SAFE HOLD MODE

The first rotation along Y_{SC} axis brought the Sun direction into plane defined by Y_{SC} axis and final Sun direction. The second rotation along XZ plane axis oriented the Sun along its final direction and the third rotation around the Sun direction enabled to reach the 3 axis stabilized final attitude. Transition to Normal Mode was commanded at 14:47:40 UTC.

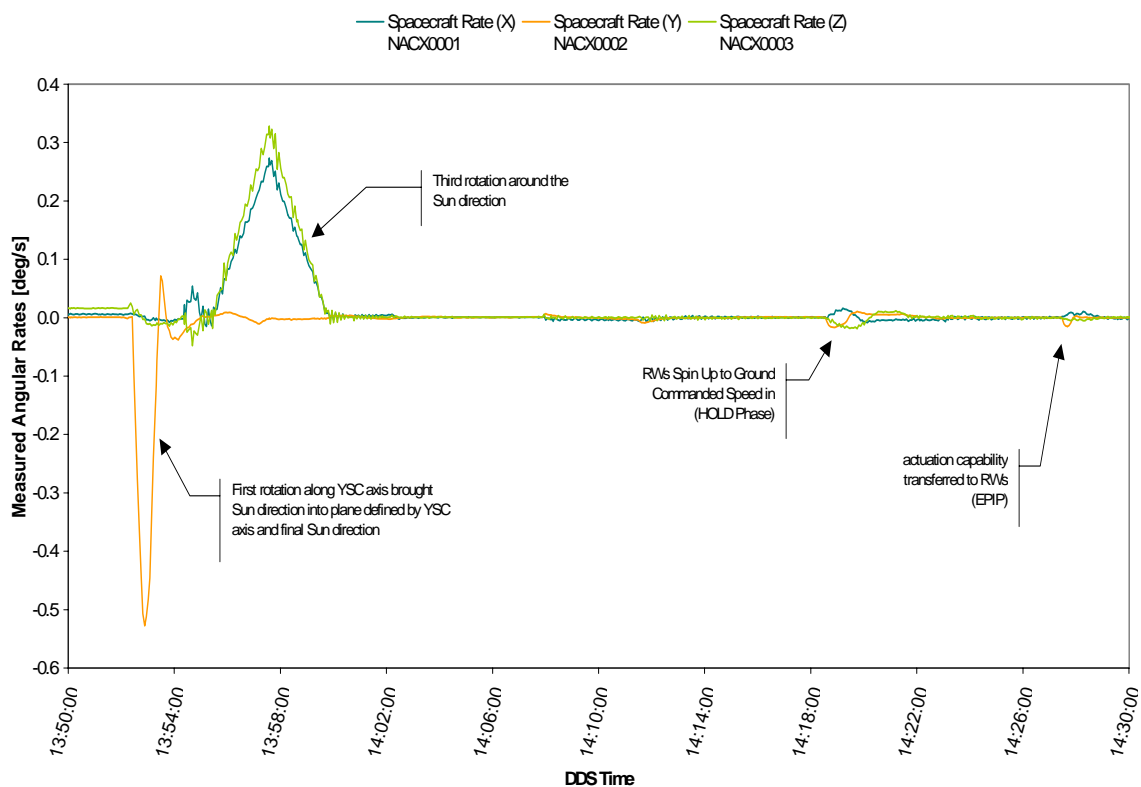
Duration [s]		Predicted		Req.	Observed
Entry	Phase	Mean	1 σ		
@ 13:52:15 UTC	SHM 1 st Stabilisation	24	13	-	61
@ 13:53:16 UTC	SHM 1 st Rotation	104	38	-	65
@ 13:54:21 UTC	SHM 2 nd Stabilisation	47	17	-	127
-	SHM 2 nd Rotation	34	28	-	-
-	SHM 3 rd Stabilisation	32	22	-	-
@ 13:56:28 UTC	SHM 3 rd Rotation	328	123	-	256
@ 14:00:44 UTC	SHM 4 th Stabilisation	25	11	-	-

-	SHM HOLD	1	0	-	1600
@ 14:27:24 UTC	SHM EPIP	260	45	-	64
@ 14:28:28 UTC	SHM EPP	2033	136	-	1152
	SHM	-	-	-	3264

SC Angular Rates [°/s]	X	Y	Z	Required
SHM	TBC	TBC	TBC	-

SA Max Pointing Error (rad)	Predicted		Observed
	Mean	1 σ	
Solar Array Y_{sc}^-	-	-	TBC
Solar Array Y_{sc}^+	-	-	TBC

SA Max Pointing Error (rad)	Azimuth	Elevation	Sun Aspect Angle	Required
SHM HOLD entry	TBC	TBC	TBC	-
SHM HOLD	TBC	TBC	TBC	-
SHM EPIP	TBC	TBC	TBC	-
SHM EPP	TBC	TBC	TBC	-



7.3.3.2 ABSOLUTE POINTING ERROR OF THE HGA

During spacecraft maintenance activity in CSG, several APM movement overshoots were experienced on the PFM spacecraft while the HGA was commanded to rotate over large azimuth and elevation angles. These spurious overshoots could not be reproduced on PFM and after thorough investigation supported both by analysis and EQM testing, the APM design was deemed sufficiently robust the gain of the controller was however altered in order to give more margin against overshoot. Under these circumstances great attention has been paid to the in-flight deployment of the high gain antenna. In particular memory cell acquisition at 8Hz of the APM encoder raw measurements was performed over the whole deployment sequence. This sequence consisted of three successive rotations, which are recalled on Figure 7.3 from following page. Post treatment of memory cell acquisition has shown fully nominal behaviour with no overshoot occurrence or spikes observed on the APM encoder angular measurements.

Since it was originally suspected that occurrence of spikes of the encoder lines were position dependent, the angular excursion over rather long-term period have been monitored. The following figure shows the evolution of both measured elevation and azimuth angles over the commissioning period. Most of the operational range has been explored without any observed overshoot even under once a day HGA re-pointing work around confirming thus the good performance of the APM.

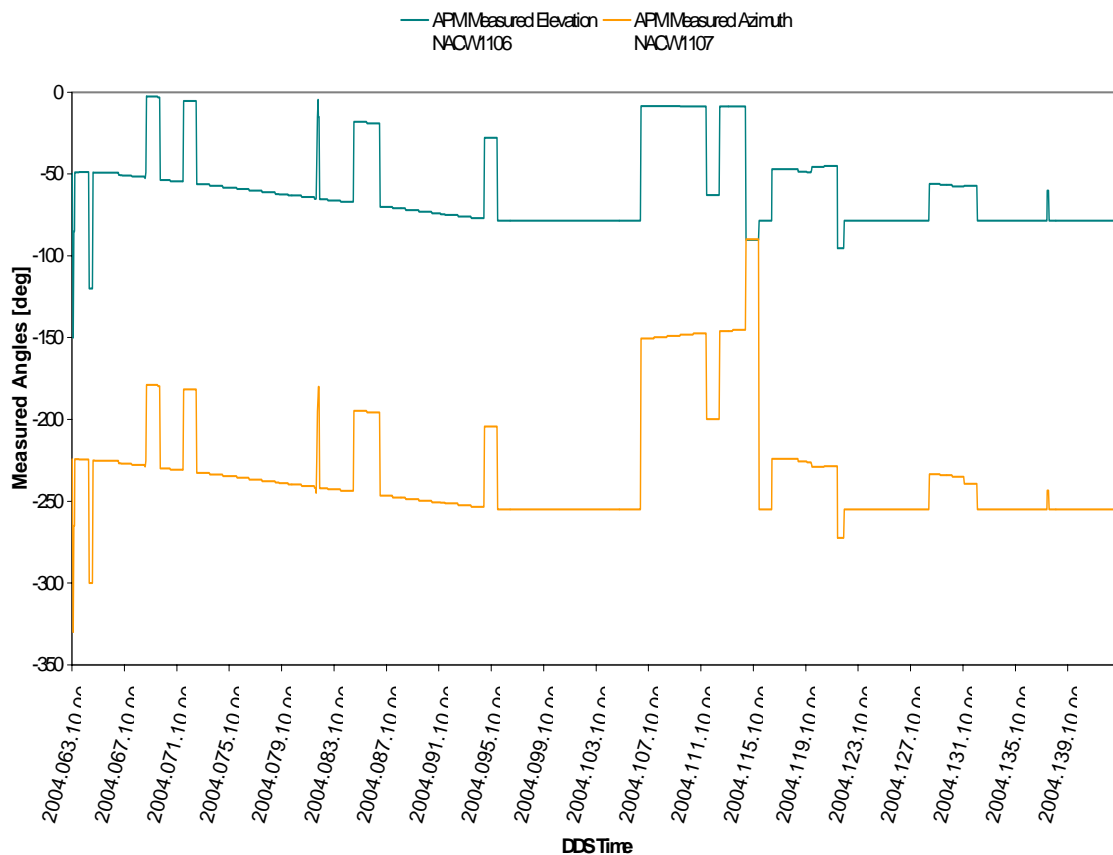


Figure 7.3: APM Measured Angular Position History

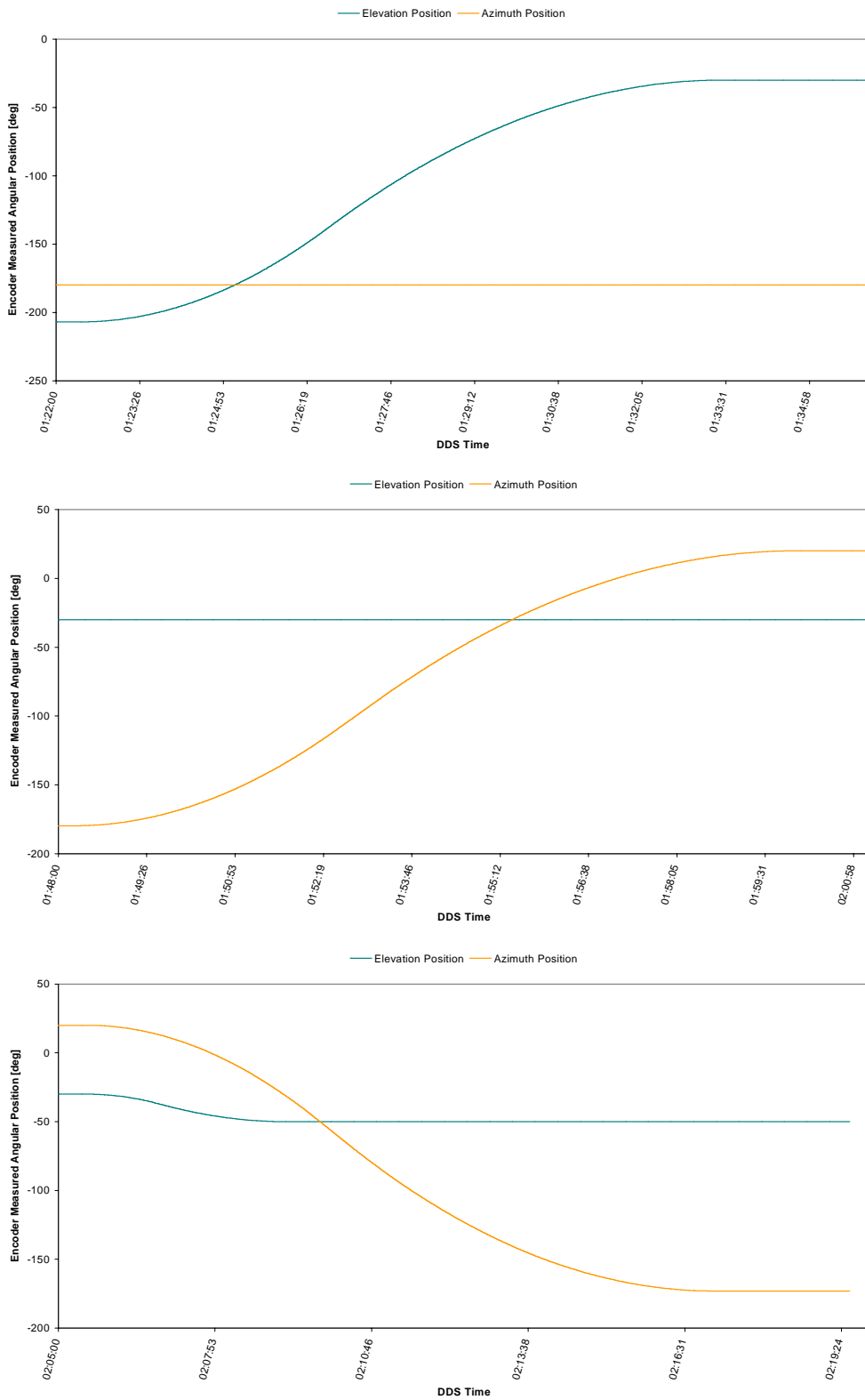


Figure 7.4: HGA Deployment Rotations

7.3.3.3 APE AND RPE FOR OPERATIONAL PHASES

During the spacecraft commissioning the pointing requirements were not very stringent and consequently there has been no need for an intensive evaluation of the absolute and relative pointing performances under either observation or detection phases. Moreover full STRs misalignments calibration and STR to CAM misalignment calibration, which play a major contribution in the overall pointing performances, were not planned over this commissioning period. Nevertheless operational experience gained over the first months of this mission together with the preliminary evaluation from flight dynamics has given good confidence that pointing requirements will be met with sufficient margins. From DOY 091 to DOY 094, during MIRO slews high frequency attitude measurements were downlinked to allow preliminary evaluation of the spacecraft pointing performance. The results refer to the first pointing on DOY 091 but are consistent with figures observed on other days of MIRO commissioning.

The depointing of the spacecraft Z-axis based on the on board estimated attitude w.r.t. the on ground attitude profile (which is delivered to the DDS) is always below 18 mdeg. The maximum depointings around the individual SC axes are:

+/- 18 mdeg around X

+/- 10 mdeg around Y

+/- 3 mdeg around Z

This appears to slightly exceed the 12.6 mdeg value for around the X axis listed in the AOCS pointing budget.

The depointing of the spacecraft Z-axis based on the on board estimated attitude w.r.t. the on board attitude profile is below 12.5 mdeg. This is slightly within the 12.6 mdeg which are assumed in the AOCS pointing budgets. The depointing shows the same periodic behaviour as spacecraft rates, i.e. the controller shows a time lag.

The difference between previous results are most likely due to the conversion of the segment start and end times into integer OBT counts. It seems that the times converted into OBT are always truncated (not rounded). This resulted e.g. in one case in an offset of about 0.9 sec of the segment end time. For this segment, the depointing between the on ground and on board attitude profile reached about 5 mdeg around the X and Y axes close to the segment end time.

The depointing of the spacecraft z-axis based on the STR estimated attitude w.r.t. the on ground attitude profile is also always below 18 mdeg. The depointing of the STR estimated attitude and the on board estimated attitude is in the order of 4 mdeg, which is close to the specification of the noise equivalent attitude error of the STR.

The on-board alignment between STR A and STR B is off from the actual alignment by about 40 mdeg (as already observed when the guidance options were changed). This is a mean value. Over time, the relative alignment shows (apart from temporal noise) a variation depending on the spacecraft attitude which is most probably due to the STR random bias (thermo elastic distortion could be another reason). This variation is in the order of 5 mdeg which is consistent with the budget value in the AOCS pointing budget.

In conclusion, the contribution of spacecraft attitude dynamics, estimation and control to the AOCS pointing budget of AOCS pointing budgets seems slightly exceeded. Due to the margin of about 8 mdeg in the total budget, the total error is just within the required limit of 30 mdeg. The main reason for the higher depointing is the difference between the segment start and end times in UTC and OBT due to truncation. The performances of the stellar estimator and the STR (noise and bias) are consistent with the budget. The higher depointing is still small compared to the margins, which are taken in the system requirement on the absolute pointing accuracy of 0.1 deg. The pointing performance will be re-addressed during CVP part 2.

7.3.3.4 DELTA-V ACCURACY

In complement to delta-V accuracy addressed in the ground segment performance report this section present more specifically performance of the ramp-up phase for OCM. In order to limit transients and excitation of equivalent flexible modes, a thrust ramp is actually implemented in OCM. The thrust is linearly increasing from $\tau=0.05$ to $\tau=1$ in 1500 sec, where τ is the thrust ratio. According to the measured angular rates, it could be confirmed that no re-tuning of the OCM controller is needed to adapt actual SA flexible mode frequency. In accordance with simulations predicting angular rates lower than $0.035^\circ/\text{s}$ for BOL configuration, the measured rates have not exceeded $0.02^\circ/\text{s}$ during the ramp-up phase of DSM. The associated acceleration has apparently not affected quality of STR measurements by pushing the tracked stars outside their respective tracking windows.

The statistics on the maximum values of the overall disturbance torques observed during simulations at BOL have led to typical values of 0.48 and 0.57Nm respectively around X_{SC} and Y_{SC} axis. The estimations of disturbance torque are fully consistent with the predicted values. As expected, disturbing torques are maximum about X_{SC} and Y_{SC} axis, i.e. perpendicular to the thrust direction. The on-board estimated disturbing torques are increasing with the applied force (increase due to the ramp) and are stabilized a few seconds after the end of the increasing phase of the ramp. A drop is observed due most likely to the residual effect of liquid sloshing modes on X and Y axis.

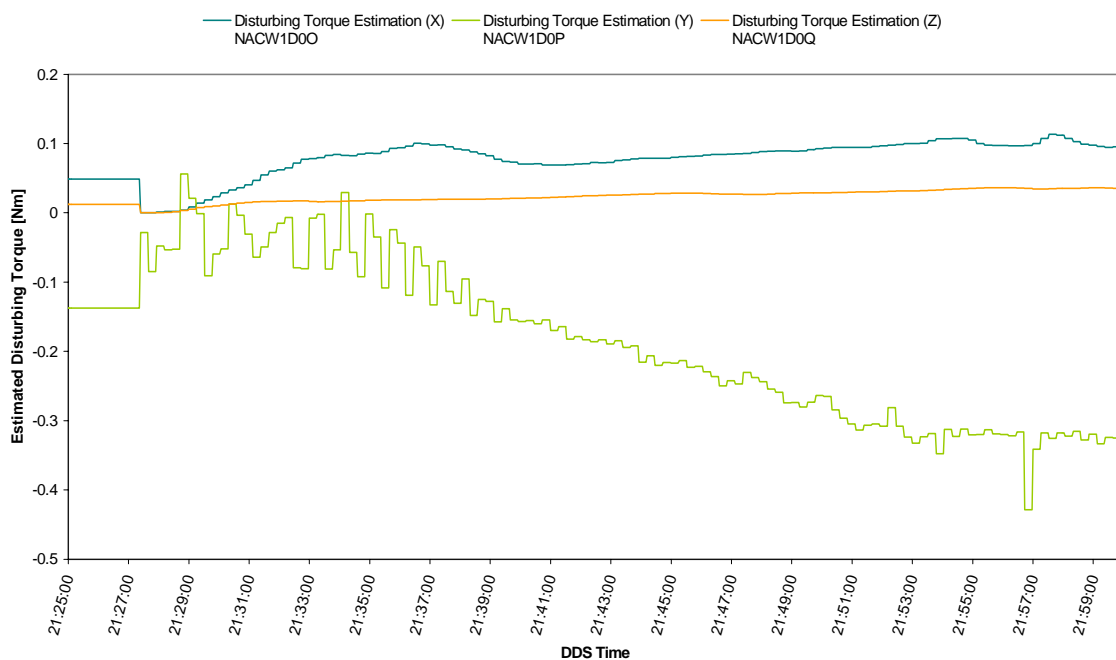
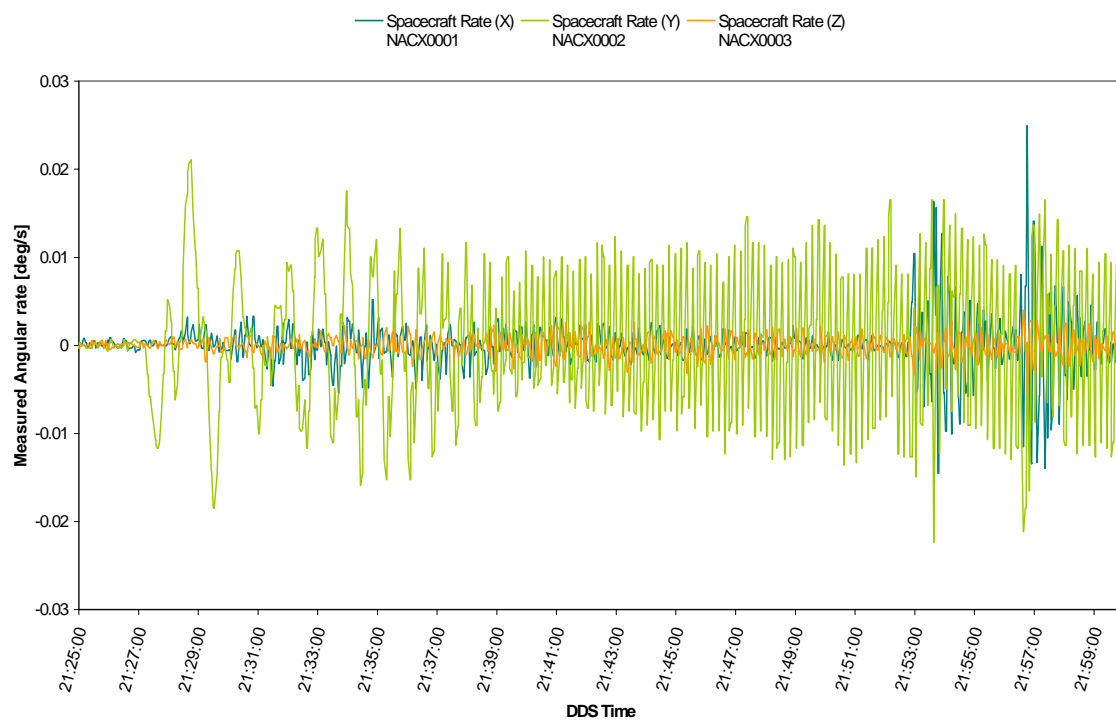


Figure 7.5: Deep Space Manoeuvre Ramp-Up Phase

7.3.4 FUEL CONSUMPTION

The fuel consumption and the associated number of thruster cycles observed on first day of mission DOY 062 are summarized in the two following Tables. These figures are in particular to be related to daily consumption for SHM and SKM/ESM modes of respectively 72g/day and 90g/day, as anticipated in the AOCS budget. In what concerns SKM and ESM, the observed total consumption was 25g over 6425 seconds resulting into a consumption of approximately 336g/day. The daily consumption of 90g was extracted from simulation set #3.5 in AOCS note RO-MMT-TN-2083. However, the scenario of set #3.5 included only 120 simulations ran over different conditions than the one observed during the LEOP phase (BOL during Mars fly-by, EOL during Deep Space Cruise) making thus typical value not easily comparable to the actual consumption value (maximum value in steady-state configuration of ESM loose is not mentioned in AOCS budget). The fuel consumption in Hold Phase which is not allocated to the reaction wheels spin-up have been roughly calculated between 14:06:17 UTC and 14:14:09 UTC. The estimated 3.7g resulted in 677g/day fuel consumption, which exceeded both the mean and maximum values of 72g/day and 164g/day quoted in AOCS budget. However, the over-consumption is largely due to the residual rates induced by excitation of the solar array flexible mode after third rotation. It was therefore not possible to reach steady state conditions that would have render comparison to the predicted values more conclusive... Although is it obviously difficult to have straightforward correlation between the observed fuel consumption and the statistical results from the AOCS simulations, performances are somehow higher than the predicted performances but deemed still within acceptable limits.

Pulse Budget	Predicted			Observed
	Max	Mean	1 σ	
SAM (SA Stowed)				
SAM	312	648	444	1516
SAM (SA Deployed)				
RRP	406	136	81	140
SCP	540	235	92	706
SAP	278	148	51	1606
StAP	112	63	23	1986
SAM	73	12	21	4438
SKM				
SAP	278	148	51	0
StAP	112	63	23	166
SAR	1360	-	-	132
ESM	1175 ⁽¹⁾	-	-	246
Total SKM	-	-	-	544
SHM				
SHM	936	567	147	4060

⁽¹⁾ Including EAH Phase

Table 9: Number of Thruster Pulses

Consumption [g]	Predicted			Observed
	Max	Mean	1 σ	
SAM (SA Stowed)				
RPP	857	384	174	70
SCP	126	77	24	35
SAP	291	213	31	140
SPP	5	1.6	1	2
BPP	150	115	13	68
SAM	1346	792	197	315
SAM (SA Deployed)				
RRP	2947	1646	599	6
SCP	831	522	165	298
SAP	453	326	66	248
StAP	46	21	9	86
SAM	12	3	3	638
SKM				
SAP	453	326	66	8
StAP	46	21	9	3
SAR	262	132	51	4
ESM	350 ⁽¹⁾	76	37	10
Total SKM	-	-	-	25
SHM				
SHM 1 st Stabilisation	37	6	5	51
SHM 1 st Rotation	348	180	67	29
SHM 2 nd Stabilisation	32	142	7	98
SHM 2 nd Rotation	104	34	30	-
SHM 3 rd Stabilisation	27	5	6	-
SHM 3 rd Rotation	353	224	75	186
SHM 4 th Stabilisation	14	1	2	-
SHM HOLD	0.4	0.1	0.1	45
SHM EPIP	224	118	30	0

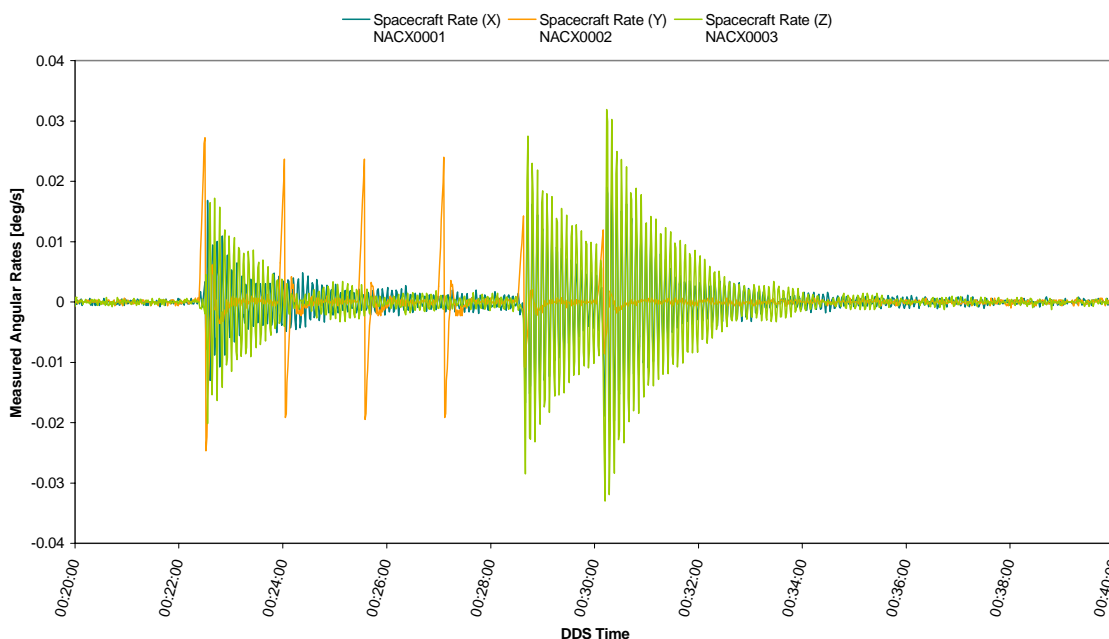
SHM EPP	-	-	-	0
SHM	1139	710	110	410

⁽¹⁾ Including EAH Phase

Table 10: Fuel Consumption Summary

Major contribution to the fuel consumption over long period is obviously WOLP. On DOY 066 wheel off-loading was performed before RW 4 was switched ON and subsequent characterisation of friction torque was conducted. The characteristics and timeline for this WOLP are to be found in the following Table and associated Figures. The maximum theoretical value of 82g for WOLP is reported in the AOCS budget while according to simulation campaign the typical consumption should be 15.94g. The observed consumption of 16g for a total transfer of momentum of 21.45Nms could be considered satisfactory.

H _{RWS}	[Nms]	@ 2004.66.00.22.30	@ 2004.66.00.32.05
RW 1		18.41	10.00
RW 2		-18.03	-5.00
RW 3		-5.80	-7.00
RW 4		0.00	0.00



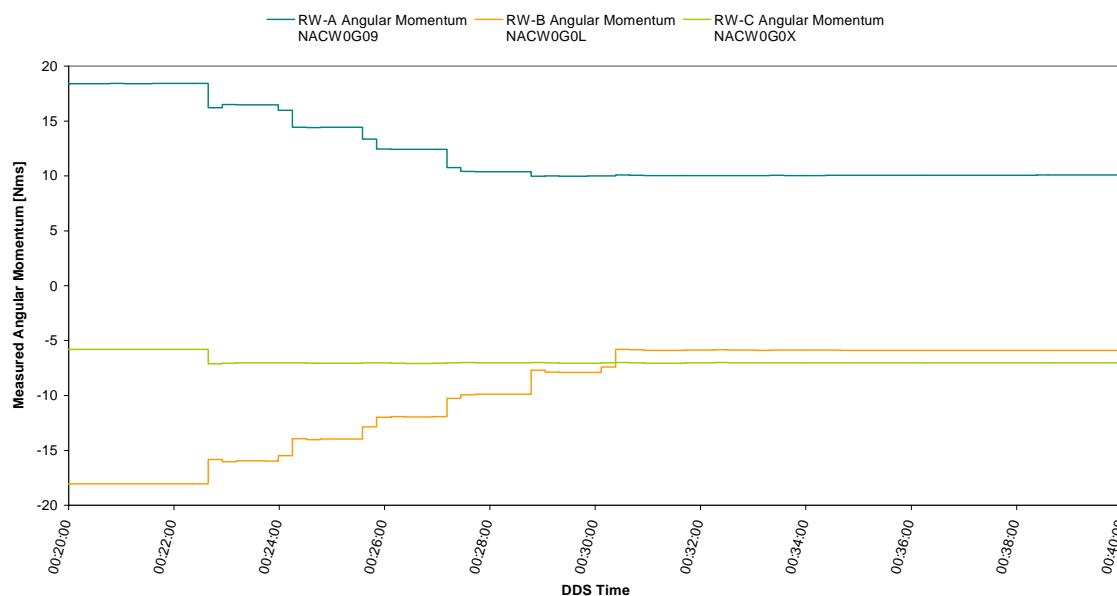


Figure 7.6: Wheel Off-Loading Characteristics

7.4 LESSONS LEARNED

TBC

7.5 CONCLUSION

The ROSETTA AOCS system has performed extremely well in its first months of operation and there are no significant AOCS problems outstanding at this time. However, some minor anomalies have been uncovered which will require some corrective actions like uplinking patches of either AOCS or STR software.

The AOCS system has consistently maintained spacecraft into the correct commanded attitude enabling the ROSETTA Operation Team to devote most of its effort and attention to payload commissioning. It has also to be noted that fairly complex AOCS FDIR has not unexpectedly interfered with normal operations and that on no occasion during the complete commissioning period the previously reported anomalies caused the spacecraft to enter its Safe Mode.

The analysis of in-orbit data is continuing to confirm correct behaviour of ROSETTA AOCS and full compliance of performances against system specifications.

The authors would like to acknowledge contribution of Flight Dynamics Team at ESOC and particularly Mathias Lauer in preparing this performance report.

8 RCS

This part of the report describes the behaviour and functional performances of the RCS as revealed by the first in-flight results.

Since separation, the RCS subsystem was fully nominal as summarised below. The RCS is operating since separation by means of its nominal thrusters.

8.1 From Launch to Separation

The RCS system was loaded with propellant and pressurised on ground according to the following:

- MON-1: 1059.5 kg
- MMH: 659.6 kg
- MON-1 tank pressure @ 24°C: 14.5 bar (abs)
- MMH tank pressure @ 24°C: 14.5 bar (abs)
- He tank pressure @ 24°C: 182 bar (abs)

The no-go launch criterion for the tank pressure was: pressure \geq 14.7 bar.

In order to fulfil the launch criterion with some margin, the temperature of the tanks was targeted to 22°C to provide a pressure level close to 14 bar. The final launch tank temperature on March 2nd, was about 20°C (see discussion of TCS paragraph 3.1) with pressure of 14.0 bar for MON-1 and 14.3 bar for MMH. When telemetry was acquired after separation and after priming of the thrusters lines, the pressure levels were:

- MON-1 tank pressure: 14.1 bar
- MMH tank pressure: 14.7 bar
- He tank pressure: 179 bar

The venting and priming of the nominal and redundant thrusters lines was performed by the automatic sequence initiated after separation. The opening of all FCV's and LV's for venting the lines could be monitored together with the pressure drop associated with the venting. Subsequent operation of the 'normally closed' pyro-valves 23, 24, 25 and 26 primed the lines up to the thrusters LV's⁴. Pyro firing went nominally as also reported in paragraph 2.5.3.

⁴ Because the redundant thrusters have never been fired so far, the redundant thrusters and their valves have not been filled with fuel yet.

The thrusters activity to stabilize the spacecraft after separation and after solar array deployment is documented by the chamber temperatures reported in fig. 8.1. The RCS performed exactly as expected.

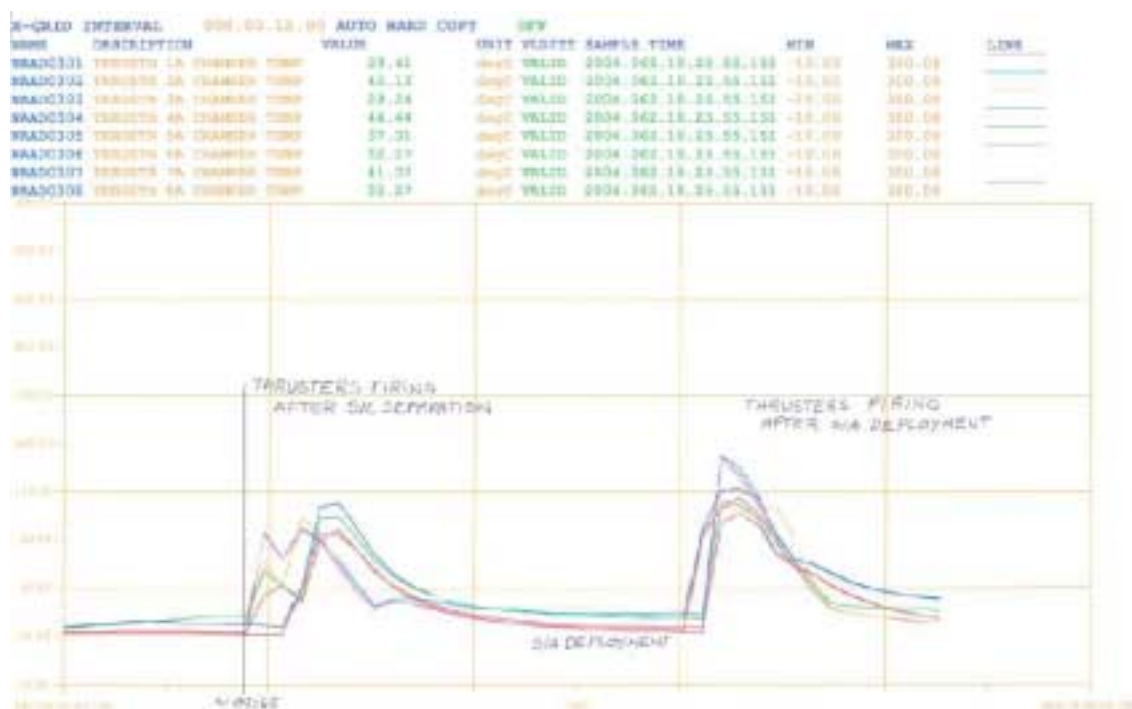


Fig. 8.1 – Thrusters activity after separation and S/A deployment. Temperatures of sensors close to the combustion chamber are reported.

8.2 LEOP Operations

The RCS subsystem performed several wheel off-loading operations during the early phases and a test of orbit correction of 1 m/s was performed on March 3rd. The activity of the thrusters used for the delta-V is documented by the temperatures reported in fig. 3.3. The performances of the RCS evaluated by ESOC (RCS ref. 1), are:

Target delta-V: 1 m/s Estimated achieved: 0.981 m/s error: 2%
 (accuracy of the measurement method: 0.3%)

8.3 First RCS Pressurisation

The first propellant tank pressurisation took place on May 6th. Before pressurisation, the tanks were thermally conditioned so as to reduce the temperature difference between

them (less than 10°) and to bring their temperature below 25°C as close as possible to 20°C. This was done by switching off all the heaters of the MMH tank and switching on the nominal and redundant ‘gauging’ heaters (LCL 16, 12 W total). The SAA was about 20° (see fig. 3.1 for SAA definition and RCS annex 1 for RCS components nomenclature). Before pressurisation, the status of the tanks was:

- MON-1 tank pressure @ 22°C: 14.4 bar
- MMH tank pressure @ 23°C: 14.7 bar
- He tank pressure @ 24°C: 182.6 bar
- He PT2: 14.6 bar

Several hours after pressurisation, at equilibrium, the status was:

- MON-1 tank pressure @ 23°C: 17.4 bar
- MMH tank pressure @ 24°C: 17.4 bar
- He tank pressure @ 23°C: 164.6 bar
- He PT2: 164.1 bar

The ‘normally closed’ pyro-valves 12, 13, 18 and 19 were fired nominally (see paragraph 2.5.3 for plots of pyro currents). Subsequently, the ‘normally closed’ pyro-valves 2 and 32 were also fired. At firing the nominal initiator of valve 2, pressure evolution of the high-pressure section could be immediately detected, showing that the first valve (NCV 2) functioned nominally on its nominal initiator. The pressure decrease of PT1 and the sudden pressurisation of PT2 can be observed in figure 8.2. PT2 increased its pressure step-wise starting from a level of 14.9 bar that it measured just before the opening of NCV2.

At the same time, the helium started to flow through the pressure regulator 1 and pressurised the two propellant tank sections as reported in fig. 8.3.

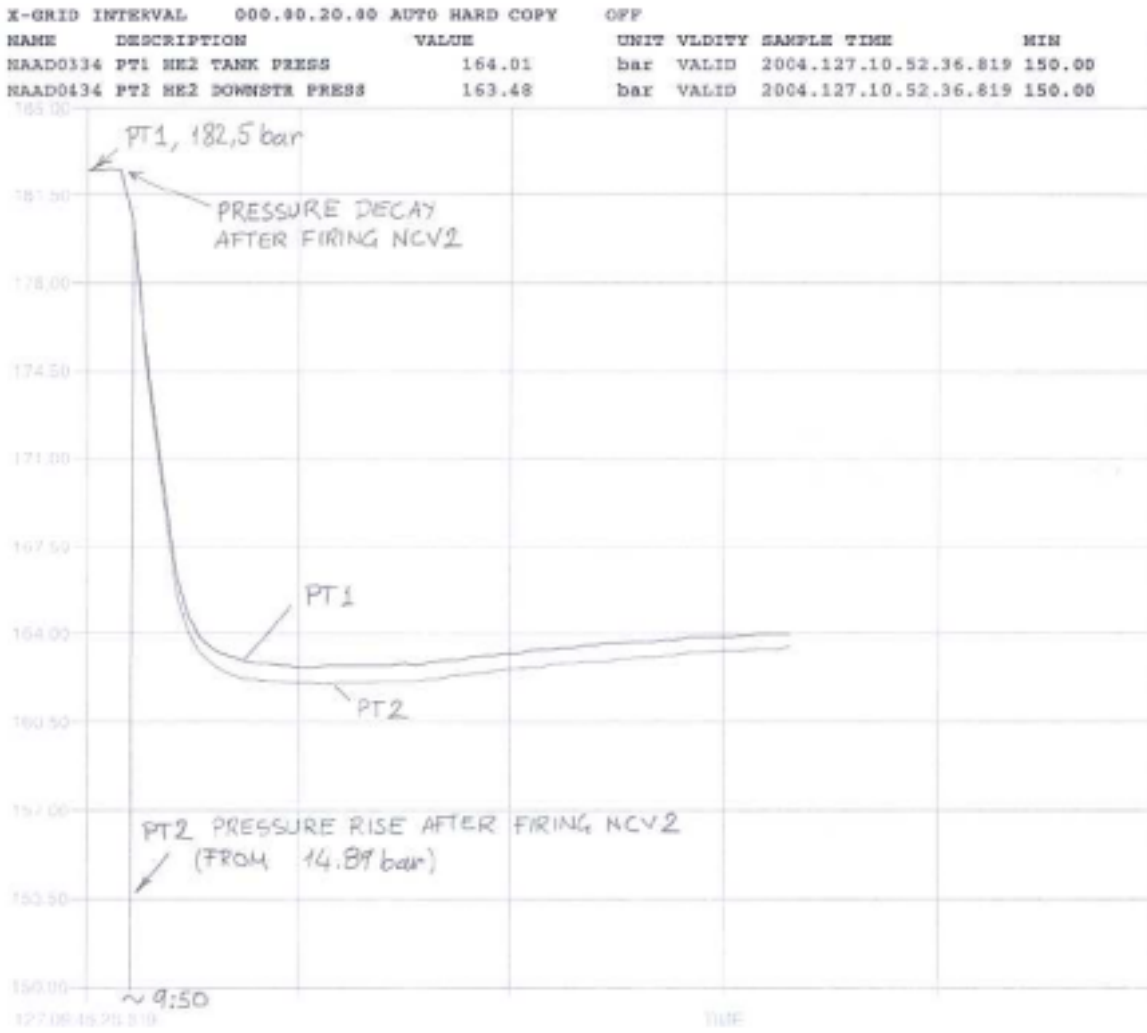


Fig. 8.2 – Pressure evolution after firing NCV2 of the helium pressurant tanks (PT1) and of the high-pressure side of the pressure regulator 1 (PT2). (On the time axis, three divisions correspond to 1 hour, absolute pressure in bar is reported on the vertical axis)

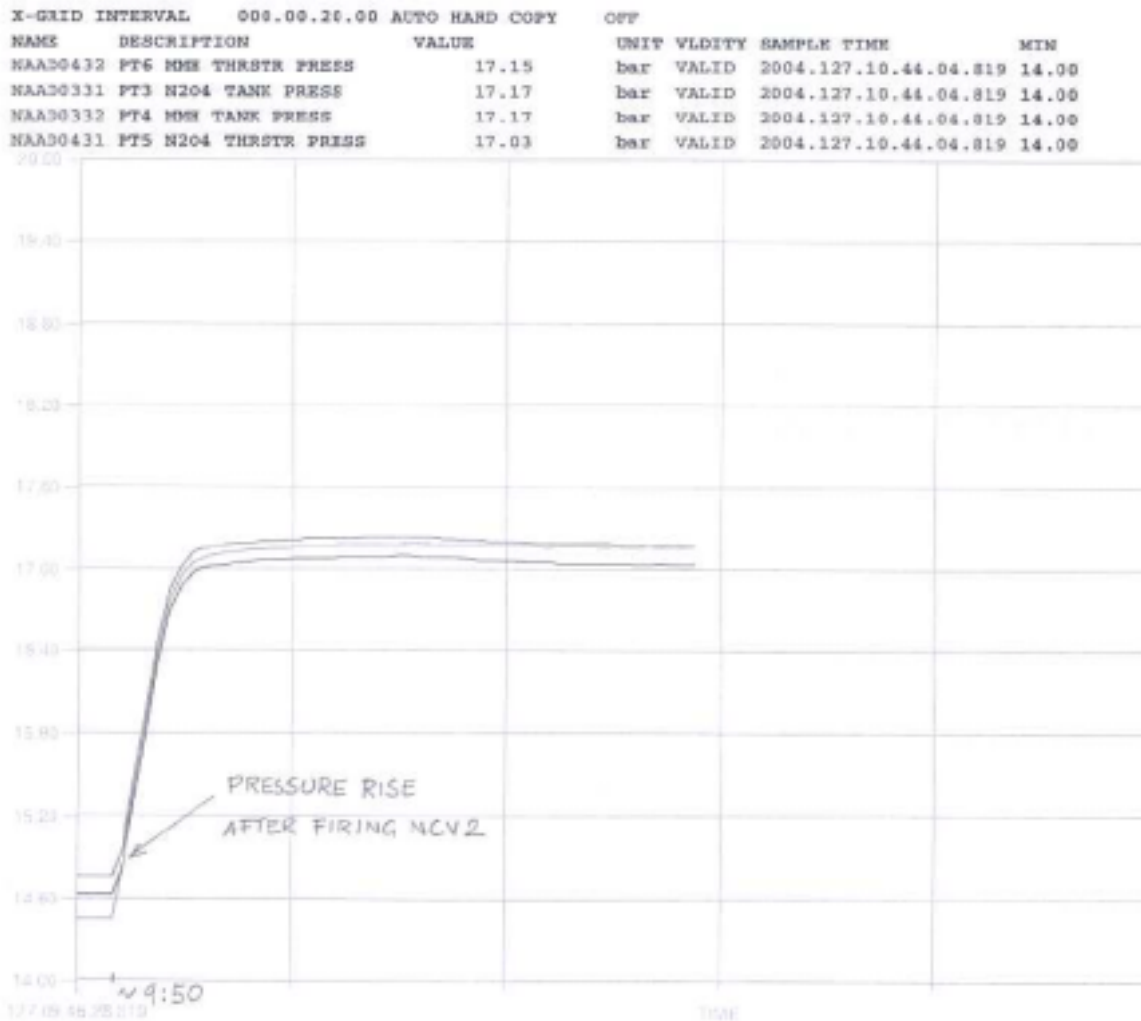


Fig. 8.3 – Pressurisation of the propellant tanks (PT3, PT4, PT5, PT6) after firing NCV2.). (On the time axis, three divisions correspond to 1 hour, absolute pressure in bar is reported on the vertical axis)

8.4 DSM1

The first DSM was performed on the night between May 10th and 11th. The targeted delta-V was 152.8 m/s. A trim manoeuvre of 5 m/s followed a few days later. The manoeuvre was performed in pressure-regulated mode. The 4 ‘delta-V’ thrusters (thrusters 9, 10, 11, 12) operated flawlessly. A typical temperature time history of the FCV’s of thrusters 12 is reported in fig. 3.4a and discussed in paragraph 3.3.3. The 4

attitude control thrusters located in the same thruster brackets (thrusters 3, 4, 5, 6) were used in pulse mode to provide control around the S/C Z-axis. A typical temperature time history of the FCV's of thrusters 5 is reported in fig. 3.4b and discussed in paragraph 3.3.3. The execution of the manoeuvre was nominal and the following performances were evaluated by ESOC (ref. 3):

Target delta-V: 152.809 m/s Estimated achieved: 152.824 m/s error: 0.01%
(accuracy of the measurement method: 0.01%)

8.4.1 Apparent Temperature Anomalies

Thruster 9 Temperature Drop – Discussion and fig. 8.4 to be provided in the final version of this report

NTO Tank Temperature Rise – Discussion and fig. 8.5 to be provided in the final version of this report.

8.5 First RCS Isolation

The first RCS isolation took place on May 24th. The tanks were brought to a lower temperature by switching off the redundant 'gauging' heater, so that the pressure could be topped-up. The status of the tanks before isolation was:

- MON-1 tank pressure @ 20°C: 17.4 bar
- MMH tank pressure @ TBD°C: 17.5 bar
- He tank pressure @ TBD°C: 141.5 bar
- He PT2: 141.7 bar

After isolation, the status was:

- MON-1 tank pressure @ 20°C: 17.4 bar
- MMH tank pressure @ TBD°C: 17.5 bar
- He tank pressure @ TBD°C: 141.8 bar
- He PT2: 27.0 bar

The above values are nominal and the pressure of PT2 (pressure regulator inlet) was lowered to a satisfactory value. This was done to limit the possible pressure regulator leaks that over long time could bring an unacceptable high pressure at the pressure regulator outlet. In fact, the MEOP of the pressure regulator outlet is limited to 22 bar.

All pyro-valves functioned nominally as reported in paragraph 2.5.3.

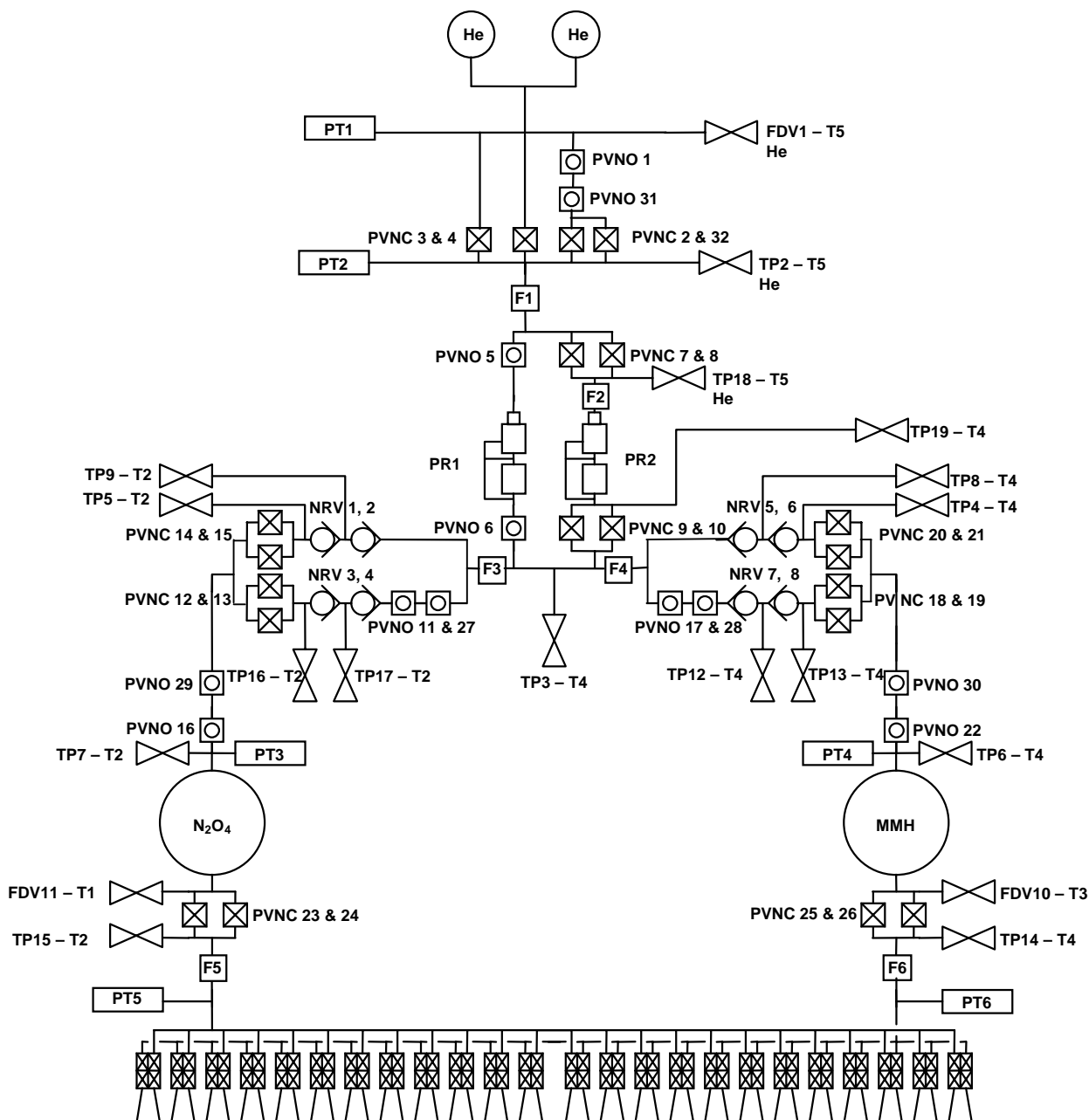
8.5.1 Apparent Pressure Anomalies

Regulator Inlet Pressure Drop – Discussion and fig. 8.6 and 8.7 to be provided in the final version of this report.

8.6 RCS REFERENCES

- 1 E-mail communication from V. Company to P. Ferri, Subject: Rosetta delta-V measurement accuracy dated May 19th, 2004

8.7 RCS SCHEMATIC AND COMPONENTS NOMENCLATURE



9 EMC

As in other ESA space missions, no specific in-orbit EMC test campaign had been foreseen during the ROSETTA spacecraft in-orbit commissioning.

During subsystem and payload operations no abnormal behaviour has been observed, which would indicate an EMC related anomaly.

10 CONCLUSION

After the Commissioning and Verification Phase part 1, the spacecraft has operated nominally with only minor anomalies. The spacecraft has performed with no major problems and no safe modes.

Only two problems need mentioning:

- Thermal
 1. Some external items of the spacecraft are in some respects hotter than predicted. Operational work a rounds have been fully investigated, documented and agreed with respect to the APM leading to no threat to the mission.
 2. ESOC will perform a number of thermal characterisations to obtain in flight thermal data to be used in future planning of near Sun operations, in order not to drive the thermal conditions beyond limits.
- Star Tracker
 1. A number of small problems have been noted regarding the loss of stars, which are still under investigation. Solutions (star catalogue and software updates) look possible to implement before the start of the next commissioning phase. At no time has the loss of stars affected the stability of the spacecraft attitude because of the implementation of the dust software.